MULTIDECADAL REMOTE SENSING OF INLAND WATER DYNAMICS

Simon Topp

A dissertation submitted to the faculty at the University of North Carolina at Chapel Hill in partial fulfillment of the requirements for the degree of Doctor of Philosophy in the Department of Geological Sciences in the School of Arts and Sciences

Chapel Hill
2021

Approved by:

Jaye E. Cable

Evan B. Goldstein

Jonathan M. Lees

Tamlin M. Pavelsky

Matthew R.V. Ross

© 2021
Simon Topp
ALL RIGHTS RESERVED

ABSTRACT

Simon Topp: MULTIDECADAL REMOTE SENSING OF INLAND WATER DYNAMICS
(Under the direction of Tamlin Pavelsky)

Remote sensing approaches to measuring inland water dynamics date back more than 50 years. These approaches rely on the unique spectral properties of different waterbodies to delineate surface extents and estimate optically active water quality parameters. Until recently, inland water remote sensing focused largely on localized study domains due to limitations in modelling methods, computing power, and data access. Recent advances in these areas have created novel opportunities for data-driven-multidecadal remote sensing of inland waters at the landscape scale. Here, I highlight the history of inland water remote sensing along with the dominant methodologies, water quality constituents, and limitations involved. I then use this background to contextualize three macroscale inland water remote sensing studies of increasing complexity. The first combines field measurements with remotely sensed surface water extents to identify the impacts of small-scale gold mining in Peru. Our results suggest that mining is leading to synergistic increases in lake area and mercury loading that are significantly heightening exposure risk for people and wildlife. I move from measuring lake extents in Peru to measuring lake color in over 26,000 lakes across the United States. This analysis shows that lake color seasonality can be generalized into five distinct phenology groups that follow well-known patterns of algae growth and succession. The stability of a given lake (i.e. the likelihood it will move from one phenology group to another) is tied to lake and landscape level characteristics including climate and population density. Finally, I move from simple parameters such as quantity and color to estimating multidecadal changes in water clarity in U.S. lakes. I show that lake water clarity in the U.S. has increased by an average of 0.52 cm yr^{-1} since 1984,

largely as a result of extensive U.S. freshwater pollution abatement measures. In combination, these three studies highlight that data intensive remote sensing approaches are expanding the capabilities of inland water remote sensing from local to global scales, and that macroscale remote sensing of inland waters reveals trends and processes that are unobservable using field data alone.

ACKNOWLEDGEMENTS

I would like to thank my advisor, Tamlin Pavelsky, who's patience, scientific insight, and kindness have been a steady source of support and inspiration. To my collaborators, colleagues, committee members, and lab mates, thank you for your time and for making science a fun endeavor. To my family, thank you for your constant encouragement. And to the Back Alley crew, thank you for the adventures and reminding me that life is about more than just work.

TABLE OF CONTENTS

LIST OF TABLES

LIST OF FIGURES

LIST OF ABBREVIATIONS

a(λ)	absorption at wavelength λ
ASGM	Artisanal and small-scale gold mining
ANN	Artificial Neural Network
APEX	Airborne Prism Experiment
AVARIS	Airborne Visible/Infrared Spectrometer
AVARIS-NG	Airborne Visible/Infrared Spectrometer Next Generation
b(λ)	backscattering at wavelength λ
BDI	below detection limit
CASI	Compact Airborne Spectrographic Imager
CCV	Calibration and continuous calibration verification
CDOM	colored dissolved organic matter
Chl-a	chlorophyll-a
CVAFS	cold vapor atomic fluorescence spectroscopy
CVI	cluster validity index
ENMAP	Environmental Mapping and Analysis Program
EPA	Environmental Protection Agency
ETM+	Enhanced Thematic Mapper
FFS	forward feature selection
GC	gas chromatographic
GLCP	Global Lake Area, Climate, and Population database
Hg	elemental mercury
HISUI	Hyperspectral Imaging Suite
HRG	High-Resolution Geometric Sensor
ICP-MS	Inductively Coupled Plasma Mass Spectrometry
ICV	initial calibration verification
IOCCG	The International Ocean-Colour Coordinating Group
LLLTO-CV	leave-location-leave-time-out cross-validation

MERIS	Medium Resolution Imaging Spectrometer
MeHg	methylmercury
MODIS	Moderate Resolution Imaging Spectrometer
MSI	Multispectral Instrument
MSS	Multispectral Scanner
NASA	The National Aeronautics and Space Administration
NDVI	normalized difference vegetation index
NDWI	normalized difference water index
NHD	National Hydrography Dataset
NOAA	National Oceanic and Atmospheric Administration
OLCI	Ocean and Land Cover Instrument
OLI	Operational Land Imager
PRISM	Portable Remote Imaging Spectrometer
PRISMA	PRecursore IperSpettrale della Missione Applicativa
R(λ)	reflectance at wavelength λ
SBG	Surface Biology and Geology Mission
SDD	Secchi Disk Depth
THg	total mercury
TM	Thematic Mapper
TSS	total suspended solids
US	United States
USGS	United States Geological Survey
Xgboost	Extreme Gradient Boosting

Chapter 1: Research Trends in the Use of Remote Sensing for Inland Water Quality Science: Moving Towards Multidisciplinary Applications[1]

Section 1: Introduction

Section 1.1: Summary

Remote sensing approaches to measuring inland water quality date back nearly 50 years to the beginning of the satellite era. Over this time span, hundreds of peer-reviewed publications have demonstrated promising remote sensing models to estimate biological, chemical, and physical properties of inland waterbodies. Until recently, most of these publications focused largely on algorithm development as opposed to implementation of those algorithms to address specific science questions. This slow evolution contrasts with terrestrial and oceanic remote sensing, where methods development in the 1970s led to publications focused on understanding spatially expansive, complex processes as early as the mid-1980s. This review explores the progression of inland water quality remote sensing from methodological development to scientific applications. We use bibliometric analysis to assess overall patterns in the field and subsequently examine 236 key papers to identify trends in research focus and scale. The results highlight an initial 30 year period where the majority of publications focused on model development and validation followed by a spike in publications, beginning in the early-2000s, applying remote sensing models to analyze spatiotemporal trends, drivers, and impacts of changing water quality on ecosystems and human populations. Recent and emerging resources, including improved data availability and enhanced processing

[1] This chapter previously appeared as an article in *Water*. The original citation is as follows: Topp, S. N., Pavelsky, T. M., Jensen, D., Simard, M., & Ross, M. R. V. (2020). Research trends in the use of remote sensing for inland water quality science: Moving towards multidisciplinary applications. Water, 12(1), 169. https://doi.org/10.3390/w12010169.

platforms, are enabling researchers to address challenging science questions and model spatiotemporally explicit patterns in water quality. Examination of the literature shows that the past 10–15 years has brought about a focal shift within the field, where researchers are using improved computing resources, datasets, and operational remote sensing algorithms to better understand complex inland water systems. Future satellite missions promise to continue these improvements by providing observational continuity with spatial/spectral resolutions ideal for inland waters.

Section 1.2: Background

Remote sensing has long been promised as a tool for large-scale monitoring of inland water quality. Dating back to the early 1970s, airborne and satellite sensors have been used to examine a wide range of water quality constituents (Wrigley and Horne, 1974; Scarpace et al., 1979). In the 50 years since, scientists have produced hundreds of peer-reviewed publications presenting models estimating biological, chemical, and physical properties of complex waterbodies (see reviews by Liu et al. (2003), Matthews (2011), Odermatt et al. (2012), and Gholizadeh et al. (2016)). Despite this proliferation of publications, existing reviews focus almost exclusively on methodological approaches rather than on the scientific contributions of remote sensing to our understanding of water quality, so characterization of the extent to which remote sensing has improved our knowledge of inland water dynamics remains limited.

The historical tendency of inland water remote sensing to focus largely on methods development (here defined as data collection and processing and/or algorithm calibration and validation), contrasts starkly with that of related fields in terms of both the scope of research questions and the scale of studies. For terrestrial remote sensing, algorithm development throughout the 1970s (e.g., Normalized Difference Vegetation Index (NDVI); Tucker (1979)) led to publications focused on spatially expansive, complex processes as early as the mid-1980s. These papers include studies on global land use (Matthews, 1983), global vegetation analysis (Tarpley et al., 1984), and connections between primary productivity and carbon cycling (Tucker

et al., 1986; Box et al., 1989). For ocean color remote sensing, early methods development led to global datasets and estimations of oceanic primary productivity by the late 1980s (Platt and Sathyendranath, 1988; Feldman et al., 1989). Comparatively, global data products for inland water quality are limited, with a few key exceptions (e.g., Zandaryaa (2018)) despite widespread acknowledgement of their importance from the inland water scientific community (Malthus et al., 2012; Lee et al., 2018). This slow evolution can be partially explained by well-known challenges related to remote sensing of complex waterbodies, as well as the limited availability of sensors appropriate for inland water quality remote sensing (Hestir et al., 2015), discussed in detail with other challenges in Section 7.

Previous reviews have provided excellent summaries of the technical approaches available to retrieve inland water quality parameters through remote sensing, as well as the current limitations of the field (Liu et al., 2003; Matthews, 2011; Odermatt et al., 2012; Gholizadeh et al., 2016; Tyler et al., 2016; IOCCG, 2018; Giardino et al., 2019a). Instead, we focus not on methodological details, but on the overall purpose and impact of past publications, how those impacts have changed over time, and how the field may evolve in the future. We quantify broad-scale trends through bibliometric analysis of search engine results. A subset of the most relevant published papers (n = 236) was identified using existing reviews, citation counts, database queries, and journal-specific searches. The identified papers were subsequently read, with key attributes documented in order to analyze trends and patterns in methodological approaches, model application, research focus, and study scale over time. Here, trend refers to a pattern with directionality over time or space. We limit our analysis to airborne and satellite remote sensing publications focusing on lakes, rivers, deltas, and estuaries, although we fully acknowledge that these publications were preceded by years of vital methods development using handheld and shipborne sensors (e.g., Bukata et al. (1981, 1988), Kishino et al. (1984), Kirk and Tyler (1986), Seyhan and Dekker (1986), and Dekker and Seyhan (1988)). Similarly, given the focus of this paper on the remote sensing of lake, river,

delta, and estuarine systems, which present their own unique challenges (Hestir et al., 2015), we excluded studies on near shore ocean waters and the Laurentian Great Lakes due to their similarity to Ocean Color Remote Sensing where well established methods already exist.

Our results highlight a nearly 30 year period focusing predominantly on methods development prior to a spike in publications, beginning in the early 2000s, applying well validated algorithms to identify spatiotemporal trends, drivers, and impacts of changing inland water quality on ecosystem functions and human populations. Study scale exhibits a similar trend towards increasingly large areas with more waterbodies studied over longer periods of time, slowly moving closer to regional and global-scale data products. Through both broad and detailed inspection of the field, our results suggest that the past decade of inland water remote sensing has led to a fuller understanding of inland water processes by focusing on challenging science questions and increased study scales. This contribution continues today with an ever-expanding body of available data, processing platforms, and methodologies.

We contextualize our analysis of the literature by: (1) summarizing the primary water constituents measured with earth observation instruments, (2) providing a brief overview of common modelling approaches to measure those constituents, and (3) discussing the limitations that have hampered past research. This contextual information is followed by the bibliometric and index analysis described above. We conclude with a discussion of potential future directions for the field.

Section 2: Earth Observation Sensors and Optically Active Waterbody Constituents

The work reviewed here focuses primarily on passive optical satellite sensors capable of large-scale remote sensing research. In general, these are either ocean color sensors such as the Moderate Resolution Imaging Spectroradiometer (MODIS) (Miller and McKee, 2004; Falcini et al., 2012; Adamo et al., 2013; Qin et al., 2015), the Medium Resolution Imaging Spectrometer (MERIS) (Matthews et al., 2010; Bresciani et al., 2011, 2012; Palmer et al., 2015b), and the Sentinel-3 Ocean and Land Cover Instrument (OLCI) (Shen et al., 2017), or land surface optical

sensors including the Landsat series (Multispectral Scanner (MSS): (Ritchie et al., 1990; Mertes et al., 1993; Kloiber et al., 2002); Thematic Mapper (TM): (Dekker and Peters, 1993; Yacobi et al., 1995; Wang et al., 2004); Enhanced Thematic Mapper (ETM+): (Ouillon et al., 2004; Tyler et al., 2006; Duan et al., 2007); and Operational Land Imager (OLI): (Watanabe et al., 2015; Lee et al., 2016)), Sentinel 2 A/B MultiSpectral Instrument (MSI) (Kutser et al., 2016; Toming et al., 2016), and SPOT High-Resolution Geometric Sensor (HRG) (Doxaran et al., 2002b). A subset of researchers have used high-resolution commercial sensors including WorldView 2 (Dvornikov et al., 2018) and IKONOS (Sawaya et al., 2003; Hellweger et al., 2007). The above sensors vary significantly in their applicability, based largely on their spatial, temporal, spectral, and radiometric resolutions. Temporal and spatial resolutions determine the scale of processes that can be captured by a given sensor. In general, land surface sensors have a finer spatial resolution (~10–30m) but coarser temporal resolution (~1–2 weeks), allowing them to detect spatial patterns in water quality in smaller waterbodies (e.g., small lakes and rivers) but with only 1–2 observations per month depending on the sensor and cloud cover conditions. Comparatively, ocean color sensors are characterized by coarse spatial resolutions (~300–1000 m) but finer temporal resolutions (~daily), limiting observations to large waterbodies but facilitating examination of processes that occur at short timespans. A more in-depth discussion on the effects of varying resolutions across ocean and terrestrial sensors can be found in Olmanson et al. (2011) and the Committee on Earth Observation Satellites (CEOS) (2018). Additionally, technical discussions and summaries of the spatial, temporal, spectral, and radiometric resolutions of the above sensors are provided by Gholizadeh et al. (2016) and Matthews (2011).

Since water is highly absorptive within the near and shortwave infrared spectrum, the majority of water-leaving radiance occurs within the visible spectrum with slight variations dependent on temperature and salinity (Buiteveld et al., 1994; Röttgers et al., 2014). The primary exception is in optically complex waters (due to high turbidity and/or bottom

reflectance), where sediment reflectance exceeds the absorptive properties of water in the near and shortwave infrared wavelengths (Sathyendranath, 2000; Doxaran et al., 2002b). Relatively high absorption within the visible spectrum leads to a low range of reflectance values when compared to land surface remote sensing. This low range requires high sensitivity (i.e., high radiometric resolution) to detect small changes in reflectance (Matthews, 2011). Different concentrations of varying water quality parameters lead to various absorption features and backscatter peaks within the water leaving radiance. The spectral resolution, measured by the range of wavelengths captured by individual sensor bands, needs to be sufficiently fine to capture spectral peaks and accurately estimate the contribution of a given water quality parameter to the overall spectral signature (Hestir et al., 2015). The sensors mentioned above are all multispectral sensors, meaning that they have a small number of relatively wide bands (~10 nm to ~80 nm) placed within the visible to mid-infrared spectrum. These coarse bandwidths can complicate retrieval of water quality parameters (Hestir et al., 2015). In order to better capture the specific absorption features and backscatter peaks within a waterbody's spectral signature, a subset of publications have utilized hyperspectral sensors that provide hundreds of narrow (1–10 nm), contiguous bands spanning the visible to shortwave infrared spectrum (see Govender et al. (2007)). Currently, the majority of hyperspectral sensors are airborne or in planning stages for future satellite missions (Bioucas-dias et al., 2013). Within inland water remote sensing, applications of hyperspectral remote sensors include the use of Hyperion (Brando and Dekker, 2003; Fang et al., 2008), the Compact Airborne Spectrographic Imager (CASI) (Wass et al., 1997; Hunter et al., 2008), the Airborne Prism Experiment (APEX) (Knaeps et al., 2015), and NASA's HyMAP scanner (Choe et al., 2008), Airborne Visible/Infrared Spectrometer (AVIRIS) (Palacios et al., 2015), Airborne Visible/Infrared Spectrometer-Next Generation (AVIRIS-NG) (Jensen et al., 2019), and Portable Remote Imaging Spectrometer (PRISM) (Fichot et al., 2016).

Regardless of sensor, the optically active water parameters that contribute to the total water-leaving signal are phytoplankton, organic and inorganic suspended solids, and colored dissolved organic matter (CDOM) (Morel and Gordon, 1980; Mobley, 1994; Sathyendranath, 2000) (Table S1). The sum of these three individual constituents, in combination, attribute to differences in overall water clarity, which is frequently used as a proxy for water quality (McCullough et al., 2012; Lee et al., 2018). Publications leveraging relationships between optically inactive constituents, which have no detectable spectral signal, and the optically active constituents listed above have provided remote sensing models for nitrogen and phosphorous (Lillesand et al., 1983; He et al., 2008; Torbick et al., 2013), dissolved oxygen (Wang et al., 2004; Toming et al., 2016), and heavy metals (Fichot et al., 2016). However, compared to optically active parameters, these optically inactive constituents require site specific algorithms due to varying regional correlations with optically active water quality constituents. Publications examining the remote sensing of inactive constituents date back to the early 90s (Baban, 1993; Dekker and Peters, 1993); however, they appear relatively infrequently within the literature and are not discussed in detail here. Below, we describe the optically active constituents with their distinct spectral signatures.

Section 2.1: Chlorophyll-A

Chlorophylls are the photosynthetically active compounds that convert light into energy for photosynthesis. Remote sensing studies primarily focus on chlorophyll-a (chl-a), which is the most abundant chlorophyll and is present within all plants, algae, and cyanobacteria that photosynthesize. In aquatic systems, it is used as a proxy measure of total algal biomass (Kutser, 2009). The algal biomass of a waterbody controls its overall biological productivity, also known as trophic state, making it an ideal indicator of ecosystem integrity (McCormick and Cairns, 1994; Carvalho et al., 2013). While not all algal blooms are inherently harmful, blooms containing certain species, most commonly phycocyanin-producing cyanobacteria, are toxic to humans, livestock, and wildlife (Svirčev et al., 2013). Anthropogenically driven nutrient loading

and climate change in recent decades have increased the size and frequency of these harmful algal blooms worldwide (Paerl and Huisman, 2009).

Optically, the spectral signature of chl-a varies depending on its concentration in relation to other water quality parameters and the composition of phytoplankton phenotypes producing the signal (Dierssen et al., 2006; Zhou et al., 2018). For low biomass, oligotrophic to mesotrophic waterbodies, the chl-a spectrum is characterized by a sun-induced fluorescence peak around 680 nm (Gitelson et al., 1994; Gower et al., 1999, 2004). For high biomass, eutrophic waterbodies, the florescence signal is masked by absorption features and backscatter peaks centered at 665 nm and 710 nm respectively (Matthews et al., 2012). The ratio between these two wavelengths has been used to accurately estimate chl-a concentrations in numerous studies (Gitelson et al., 1993; Dall'Olmo and Gitelson, 2006; Le et al., 2011). Beyond basic constituent retrieval, research focusing on chlorophyll includes the detection of harmful cyanobacteria (Kudela et al., 2015; Lunetta et al., 2015; Oyama et al., 2015) and phycocyanin (Hunter et al., 2008; Medina-Cobo et al., 2014), assessment of trophic state (Duan et al., 2007; Sheela et al., 2011; Watanabe et al., 2015), and algal bloom development and dispersion modelling (Hedger et al., 2002; Bresciani et al., 2013; Zhang et al., 2013; Curtarelli et al., 2015).

Section: 2.2: Total Suspended Solids

Total suspended solids (TSS) refers to both inorganic and organic particles held in suspension throughout a water column. Controls on the composition of organic and inorganic particles vary geographically, with some areas driven primarily by inorganic sediments and others by phytoplankton. In the literature it is referred to variously as total suspended matter, suspended sediment concentration, and particulate matter, though the precise definitions of these terms sometimes vary. Monitoring TSS fluxes has strong implications for biogeochemical cycling in terms of nutrient transport (Rügner et al., 2013), heavy metal loading (Nasrabadi et al., 2016), light conditions (Julian et al., 2008), and global carbon budgets (Mendonça et al., 2017). Terrestrial carbon deposition into lakes and reservoirs, largely in the form of TSS, is

double that of deposition into the ocean (Cole et al., 2007; Adrian et al., 2009), despite lakes comprising only 3%–3.7% of the total land area (Downing et al., 2006; Verpoorter et al., 2014). Simultaneously, the settling out of TSS into lake bottom sediments provides a carbon sink, with current global carbon sequestration estimates ranging from 0.06–0.27 Pg year^{-1} (Cole et al., 2007; Mendonça et al., 2017). On a local scale, high TSS reduces light penetration through increasing turbidity and leads to benthic smothering, impacting species composition and primary productivity from macrophytes (Bilotta and Brazier, 2008; Kefford et al., 2010). Finally, TSS concentrations and flux in rivers capture the landscape processes controlling delivery of erosional products from land to ocean (Syvitski, 2005; Overeem et al., 2017).

Spectral signatures of TSS concentrations can vary significantly based on the particle size and composition of organic to inorganic materials (Novo et al., 1989; Spyrakos et al., 2017). Organic-dominated systems derive their spectral signatures from algae concentrations and can share the pronounced absorption features and backscatter peaks described above for chlorophyll (Shi et al., 2013). As inorganic TSS concentrations increase within a waterbody, the location of the spectral maximum moves from around 550 nm into the red or near-infrared wavelengths (Doxaran et al., 2002b) with waterbody specific variation dependent on chlorophyll and CDOM concentrations. Remote sensing studies examining TSS focus largely on riverine and coastal systems, with notable studies including estimates of TSS delivery to the ocean (Overeem et al., 2017), variability in sediment plume size (Walker, 1996; Falcini et al., 2012; Brando et al., 2015), impacts of reservoirs on sediment concentration (Pereira et al., 2017), impacts of land use change on sediment delivery (Telmer et al., 2006), and variability of sediment in lagoons (Volpe et al., 2011). TSS concentrations can be correlated with various optically inactive water quality parameters and have subsequently been used to infer the concentration of phosphorous (Gholizadeh et al., 2016), mercury (Telmer et al., 2006), and other metals (Choe et al., 2008) at local scales.

Section: 2.3: Colored Dissolved Organic Matter

Colored (or 'chromophoric') dissolved organic matter is the colored portion of total dissolved organic carbon. Sources of CDOM can be either autochthonous (i.e., phytoplankton) or allochthonous (i.e., terrestrial carbon). Of the two sources, allochthonous carbon leached out of surrounding soils is generally the dominant control of total lake and river dissolved organic carbon (Sobek et al., 2007). Photo and biodegradation of CDOM can contribute to elevated levels of CO_2 within lacustrine systems (Tranvik et al., 2009). Recent studies of CO_2 concentrations in Chinese (Wen et al., 2017) and US (McDonald et al., 2013) lakes found that ~60%–70% were supersaturated with CO_2. Globally, this oversaturation leads to 0.35–0.43 Pg $year^{-1}$ of carbon off-gassed into the atmosphere, in addition to an estimated 1.8 Pg $year^{-1}$ emitted from streams and rivers (Raymond et al., 2013). At low levels, CDOM absorbs harmful ultraviolet radiation with minimal impact on light penetration within the visible spectrum (del Vecchio and Blough, 2006). As concentrations increase, absorption of low-wavelength light by CDOM regulates the light availability of primary producers, controlling net productivity and trophic structure (del Vecchio and Blough, 2006; Thrane et al., 2014). Continued monitoring of CDOM directly, and as a proxy for total dissolved organic carbon, provides a better understanding of carbon inputs and processing in freshwater systems.

Highly absorptive in the visible spectrum, elevated levels of CDOM lead to stratified, dark waterbodies with limited light penetration (Houser, 2006). Similar to TSS, the reflectance spectra of waterbodies with varying concentrations of CDOM are highly dependent on the composition of other optically active constituents, and in certain areas can be complicated by the presence of colloidal iron, which shares similar optical properties (Kutser et al., 2015a). CDOM's contribution to water-leaving radiance is characterized by an exponential increase in absorption as wavelength decreases (Olmanson et al., 2016). Intuitively, this would suggest that CDOM models should incorporate wavelengths in the blue spectrum; however, excessive absorption by CDOM and low natural water-leaving radiance at low wavelengths reduces the

usable signal (Bricaud et al., 1981; Kirk and Tyler, 1986). As a result, algorithms commonly incorporate a green/red ratio (e.g., Brezonik et al. (2005), Kutser et al. (2005, 2009a); Toming et al. (2016)). Remote sensing studies focusing on CDOM range in application from identifying trends in inland water carbon content (Chang and Vannah, 2012; Kutser et al., 2015b) to examining landscape-level drivers of CDOM distributions (Dvornikov et al., 2018; Griffin et al., 2018a). Work in rivers highlights controls of carbon export in arctic landscapes (Griffin et al., 2011) and relationships governing CDOM variation in river estuaries along with the resulting impact on correlated concentrations of methylmercury (Fichot et al., 2016). An in depth review of CDOM and its optical properties was published by Coble (2007).

Section: 2.4: Water Clarity

The combination of chlorophyll, suspended sediments, and CDOM collectively contributes to overall water clarity. Most commonly, Secchi Disk depth or turbidity are used as relative measures of clarity. The former metric, developed more than 150 years ago, quantifies the maximum visible depth of a white and black disk lowered into a waterbody (Cialdi and Secchi, 1865; Wernand, 2010). In comparison, turbidity is an explicit measurement of light scattering within a water column caused by suspended and dissolved particles. Water clarity regulates freshwater ecosystems through light attenuation and control over epilimnion depth (Mazumder and Taylor, 1994). Numerous studies have examined the role of water clarity in thermal stratification (Gunn et al., 2001; Heiskanen et al., 2015), lake metabolism (Schwarz and Hawes, 1997; Obrador et al., 2014), and biodiversity (Bilotta and Brazier, 2008). Generally, a shallower thermocline and reduced light penetration associated with degraded water clarity reduces photosynthesis of submerged macrophytes and other primary producers (Bilotta and Brazier, 2008; Izagirre et al., 2009).

Remote sensing retrievals of water clarity almost universally use wavelengths and band ratios that include the red spectrum in some way (e.g., Verdin (1985), Baban (1993), Nelson et al. (2003), Bayley et al. (2007), Wu et al. (2008), McCullough et al. (2012), Hicks et al. (2013),

Rose et al. (2017)). Reflectance at these wavelengths accounts for total sediment and chlorophyll concentrations such that increasing brightness is associated with decreased water clarity (Matthews, 2011). Water clarity has long been acknowledged as a proxy for nutrient availability and chlorophyll concentrations within lakes (Hutchinson, 1973; Carlson, 1977; Megard et al., 1980); as a result, remote sensing studies frequently use it as a proxy for overall lake trophic status (oligotrophic, mesotrophic, or eutrophic) (Peckham et al., 2006; Olmanson et al., 2008; Sheela et al., 2011).

Section 3: Modelling Approaches

Models that leverage the relationship between a waterbody's optical qualities and its concentration of optically active water quality constituents are commonly referred to as bio-optical algorithms (Morel, 2001). In inland waters, these models can be categorized as empirical, semi-analytical, or machine learning based (Appendix A: Table S2). While inherently empirical, we distinguish machine learning techniques separately due to their computational complexity and ability to handle non-linear relationships. As discussed below, all three of these modeling approaches have benefits and shortcomings in terms of applicable scale, model transparency, and model complexity.

Section 3.1: Empirical Models

The most common approach to inland water remote sensing involves fitting a standard linear regression between spectral band/band ratio values and temporally coincident in situ water quality measurements. One inherent limitation of this approach is its non-generalizability across large spatial and temporal scales where variations in atmospheric and water composition create large variability in observed spectral signatures of water quality parameters. As such, empirical models are restricted to confident predictions only within the range and setting of the input data. This restriction limits their application across spatiotemporal domains. At a local scale, empirical modelling accounts for the site-specific optical qualities of the water, but with increasing spatial or temporal scales, optically non-homogenous waterbodies and changing

atmospheric conditions complicate parameterization (Politi et al., 2015). These shortcomings are often outweighed by the benefits of model transparency, simplicity, and minimal computational requirements.

The family of empirical models can be split into purely empirical and semi-empirical approaches. The purely empirical approach derives relationships using input band and band ratio values as coefficients, often generating multiple models and choosing the best fit through comparison of error metrics. Purely empirical approaches date back to the 1970s and 80s, with notable applications examining trophic state in Wisconsin (Scarpace et al., 1979) and Minnesota (Lillesand et al., 1983), and turbidity and chlorophyll in Australian lakes (Carpenter and Carpenter, 1983).

In contrast, semi-empirical models use multi-band index values with some basis in the physical properties of the constituent of interest. These models largely focus on the measurement of water clarity, chl-a, cyanobacteria, and TSS. Like terrestrial vegetation indices (e.g., NDVI), they are designed to enhance the spectral properties of the constituent of interest while reducing noise from extraneous optical parameters; however, unlike semi-analytical approaches (described below), semi-empirical models don't incorporate any inverse modelling of the inherent optical properties of a given waterbody. Notable semi-empirical indexes include the normalized difference chlorophyll index (Mishra and Mishra, 2012), the maximum chlorophyll index (Gower et al., 2005), the Floating Algal Index (Hu, 2009), and the normalized difference suspended sediment index (Shahzad et al., 2018). Application of these semi-empirical indexes has contributed to robust algal bloom detection (Huang et al., 2014), determining the presence of harmful cyanobacteria concentrations associated with eutrophication (Zhou et al., 2018), and modelling sediment concentrations in rivers and deltas (Shahzad et al., 2018). Due to their basis in physical properties, semi-empirical models are more generalizable than purely empirical approaches. However, they necessitate measurements of specific wavelengths that capture

absorption features and scattering peaks, restricting their applicability to sensors with suitably placed band centers and sufficient spectral resolution.

Section 3.2: Semi-Analytical Models

Analytical and semi-analytical models are physics based and involve parameterization based on the inherent optical properties (IOPs) of water and the atmosphere, where IOPs refer to the optical properties of the medium of interest that are independent of the ambient light field (Mobley, 1994; Sathyendranath, 2000). The IOPs of a given waterbody are modelled in coordination with apparent optical properties (including illumination conditions, sensor orientation, and field of view) to construct theoretical absorption and backscattering values which can then be decomposed through an inverse equation to estimate optically active water quality constituents (described below) (Morel and Gordon, 1980; Sathyendranath, 2000; Morel, 2001; Giardino et al., 2019a). For purely analytical models, the inverse equation is parameterized based purely on light physics; however, these are rarely used for optically complex waters where the interactions of numerous water quality constituents become difficult to model. As a result, semi-analytical models, which incorporate in situ measurements to parameterize the inverse equation, are the primary form of physics based algorithms developed for inland water quality remote sensing retrievals (Matthews, 2011). This modelling approach evolved from the reflectance approximation developed by Morel (1977), who studied turbidity and chlorophyll in ocean waters. Compared to empirical and semi-empirical algorithms, semi-analytical models are mechanistic, make apriori assumptions regarding light physics, and are theoretically generalizable outside the range of a given study; however, the application of any single model to optically nonhomogeneous waterbodies requires large amounts of in situ validation data and remains challenging (Malthus et al., 2012).

A prerequisite to this modelling approach is understanding the light physics that control reflectance as particle size, composition, and concentration vary. These properties are modelled through the absorption and backscattering coefficients of all the optically active constituents

found within the study area (Equation 1). While derivations of semi-analytical models come from numerous sources (e.g., Gordon et al. (1975, 1988), Philpot (1987); Stumpf and Pennock (1989)), the basic form of the preliminary equation follows Equation 1.

$$R(\lambda)=Y^{*}\frac{b(\lambda)}{a(\lambda)+b(\lambda)} \quad 1)$$

Here, the total reflectance just below the water's surface (*R*) at wavelength λ is equal to the backscattering at the given wavelength over the absorption plus the backscattering at the given wavelength times an empirically or analytically derived constant *Y.* The absorption and backscattering coefficients can be further broken down into absorption and backscattering for each optically active constituent. (e.g., $b(\lambda) = b_{water}(\lambda) + b_{cdom}(\lambda) + (\lambda)b_{chl} + (\lambda)b_{tss}$). Values for *R* are either generated through in situ measurements of reflectance and water quality or theoretically generated using physical modelling software such as HydroLight (Mobley and Sundman, 2008). These generated spectral signatures are then used to parameterize an inverse model that decomposes *R* into optically active constituent concentrations through their absorption and backscatter coefficients. One benefit of this inverse modelling procedure is the ability to estimate multiple water quality parameters simultaneously. However, model development is inherently complicated and, depending on if atmospheric corrections have been applied, requires information about atmospheric composition, bottom reflectance, and extensive in situ sampling. Even so, the literature contains numerous examples of successful applications of semi-analytical models across large spatiotemporal scales. Early development of semi-analytical modelling for inland waters was led by researchers such as Dekker (Seyhan and Dekker, 1986; Dekker et al., 1991) and Kutser (Kutser and Arst, 1994) examining chl-a, TSS, and CDOM. More recently, Heege et al. (2014) developed a semi-analytical algorithm for turbidity across the Mekong Delta with strong validation results using MODIS, Landsat, and RapidEye, Lymburner et al. (2016) applied a semi-analytical algorithm to a multi-decadal study of TSS in Australian lakes, and both Volpe et al. (2011) and Zhou et al. (2017) applied semi-

analytical algorithms across multi- and hyper-spectral data to detect TSS in shallow lagoons. For a more detailed description of semi-analytical modelling, see Dekker et al. (2001, 2002), Giardino et al. (2019a), Morel (2001), and IOCCG (2000).

Section 3.3: Machine Learning Models

In recent years, increases in computational capacity and available data have created opportunities for novel approaches to data analysis. While inherently empirical, machine learning approaches are differentiated by their ability to operate in multidimensional space with complex non-linear relationships (Olden et al., 2008). The spectrum of machine learning methods for remote sensing applications is broad (Camps-Valls, 2009; Lary et al., 2016); here, we focus on the benefits and limitations of machine learning methods generally, along with some notable examples in the field of inland water remote sensing. A more detailed review of machine learning methodology for remote sensing was published by Lary et al. (2016).

Within inland water remote sensing, machine learning algorithms including artificial neural networks (Schiller and Doerffer, 1999; Song, 2011; Imen et al., 2015), genetic algorithms/programming (Song et al., 2013; Chang et al., 2014), support vector machines (Sun et al., 2014), random forest/boosted regression trees (Lin et al., 2018), and empirical orthogonal functions (Qi et al., 2014; Duan et al., 2017) have all shown promise in accurately estimating water quality parameters across a variety of spatiotemporal scales. As with traditional empirical models, machine learning approaches are only applicable within the range and setting of data used to train a given model. However, unlike traditional empirical models, most machine learning models use iterative learning to reduce overall error and maximize model fit (Hastie, 2009). Depending on the parameterization of the model and the amount of training data available, this approach may lead to over-fitting of the data, especially in models with numerous input variables subject to collinearity such as adjacent hyperspectral bands (Rocha et al., 2017). To avoid overfitting, machine learning methods require the provision of separate training and testing datasets that contain representative samples of the parameters of interest. The power

and scalability of most machine learning algorithms is dependent on the quality and range of the training and testing data. Given the proper inputs, these algorithms can produce generalizable models that capture complex, non-linear relationships between remotely sensed reflectance and biogeophysical parameters. While modelling chl-a and turbidity in Lake Chagan, China, Song (2011) found reductions in root mean square error of 76% and 65%, respectively, when comparing traditional regression techniques to artificial neural networks. Similarly, Xiang et al. (2015) found a 20% increase in trophic state classification accuracy when using machine learning compared to multivariate regression.

Section 4: Challenges and Limitations Within the Field

The literature reviewed here highlights that, despite the diverse modelling approaches discussed above, several barriers still exist that limit the progress of inland water remote sensing. Specifically, sensor design, atmospheric effects, dynamic waterbodies, and institutional barriers, all of which present legitimate challenges to increasing the scale and robustness of remote sensing algorithms. Here, we discuss these issues in detail to provide context on the limitations of the reviewed literature.

At the most basic level, many sensors are limited in the types of observations they can make. Multispectral, broad-band satellites like the Landsat TM/ETM+ series were engineered for terrestrial applications and lack the spectral resolution, band centers, and signal-to-noise ratios ideal for complex waters. Their relatively infrequent return periods make them more suited to detecting long-term changes as opposed to daily or weekly variation. Ocean color sensors including MODIS, SeaWiFS, and MERIS have higher spectral resolution and frequent return periods, but they lack the spatial resolution to capture narrower inland water bodies, particularly rivers (see Matthews (2011) and Hestir et al. (2015) for detailed discussion). The newest generation of sensors has been designed to overcome some of these issues (Tyler et al., 2016; Giardino et al., 2019a), though the limited precision of broad spectral bands remains a challenge. While they lack certain band centers useful for inland water remote sensing, new

sensors such as the Landsat 8 Operational Land Imager (OLI) and the Sentinel 2 MultiSpectral Instrument (MSI) have increased signal to noise ratios, improved radiometric and temporal resolution, and aerosol-specific bands making them better equipped to handle the size and complexity of inland waters (Concha and Schott, 2016; Pahlevan et al., 2017).

Regardless of sensor choice, among the largest barriers to remote sensing of inland waters is controlling for varying atmospheric effects. The signal to noise ratio of top-of-atmosphere radiance over waterbodies can vary substantially with different atmospheric water vapor and aerosol concentrations. In order to accurately estimate water quality parameters, the atmospheric effects need to be controlled for through precise atmospheric corrections (Brivio et al., 2001; IOCCG, 2018). These corrections are particularly important over large spatiotemporal domains because atmospheric conditions can vary significantly. Historic correction procedures are largely based on open ocean remote sensing and assume zero water leaving radiance beyond the visible spectrum (Gordon and Wang, 1994). This assumption does not hold over optically complex waters where chlorophyll, suspended sediment, and bottom reflectance lead to true non-zero radiance in the near infrared. The result is an overestimation of aerosol thickness and an overcorrection of visible wavelengths in turbid waters (Schroeder et al., 2007). Progress has been made improving atmospheric correction algorithms over complex waters through the use of radiative transfer functions (Schroeder et al., 2007), pseudo-invariant features (Concha and Schott, 2016), dark pixel extraction (Vanhellemont and Ruddick, 2018), and SWIR-based correction procedures (Wang et al., 2013; Novoa et al., 2017); however, many methods lack transferability between sensors making it difficult to compare surface reflectance products across platforms (Pahlevan et al., 2019). Atmospheric correction is further complicated by adjacency effects from surrounding land. Radiation reflected from relatively bright land is scattered by the atmosphere, increasing noise over adjacent, relatively dark waterbodies. Solving adjacency issues typically involves computationally expensive radiative transfer functions, though recent progress has been made using models that reduce computational

requirements by approximating atmospheric scattering within the correction procedure (Kiselev et al., 2015).

Independent atmospheric challenges are exacerbated by the dynamic nature of waterbodies themselves. Changing water conditions and bio-fouling of in situ sensors can make it difficult to capture coincident field and satellite observations necessary for model development (Garaba et al., 2014; Garaba and Zielinski, 2015). From a reflectance standpoint, algal mats, surface macrophytes, and sun glint (specular reflection of sunlight towards the sensor) all contribute extraneous signals to observed water-leaving radiance. The body of literature on these issues is significant, and processing schemes to isolate and/or remove these signals are continually improving. For sun glint, removal schemes can range from relatively simple empirical models such as those tested by Kutser et al. (2009b) to more complicated radiative transfer functions (Martin et al., 2016). For algal mats and floating macrophytes, semi-empirical threshold-based algorithms including the Floating Algal Index (Hu, 2009), Maximum-Peak Height (Matthews et al., 2012), and adaptations of classic NDWI indexes (Oyama et al., 2015) have all provided robust delineation of water from adjacent algal and macrophyte signals. Additionally, varying sediment types between regions can affect the relationship between reflectance and measurements of TSS (Novo et al., 1989). These variations can be partially accounted for using band ratio algorithms that are generalizable across sediment types (Doxaran et al., 2002a).

The above technical barriers represent legitimate challenges to extracting water quality constituents from dynamic inland systems. However, existing retrospectives on the past 50 years in the field indicate that technical barriers alone are not responsible for the slow progress towards applying remote sensing as a tool to better understand inland water systems. Bukata (2013) insightfully proposes that one explanation may be the relatively isolated nature of the field and the historic lack of collaboration with related ocean color remote sensing. This observation is supported by Downing (2014), who describes the fields of oceanography and

limnology as “twins, mostly separated since birth”. This lack of institutional communication has had ripple effects, reducing collaborative projects and limiting funding sources. Collaboration is further reduced through the inherent scale of the research. Technical challenges with spatiotemporally expansive studies generally constrain inland water research efforts to localized scales. This pattern contrasts with ocean remote sensing, where international study areas have led to numerous, well-funded, multinational research efforts (Palmer et al., 2015a). Communication and collaboration leading to these large research efforts is facilitated by international organizations like the International Ocean-Colour Coordinating Group (IOCCG). Recent work done by the IOCCG (IOCCG, 2018), as well as emerging groups like AquaWatch (https://www.geoaquawatch.org/), are working towards similar goals for inland water remote sensing researchers, but these efforts are still in their infancy compared to their ocean color counterparts. The nature of the field and its apparent lack of cohesion may, in part, stem from the fact that it is spread across many different disciplines. A Scopus search query of inland water quality remote sensing returns publications from over 350 distinct journals spread across hydrology, ecology, biogeochemistry, environmental management, and engineering, indicating that much of the research is spread across different niches and sub-disciplines. However, the following review of the literature indicates that efforts to overcome these technical and institutional barriers have made significant progress in improving inland water quality remote sensing efforts, particularly over the past decade. Below we highlight this progress through an analysis of how remote sensing of inland water quality has been used to answer challenging science questions. Additionally, we contextualize these recent advances within the literature and discuss how researchers are working towards further addressing them in the future (Section 7).

Section 5: Evolution of Inland Water Remote Sensing Publications

In order to analyze the progression of publications on remote sensing of inland water quality, we carried out two analyses: the first identifies general trends in publication patterns, while the second analyzes trends in modelling approaches and research focus.

Section 5.1: Overarching Trends in the Field of Inland Water Remote Sensing

General trends were identified through a bibliometric analysis of search results from the Elsevier Scopus database (conducted July 2018). Database titles, keywords, and abstracts were searched for the terms 'remote sensing', 'water quality', and either 'lake', 'reservoir', 'river', 'delta', 'estuary', or 'inland waters' (along with variants, i.e., 'lake' and 'lakes'). The search results returned 1,186 distinct articles published in peer-reviewed journals dating back to 1970 (Figure 1.1). Bibliometric data were extracted from the query using the Bibliometrix package in R (Aria and Cuccurullo, 2017).

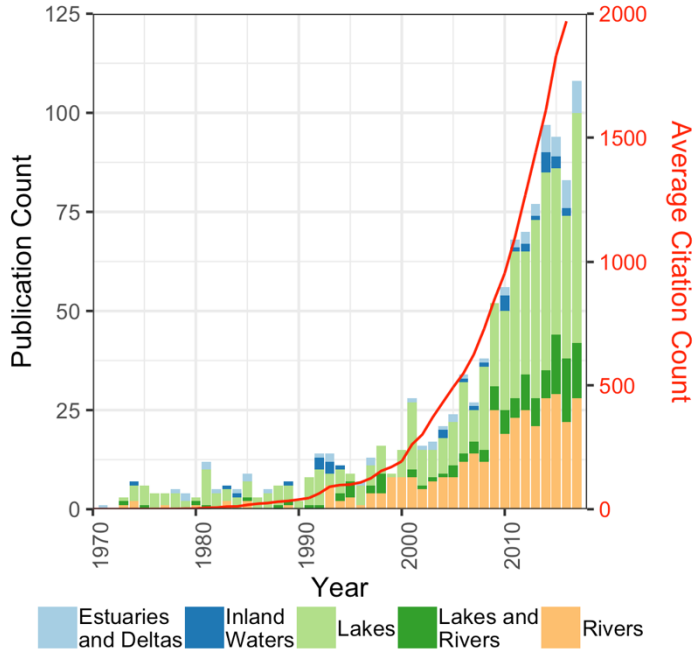

Figure 1.1. Published papers per year returned from Scopus search queries and grouped by search term. Average citation count is the sum of citations for all papers averaged over the number of years since their publication.

The results of the Scopus bibliometric analysis indicate that inland water quality remote sensing has been growing dramatically since its introduction in the 1970s. The annual average increase in publications over the study period is 8.9%, but examination of the trend indicates that it is best represented by a simple power law function (R^2 = 0.848), with a sharp increase in publications starting in the early 2000s. Power law functions allow for the calculation of a doubling time which represents the amount of time it takes a population to double in size

starting from any given timepoint. Bornmann and Mutz (2015) calculated the doubling time and average annual growth rate for total academic publishing between 1980 and 2012 to be approximately 23.7 years and 2.96% respectively. For the same period, remote sensing of inland water quality grew at three times that rate, with a doubling time and average annual growth rate of 8.3 years and 10.01% respectively. The most pronounced year-on-year jump occurs right after 2008, which corresponds to the public release of freely available Landsat imagery by NASA and the US Geological Survey. After removing the overall trend of the power law function, a t-test on the residuals for the 5 years before and after 2008 indicates a significant increase in publications for the period after Landsat was made public (95% CI = 0.3–0.7, p = 0.0016). This result is consistent with previous research showing that for multiple earth observation fields, the release of the Landsat archive resulted in more frequent and larger-scale studies (Wulder et al., 2012).

Further analysis of the bibliometric data shows that while contributions to the literature come from a diverse set of sources, there are a few distinct countries, journals, and authors that are disproportionately active within the field. Publications from the United States and China are responsible for 26.1% and 21.4% of the total publications respectively (Figure 1.2). Similarly, while there are contributions to the literature from 3362 authors or co-authors, publications that include the top ten most productive authors comprise 17% of the total search results (Table 1.1). The cumulative contribution of publications from the top ten journals comprise nearly one third of the entire search. Of the 378 publications from these top ten journals, 60% are from strictly remote sensing journals. When expanded out to the entire query, 18% of the returned journals include a remote sensing term in their title and account for 33% of all publications. This pattern is worth noting for two reasons. First, remote sensing journals are more likely to contain methods development papers. Secondly, it suggests that many publications are focused primarily on communicating advances within the remote sensing community, with perhaps less

outreach to hydrologists, ecologists, and other scientists not inherently focused on remote sensing.

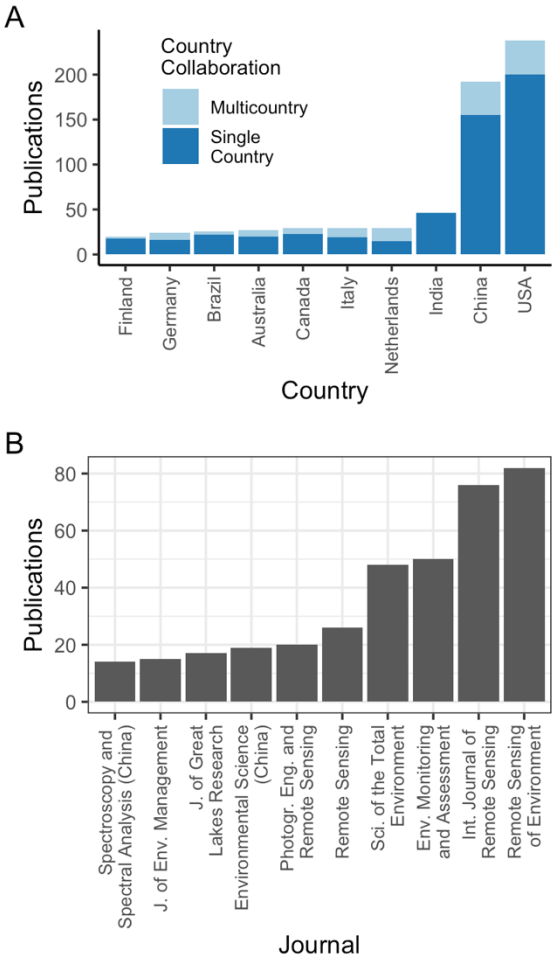

Figure 1.2. Distribution of publications returned from Scopus query for the top ten most productive countries (A) and top ten most published journals (B).

Table 1.1. Summary data from Scopus query for inland water quality remote sensing.

Scopus Query Summary	
Total Publications	1186
Distinct Journals	342
Distinct Keywords (Scopus)	7706
Distinct Keywords (Authors)	2447
Average citations per publication	16.6
Authorship Summary	
Distinct Authors	3,362
Authors per Documents	5.24
Contributions Summary	
Contribution from top 10 Countries	676 (54.8%)
Contribution from top 10 Authors	209 (16.9%)
Contribution from top 10 Journals	378 (30.6%)

Section 5.2: Detailed Analysis of Literature Patterns and Scale

In order to more deeply examine trends in remote sensing of water quality, we identified a subset of 236 papers within existing reviews (Matthews, 2011; Odermatt et al., 2012; Gholizadeh et al., 2016) and from keyword searches containing common inland water remote sensing terms (e.g., combinations of ‘remote sensing’, ‘lakes’, ‘rivers’, ‘chlorophyll’, ‘CDOM’, ‘TSS’, and ‘inland waters’) in relevant databases (Article+, Google Scholar, Scopus, and Web of Science). Papers were chosen based on a combination of their search relevance, citation count,

and subject focus. While we strived to be comprehensive in the inclusion of papers, some relevant studies were inevitably missed. We conducted more intensive journal-specific searches within high impact journals including Science, Nature, PNAS, WRR, Association for the Sciences of Limnology and Oceanography journals, and Ecological Society of America journals to ensure the inclusion of studies that utilized remote sensing but focused more on scientific application of remote sensing than on methods development. A significant and worthwhile body of work exists using remote sensing to study water quality in complex near coast ocean environments as well as the Laurentian Great Lakes (see reviews Liu et al. (2003), Matthews (2011), Odermatt et al. (2012), and Gholizadeh et al. (2016)). While critical to the development of inland water quality remote sensing methods, this body of work was excluded from this review in order to better focus on lake, river, and estuary remote sensing applications and how those applications have changed over time. Similarly, studies using strictly in situ reflectance were excluded because our focus was on remote sensing from satellites or airborne platforms. The final subset was read to analyze overarching trends in research focus and scale. Each of the resulting 236 papers was subsequently classified into one of the four categories outlined below.

1) Purely methodological: The purpose of the paper is to present and validate a new model or methodology. Results consist of model validation and error metrics. No figures depicting spatial or temporal patterns are present.
2) Methodological with pattern analysis: The paper is predominately methods development and validation but includes some figures applying the proposed model either spatially or temporally.
3) Trend/pattern analysis: The purpose of the paper is to examine spatiotemporal patterns and/or trends in water quality within the study area, with trends defined has having directionality over space or time. Model validation results are presented for transparency, but the bulk of the results and discussion focusses on either spatial or

temporal trend analysis. The preponderance of figures and tables depict maps, time-series, or other spatiotemporal analyses.

4) Water quality science research with a focus on impacts and drivers: The paper contains specific hypotheses and/or science questions to be directly addressed. Results and discussion focus on spatiotemporal dynamics of water quality as well as the drivers and/or impacts of changing water quality. The preponderance of figures and tables present within the paper depict either trends or relationships between the parameter of interest and associated drivers/impacts.

Key questions that determined the classification of the papers included:

1) Is there a specific hypothesis or science question addressed?
2) Is there any spatial or temporal analysis of patterns or trends in the study area?
3) Are the majority of the figures and tables focused on validating a proposed model, or are they examining trends, drivers, and impacts of inland water quality?

With regards to the third criterion, figures and tables within each paper were categorized into the four groups depending on whether they provided background information, model validation, or spatiotemporal analysis (details in Appendix A: Table S3). The final index (Appendix A) depicts a field of research that has evolved, particularly in the last decade, from almost universally methods-focused into one in which new methodologies, data products, and increased computing power are creating opportunities to address science questions related to water quality in novel ways.

The overall trend in the publication counts of the detailed dataset closely parallels the power-law trend in the broad Scopus query, including a comparable spike in publications after 2008. Similarly, 75% of the studies resulting from the various searches focus on lakes and lake related water quality parameters (Figure 1.3). Eutrophication-associated parameters (chlorophyll, clarity, and cyanobacteria) are almost entirely measured in lake systems. In

contrast, studies focusing on rivers, deltas, and estuaries are almost exclusively measuring sediment loading and transport parameters (TSS and turbidity).

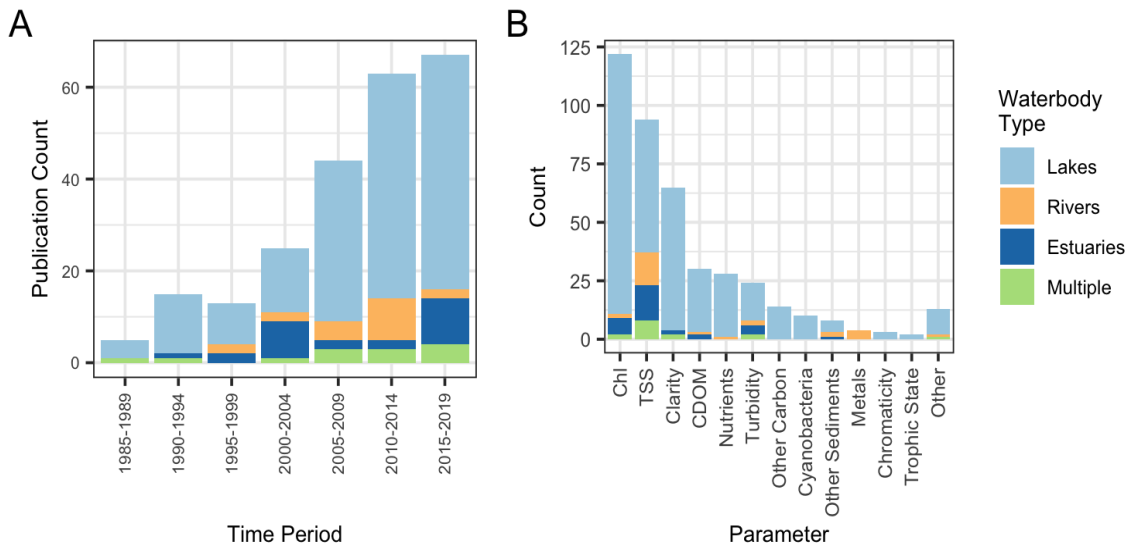

Figure 1.3. Publication counts within the detailed index binned by time (A) and water quality parameter of interest (B). Colors represent type of waterbody being researched.

In total, the included papers presented 411 models for constituent retrieval. Of these, only 70% reported some measure of goodness-of-fit or absolute error, and only 23% reported some measure of validation, with validation defined as an error metric derived from data not used in building the model. The most commonly reported metric was a coefficient of determination (R^2), with mean recorded values of 0.76 (σ = 0.184) for model fit and 0.79 (σ = 0.159) for model validation (Figure 1.4). Simple linear regression of R^2 values over time indicate that model fit has decreased (p = 0.011) and model validation has shown no significant trend (p = 0.633). However, more recent models frequently cover larger spatiotemporal domains and represent more difficult constituent retrieval, possibly leading to reduced model fit. While R^2 values are not the most robust stand-alone metric of model performance (Willmott, 1981), comparisons utilizing other common metrics are difficult due to the lack of standardization between reported metrics within the reviewed publications. In total, over 35 different error metrics were identified within the literature. Many of these represent differences in terminology

as opposed to the actual statistical measure. For example, root mean square error (RMSE) is referred to in nine different ways in total, with variations both in terminology (e.g., root mean square error and root mean square deviation) and metric transformation (e.g., percent, normalized, relative, and log values). Similar ranges of variation occur for mean/median absolute error (MAE), standard error (SE), relative error (RE), and bias. This disparity in reporting measures makes it difficult to accurately compare model error across studies without significant burden on the reader. However, examination of the most common metric, R^2, suggests consistently strong model fits dating back to the 1970s (Figure 1.4). These results suggest that the potential has long existed for remote sensing to contribute to addressing scientific questions related to water quality. The reasons for the lag between methods development and scientific application remain uncertain. Two possible explanations are that the empirical models that dominate early literature were too site-specific to be useful at larger scales, or that perceptions of the usefulness of remote sensing in water quality research differed between the remote sensing community and fields like hydrology, limnology, and ecology.

Figure 1.4. Reported R^2 values for model fit and model validation along with linear regressions of R^2 over time.

Trends in modelling approach indicate a fairly static field up until the early 1990s, with empirical modelling approaches comprising 50%–80% of all publications for nearly 20 years (Figure 1.5). The mid-2000s show an increase in publications employing machine learning models and pre-produced satellite products. The emergence and subsequent decline of

product-based studies from 2008–2015 likely corresponds to the launch of the Medium Resolution Imaging Spectrometer (MERIS) in 2002 and its decommission in 2012. MERIS presented a unique step towards global products through the development of the BEAM processing toolbox (Brockman Consult in collaboration with the European Space Agency), which utilizes a neural network scheme to simultaneously conduct atmospheric correction and water quality estimates. BEAM provided ready-made water quality products to inland water and ocean researchers alike, though validation of the products was regionally inconsistent (Alikas and Reinart, 2008; Okullo et al., 2011; Kallio et al., 2015).

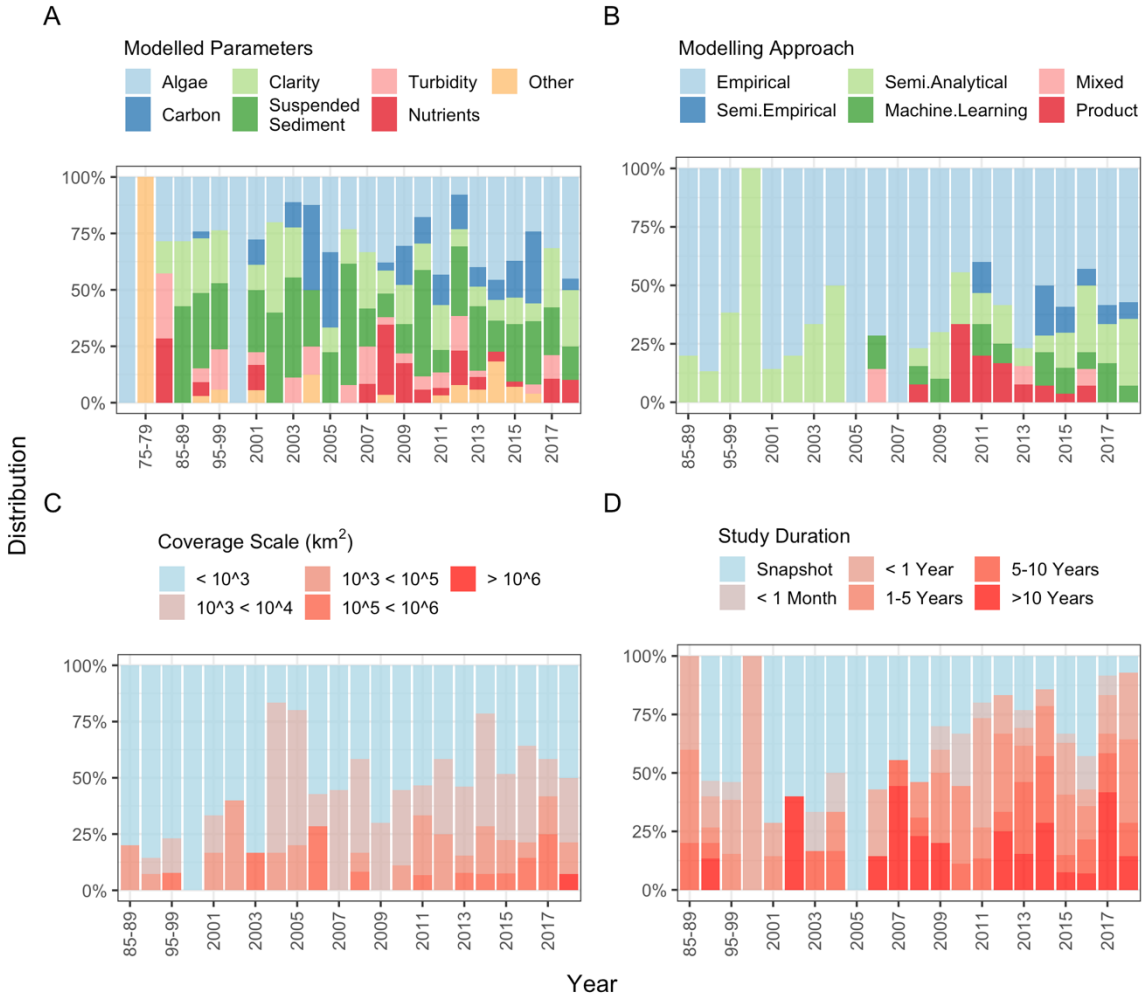

Figure 1.5. Temporal distributions of modelled parameters (A), modelling approach (B), study spatial scale (C), and study temporal scale (D). Results for 1975–1999 are reported in five-year windows due to the relatively small number of studies published during this time period.

The development of BEAM's neural network scheme and the rise in machine learning approaches starting around 2000 is likely attributable to increased computational capabilities and a proliferation of specialized software in common programming environments like R and Python. For the former, packages like Rpart (Therneau and Atkinson, 2019), originally released in 1999, and nnet (Venables and Ripley, 2002) created previously unavailable access to decision tree and neural network modelling approaches. For Python, software development throughout the 2000s led to comprehensive machine learning libraries such as Scikit-learn (Pedregosa et al., 2011), which provided both access to common machine learning algorithms and a framework for their calibration and validation. These machine learning tools, among others, emerged in part due to an increased need for open source software that promoted study replicability, researcher access, and collaborative code development for machine learning researchers across fields (Sonnenburg et al., 2007).

The emergence of machine learning approaches in remote sensing of inland waters is paralleled by an increase in semi-empirical models. Initially, this late appearance of semi-empirical models appears unintuitive since they are computationally inexpensive and closely parallel older terrestrial indexes like NDVI; however, their emergence is likely explained by a proliferation of data from ocean color sensors such as SeaWiFs (launched 1997), MODIS Terra and Aqua (1999 and 2002 respectively), and MERIS (2002). With MERIS specifically, its high spectral resolution and chlorophyll-specific band centers allowed for better detection of absorption features and backscatter peaks that facilitate semi-empirical models (Gower et al., 1999). However, due to their coarse spatial resolution, these studies are mostly limited to larger lakes. These sensors were subsequently joined by the hyperspectral sensor Hyperion in 2000, which created new opportunities for semi-analytical water constituent retrieval (Brando and Dekker, 2003).

The temporal trends described above show distinct spatial patterns with an overall dominance of studies located in the U.S., Europe, and China (Figure 1.6). China and the U.S.,

respectively, comprise 20% and 24% of the total studies included, with a notable clustering of long-term, large-scale studies in the Yangtze Basin. Spatiotemporal trends in publication dates depict a temporal expansion outward, with the earliest studies located almost exclusively in the U.S and subsequent publications spreading out across the globe. However, it should be noted that this trend may be partially attributable to a language bias in early publications where there is less access to non-English papers.

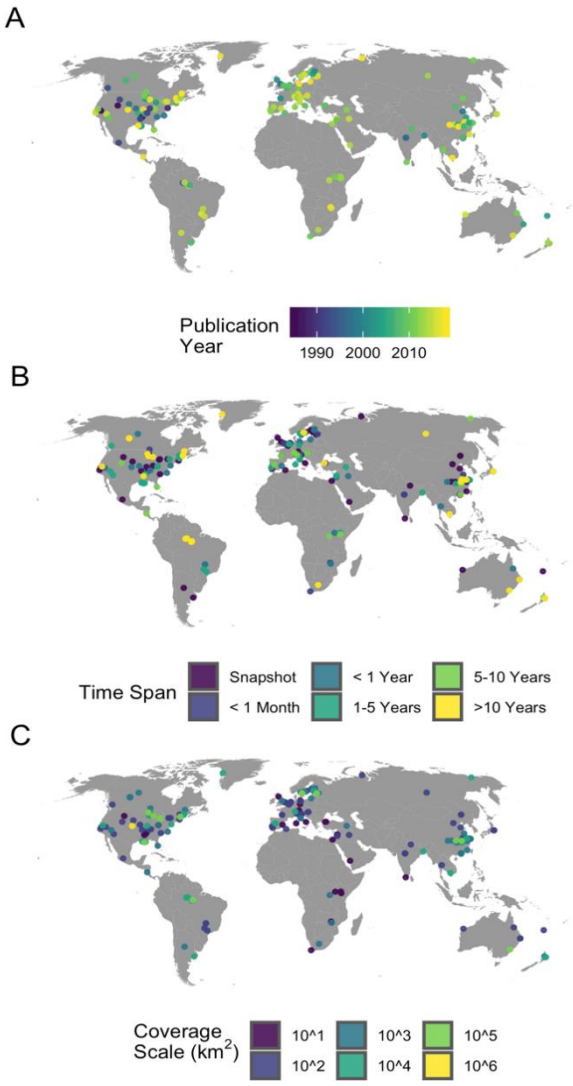

Figure 1.6. Spatial distribution of study publication date (A), timespan (B), and spatial scale (C).

Section 6: From Methods to Applications: An Overview of Inland Water Remote Sensing

The study of water quality in lakes, rivers, and estuaries using remote sensing has expanded substantially over the past 50 years. When considering the *intent* of the publications

as opposed to just the number, it is apparent that only in the past 10–15 years has inland water remote sensing consistently been used as a powerful analytical tool informing the broader inland water literature. In the papers reviewed for this analysis, twice as many studies were published in the past ten years as in the previous 28 years combined, a rate much faster than the growth of academic publishing as a whole. Of papers published since 2008, nearly 30% focus on examining drivers and impacts of water quality, compared to only 7% for the period prior (Figure 1.7).

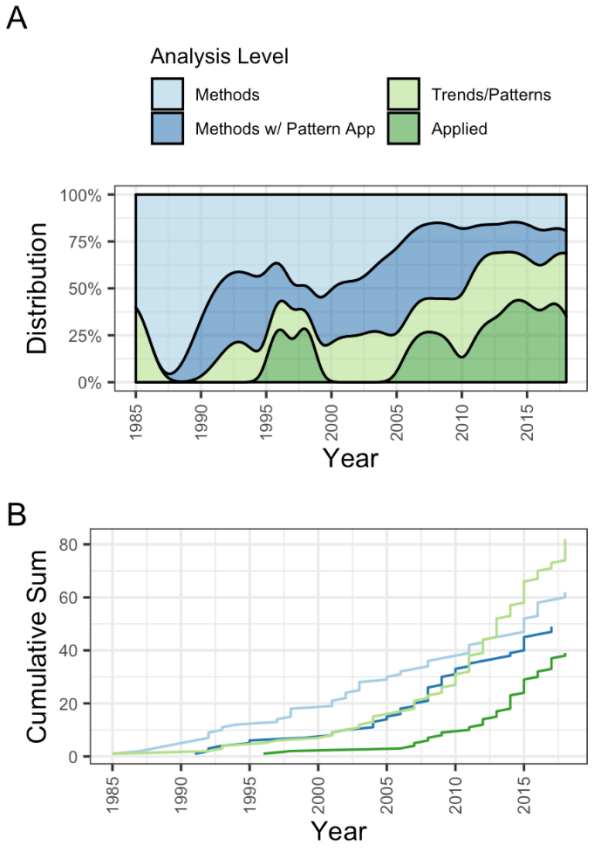

Figure 1.7. Distribution of publication focus through time (A). Cumulative sum totals (B) for methods categories (n = 113; 49%), trend/pattern papers (n = 81; 35%), and water quality science papers (n = 38; 16%) show decreasing dominance of methods over time.

Studies are also expanding into longer time-frames and over larger spatial scales (Figure 1.5). Pre-2008, the average study covered tens of square kilometers over a 2 year period. Post-2008, the average study examines hundreds of square kilometers over a period of 5 years. This expansion requires the caveat that study scale is used as a proxy for the number

of distinct lakes, and some of the increase in study scale may result from an increase in the average lake size rather than the total number of optically unique waterbodies. Similarly, longer-term studies largely focus on simpler metrics such as water clarity and TSS, in part due to ongoing challenges modelling the more complex spectral signatures of chl-a and CDOM. Satellites like Landsat provide long time series of observations but lack the radiometric and spectral resolution to model more complex parameters. Pearson's Correlation Coefficients (Pearson, 1896) were calculated to identify relationships between study scale, duration, publishing date, and category. The category variable was converted to a numeric (1–4) in order of level of analysis (1, methods development; 2, methods with pattern analysis; 3, trend/pattern analysis; 4, water quality science). While the categorical classification of the included papers is partially subjective, their correlations with other study parameters are still included to provide insight into how the scientific application of publications has changed with study scale and duration. The resulting correlation matrix (Table 1.2) depicts a clear pattern between study scale and impact over time. All four of the included variables were positively correlated at a 99% significance level (with the exception of study category and scale, $p = 0.014$). While none of the correlations are particularly strong, their significance and consistency indicate that studies published later tend to cover larger spatiotemporal domains and focus more on analyzing water quality dynamics and impacts than on methods development.

Table 1.2. Correlation matrix of key study parameters. All correlations are significant at a 99% confidence interval (***). Study category rescaled to 1–4, representing the four levels of analysis from purely methodological to water quality science papers.

	Pub. Year	Study Duration	Study Scale	Study Category
Pub. Year	1	0.171	0.255	0.342
Study Duration	***	1	0.326	0.32
Study Scale	***	***	1	0.173
Study Category	***	***	***	1

This shift in study focus, scale, and duration all suggest that remote sensing is becoming a useful tool in understanding inland water quality rather than an area for methodological study among remote sensing specialists. Publications representative of this shift towards hypothesis-driven science vary significantly in their focus, with emphasis on hydrological processes, drivers of water quality, public hazard identification, and impacts of degraded water quality (Appendix A: Table S4).

Studies examining drivers of water quality at local to regional scales comprise the largest group of water quality science publications. Recent work has examined climatic, anthropogenic, and landscape-scale variables that interact with complex biogeophysical water quality properties. Work by Lymburner et al. (2016) presents a 30 year analysis of TSS in Australian lakes, showing distinct relationships between El Niño Southern Oscillations and fluctuations in TSS levels. Olmanson et al. (2008, 2014), examined a 20 year record of remotely sensed water clarity for over 10,000 lakes in Minnesota. Their results showed significant differences in overall trends based on land use and eco-region. Ng et al. (2011) and Curtarelli et al. (2015) both incorporated remotely sensed chl-a data into hydrologic models and found that thermal stratification and mixing were key drivers of algal bloom growth and dispersion. Work done by Rose et al. (2017) showed that controls on water clarity move from local to watershed scales during dry and wet years respectively. Other studies focusing on climatic drivers of water quality have used remote sensing to analyze the impacts of hurricanes (Wang et al., 2012), typhoons (Zhu et al., 2014), and growing season length (Sass et al., 2008a) on various water quality metrics.

Studies focusing on anthropogenic drivers have brought to light the impacts of human activities on freshwater resources for areas ranging from individual lakes to entire states. Work by Cui et al. (2009, 2013) examined the combined effects of precipitation, river flows, and dredging on TSS levels in Poyang Lake in China. They found that the combined precipitation and anthropogenic impacts degraded water quality far more than either individual driver could

on its own. At a basin scale, Ren et al. (2018) and Hou et al. (2017) conducted studies examining how the Three Gorges Reservoir affected water clarity and TSS dynamics in the Yangtze Basin. In the Peace-Athabasca Delta, Pavelsky and Smith (2009) and Long and Pavelsky (2013) utilized multi-temporal images of sediment loads to calculate river velocity and recharge for floodplain lakes.

Studies using remote sensing of water quality to address scientific questions extend beyond the field of hydrology and into biology and public health. Sandström et al. (2016) utilized remotely sensed CDOM and chl-a concentrations to analyze fish habitat assemblages and biodiversity. For public health, inland water remote sensing is helping to analyze disease distribution and drinking water hazards. Fichot et al. (2016) identified spatial patterns of methylmercury in the San Francisco Bay area using an airplane mounted hyperspectral sensor. Qin et al. (2015) developed a dynamic forecasting model capable of predicting the presence of toxic algal blooms. The model ultimately resulted in over one million tons of algal scum being removed from a drinking water reservoir in China (Qin et al., 2015). Other authors have similarly identified public threats to drinking water in Lake Mead (USA) (Imen et al., 2015) and Lake Chaohu in China (Duan et al., 2017). Two specific studies stood out through their novel use of remote sensing to facilitate epidemiological studies. Torbick et al. (2014) incorporated Landsat-derived water quality parameters into an eco-epidemiological model to examine the distribution of amyotrophic lateral sclerosis (ALS) across New England. They found that close proximity to waterbodies with elevated levels of nitrogen increased the odds of being located within an ALS hotspot by 167%. Similarly, Finger et al. (2014) incorporated remotely sensed chl-a measurements into a model of cholera dynamics within the Democratic Republic of Congo.

One additional subset of the reviewed literature merits discussion when considering advances in the field; specifically, researchers who are continuing to expand the spatiotemporal scale of their study areas. The need for global data products has received increasing attention in recent years as an essential aspect to protecting threatened freshwater resources (Malthus et

al., 2012; Hestir et al., 2015; Lee et al., 2018). Within the U.S., work towards this goal includes state-wide analyzes of Secchi Disk depth in Minnesota (Olmanson et al., 2008, 2014) and Maine (McCullough et al., 2013), and a national approach to modelling lake chl-a (Lin et al., 2018). Outside the U.S., previously mentioned work by Lymberner et al. (2016) in Australian lakes and Hou et al. (2017) in the Yangtze basin both cover areas of tens of thousands of square kilometers, albeit without including every lake in the study region. At a global level, Ho et al. (2019) recently analyzed the prevalence of harmful algal blooms in 71 lakes over the span of three decades, further increasing the spatiotemporal domain of inland water remote sensing.

Publications like those mentioned above are complemented by a host of living databases and interactive web services that are increasing access to near real-time water quality information. The Copernicus Inland Water Service provides semi-continuous (2002–2012, 2016-present) turbidity and chl-a observations for approximately 1000 of the world's largest lakes (https://land.copernicus.eu/global/products/lwq). Similarly, the Minnesota LakeBrowser provides periodic measurements of chl-a, CDOM, and water clarity dating back to 2002 for over 10,000 lakes across the state (https://lakes.rs.umn.edu/). These publicly available databases are being supplemented by private companies like EOMAP (https://www.eomap.com/) which provide remotely sensed estimates of water quality parameters on a contract basis around the globe. While validation of some of these products is difficult to obtain, they are facilitating increased access to water quality data for water managers and researchers alike. Improvements in modeling methodologies and growing access to both in situ and earth observation data are setting the stage for future studies at larger and larger scales.

Section 7: Emerging Trends in the Remote Sensing of Water Quality

The past decade has seen a dramatic growth in the resources necessary to remotely sense inland water quality. One example highlighted here is the 2008 shift to open access Landsat data—after which, publication counts rose and study scale and duration increased significantly. However, the Landsat archive is only one of numerous petabyte-size archives of

earth observation data provided by government agencies such as NASA, the USGS, NOAA, and the European Space Agency. These archives are constantly expanding and will continue to do so in the coming years. Starting in 2010, access to these data sources further increased with the release of the Google Earth Engine platform, which hosts imagery and resulting data products from over a dozen different earth observation sensors. The platform provides free access to these datasets along with cloud-based processing, dramatically increasing the computational power of remote sensing researchers across fields. For inland water remote sensing, Lin et al. (2018) combined in situ data from the 2007 National Lake Assessment (N = 1,157 lakes) with Landsat data and machine learning algorithms built into Google Earth Engine to develop a well-validated national model for lake chl-a (RMSE = 34.9 µg/L). Similarly, Overeem et al. (2017) used Google Earth Engine to model sediment export from Greenland over 14 years. Today, the platform continues to grow and increase in usefulness, adding approximately 6,000 scenes daily from various active satellite missions, with a latency of approximately 24 h (Gorelick et al., 2017). The power of Google Earth Engine essentially provides researchers with supercomputing capabilities from their local machines, dramatically increasing the scales at which earth observation research can take place. Platforms like Google Earth Engine are complimented by an ever-growing body of processing and analysis software in common programming languages like R (Fox, 2009).

While the provision of open-access satellite imagery to researchers is essential to the progression of the field, it alone cannot account for the shift in research focus and scale outlined above. Paralleling the rise in remote sensing data availability over the past decade has been a rise in the in situ data available for model calibration and validation. In the past, the burden of collecting this data frequently fell on individual researchers, significantly limiting the amount of field data available. Recent databases provided by government agencies, NGOs, and researchers alike are providing a wealth of freely available in situ data that are easily accessible. At a global level, the GEMStat database maintained through the International Centre

for Water Resources and Global Change, provides over 4 million observations of lakes, rivers, wetlands, and groundwater systems from 4000 sites spread over 75 countries (https://gemstat.org/). In the U.S., The National Water Quality Portal (WQP), released in 2012 by the USGS, EPA, and National Water Quality Monitoring Network, provides national coverage of archived state, federal, and tribal water quality field measurements. In total it assimilates and standardizes monitoring data for over 2 million individual sampling sites (Read et al., 2017). The Lake Multi-Scaled Geospatial and Temporal Database (LAGOS-NE) provides a similar assimilation of in situ water quality measurements for 17 water-rich states in the upper Midwest and Northeast United States, providing historical field data for over 51,000 lakes and reservoirs (Soranno et al., 2017). These datasets have already been used as calibration and validation data for remote sensing of water skin temperature (Schaeffer et al., 2018). In Europe, national-scale water quality data for inland and coastal waters are compiled from participating agencies into the Waterbase dataset, which is harmonized and made research ready under the WISE system (water information system for Europe) (Srebotnjak et al., 2012). These official data sources can be supplemented with novel collections aggregated through citizen science campaigns. These include Eye On Water (http://www.eyeonwater.org/) and Seen-monitoring (http://www.seen-transparent.de/) in Europe, the Secchi-Dip In in North America (http://www.secchidipin.org/), and state level efforts in Minnesota, Wisconsin, Michigan, and Maine (https://www.pca.state.mn.us/water/citizen-water-monitoring, https://www.uwsp.edu/cnr-ap/UWEXLakes/Pages/programs/clmn/default.aspx, https://micorps.net/lake-monitoring/, and https://www.lakestewardsofmaine.org/ respectively). Together these campaigns have collected hundreds of thousands of observations available to researchers. The new AquaSat database from (Ross et al., 2019) uses Google Earth Engine to extract coincident (+/− 1 day) Landsat reflectance values for in situ measurements found in the WQP and LAGOS-NE. The result is the first dataset of its kind, providing over 500,000 paired observations of reflectance values and associated water quality parameters in optically complex waters dating back to 1984. Databases

such as these provide data continuity, cost and time savings for researchers, and large calibration and validation samples for model development.

The development and expansion of new and existing databases is paralleled by the development of new sensor technology. Airborne hyperspectral sensors capable of capturing contiguous spectral signatures of water-leaving radiance have provided new levels of precision to measure optically active constituents (see reviews by Govender et al. (2007), Gholizadeh et al. (2016)). These airborne campaigns are working towards satellite missions such as NASA's Surface Biology and Geology mission (SBG, in development), Italy's PRecursore IperSpettrale della Missione Applicativa (PRISMA, launched 22 March 2019), Japan's Hyperspectral Imaging Suite (HISUI, planned 2019), and Germany's Environmental Mapping and Analysis Program (EnMAP, planned 2020) (Kneubühler and Damm-Reiser, 2018). These spaceborne imaging spectrometers will increase spatiotemporal transferability of retrieval models, improve overall constituent retrieval, facilitate biogeochemical composition analysis, enable benthic habitat identification in optically shallow water bodies, and allow for the retrieval of additional detectable water quality parameters that are currently unfeasible with broadband, multispectral sensors, all while providing global hyperspectral data at roughly 30 m resolution (Hestir et al., 2015; Giardino et al., 2019a). Traditional governmental satellite missions are being supplemented with a host of novel earth observation technologies being developed by commercial companies such as Planet (https://www.planet.com/), MAXAR (https://www.maxar.com/), and Airbus (https://www.airbus.com/). These private platforms are creating novel opportunities for hydrological remote sensing through public and academic research partnerships. For example, Planet, which operates over 150 small imaging satellites that provide daily global imagery at 3–5 m resolution, collaborated with Cooley et al. (2017) to study lake connectivity in the Yukon Flats region of Alaska at previously unfeasible spatial scales. For inland water quality, the high spatial and temporal resolution of such satellite constellations will allow for detection of short-term phenomena like algal blooms in streams and lakes that are currently too small to study with

publicly available satellite imagery. These efforts to improve research in small aquatic systems are being further aided by the increased use of unmanned aerial vehicles and even smartphones (McCabe et al., 2017).

These emerging technologies will allow the inland water quality remote sensing community to overcome historic challenges and examine new science questions. However, this process will require dedicated researchers and reliable funding sources. While emerging technologies hold promise, they also present new challenges. Hyperion, the first spaceborne hyperspectral sensor believed to be appropriate for inland waters, showed initial promise (Brando and Dekker, 2003) but ultimately proved unreliable over waterbodies due to its low signal to noise ratio and radiometric instability (Devred et al., 2013). The Planet constellation of CubeSats, while providing unprecedented spatial and temporal resolution, are subject to geolocation accuracy errors and inconsistencies in radiometric calibration between satellites (Cooley et al., 2017). These issues are in addition to well-characterized challenges including robust atmospheric correction and solving adjacency effects, both of which need to be applied across sensors to create comparable datasets. Solutions to these existing challenges will likely be developed through improvements in sensor engineering, computational capacity, and modelling approaches, as well as growing collaborative efforts by international groups such as IOCCG (IOCCG, 2008, 2018) and the Committee on Earth Observation Satellites (CEOS, 2018). As existing issues are overcome, remote sensing of inland water quality can be applied to address relevant scientific questions and conservation goals, including those outlined in the National Research Council Decadal Survey (National Academies of Sciences, 2018) and the EU Water Framework Directive (Poikane et al., 2011). Conducting such research will help solve water quality issues of global importance and better inform water managers, policy makers, and the scientific community regarding critical science questions. Some of the most pressing questions synthesized from the reviewed literature include:

- How does biogeochemical cycling of suspended sediments and CDOM in lakes and rivers contribute to the global carbon cycle?
- How are added nutrient inputs and warming air temperatures contributing to the frequency and distribution of harmful algal blooms in lakes and reservoirs?
- What is the impact of anthropogenic development, including urbanization and reservoir construction, on basin-wide water quality?
- What are the patterns and trends in the biogeochemistry of water resources in remote, vulnerable areas including the arctic and boreal regions?
- How are changes in water quality affecting the biological structure of freshwater resources at regional to global scales?
- How are changing water quality dynamics impacting important drinking water resources?

Section 8: Conclusions

The bibliometric analysis presented here highlights the dramatic growth of inland water quality remote sensing studies, far outpacing the average rate of increase in academic publishing as a whole. The past 50 years have produced hundreds of remote sensing publications accurately estimating biogeochemical water quality parameters; however, the majority of these focus on methods development rather than using remote sensing as a tool to better understand inland water quality dynamics. Detailed examination of 236 of the most relevant publications returned by search queries indicates that the past 10–15 years has brought about a focal shift within the field, where researchers are moving beyond methods development towards research focused on spatiotemporally explicit water quality dynamics. This shift is partially attributable to the development of new satellite and in situ datasets, improved access to satellite imagery, and increased computational/software capabilities. The current change in focus within the field is similar in nature to the shift that occurred in ocean

color and terrestrial remote sensing throughout the 1980s and 1990s—after which, both fields applied remote sensing to answer some of the most pressing science questions of their time. For inland water quality, the progression of research is evidenced by a subset of recent publications which have begun to leverage remote sensing to examine water quality trends, ecological and anthropogenic drivers, and resulting impacts of changing water quality on ecosystem function and water resources. This shift has been accompanied by a significant increase in the spatiotemporal scale of analysis, moving the field closer to providing national to global-scale data products for policy makers, water managers, and scientists. The increase in high quality science and study scale within the field continues to be facilitated by improved datasets and growing computational capacity. New data products like AquaSat (Ross et al., 2019) promise to continue this trajectory of growth and facilitate a new generation of inland water remote sensing research.

Based on the literature reviewed here, future inland water quality remote sensing work will benefit greatly from the following recommendations:

- Continued development of generalizable constituent retrieval models, including atmospheric corrections, that are applicable across large spatiotemporal domains and across differing sensors.
- The expanded application of robust, generalizable models to better understand global processes including erosion and deposition, terrestrial carbon and nutrient cycling, and trends in algal bloom dynamics in inland waters.
- Improved communication between experts in remote sensing and scientists in fields such as hydrology, limnology, and ecology in order to facilitate the wider adoption of remote sensing models in scientific studies of water quality.

- The development of user-friendly tools that inform local water managers of remotely sensed changes in water quality to promote sound policy and the conservation of essential freshwater resources.

Chapter 2: Artificial lake expansion amplifies mercury pollution from gold mining[2]

Section 1: Introduction

Section 1.1: Summary

Artisanal and small-scale gold mining (ASGM) is the largest global source of anthropogenic mercury emissions. However, little is known about how effectively mercury released from ASGM is converted into the bioavailable form of methylmercury in ASGM-altered landscapes. Through examination of ASGM-impacted river basins in Peru, we show that lake area in heavily mined watersheds has increased by 670% between 1985 and 2018, and that lakes in this area convert mercury into methylmercury at net rates 5-7 times greater than rivers. These results suggest that synergistic increases in lake area and mercury loading associated with ASGM are significantly increasing exposure risk for people and wildlife. Similarly dramatic increases in lake area in other ASGM hotspots suggest that 'hydroscape' (hydrological landscape) alteration is an important and previously unrecognized component of mercury risk from ASGM.

Section 1.2: Background

Informal – mostly illegal – artisanal and small-scale gold mining (ASGM) is the primary contributor to global atmospheric mercury (Hg) pollution (UNEP, 2018) and an important driver of deforestation (Asner et al., 2013; Asner and Tupayachi, 2017; Espejo et al., 2018), sediment loading (Lobo et al., 2016; Dethier et al., 2019), and biodiversity loss (Mol and Ouboter, 2004;

[2] This chapter previously appeared as a joint first-author article with Jacqueline Gerson in *Science Advances*. The original citation is as follows: Gerson, J. R*., Topp, S. N.*, Vega, C. M., Gardner, J. R., Yang, X., Fernandez, L. E., Bernhardt, E. S., & Pavelsky, T. M. (2020). Artificial lake expansion amplifies mercury pollution from gold mining. Science Advances, 6(48), eabd4953. https://doi.org/10.1126/sciadv.abd4953. *Indicates equal contributions to first authorship

Alvarez-Berríos et al., 2016; Markham and Sangermano, 2018) across the Global South. Simultaneously, ASGM provides livelihoods for tens of millions of people (Veiga et al., 2006) across over 70 countries worldwide (Telmer and Veiga, 2009). Within the Madre de Dios region of the Peruvian Amazon – a global biodiversity hotspot and home to numerous indigenous communities – ASGM has been responsible for the deforestation of nearly 14% (~95,000 ha) of the landscape between 1984-2017 (Espejo et al., 2018) and is estimated to release approximately 180 tons of Hg annually, according to a recent report by the Artisanal Gold Council (Cardo and Vargas, 2017).

During ASGM, gold-laden sediments from rivers, oxbow lakes, and floodplains are processed through a combination of sluicing and settlement ponds in which elemental Hg is added to isolate the gold. The Hg within this Hg-gold amalgam is then burned off and released into the atmosphere, while Hg-enriched tailings are dumped into nearby aquatic ecosystems. Once methylated by microbes, predominantly under anoxic conditions, methylmercury (MeHg) bioaccumulates and biomagnifies across the food web (Driscoll et al., 2013), leading to neurotoxic impacts in terrestrial and aquatic biota (Scheuhammer et al., 2007; Eagles-Smith et al., 2018) and people (Ha et al., 2017). In addition to deforestation and Hg loading, ASGM alters the landscape by creating thousands of small mining ponds (Figure 2.1), which in turn can cause site-specific externalities, such as increased malaria transmission (Sanchez et al., 2017; Ferring and Hausermann, 2019) and contamination of agricultural land (Bose-O'Reilly et al., 2016). The size and connectivity of these ponds vary, but their presence is ubiquitous and has implications for the processing and bioavailability of Hg.

In this study, we sought to understand how ASGM changes the extent of lotic (riverine) and lentic (lake) environments and how Hg loading and net methylation differ across these environments. We analyzed remote sensing data of the Madre de Dios region over the past 34 years to quantify changing areas of lotic and lentic systems and understand how mining alters the landscape to create environments suitable for Hg methylation. We also collected unfiltered

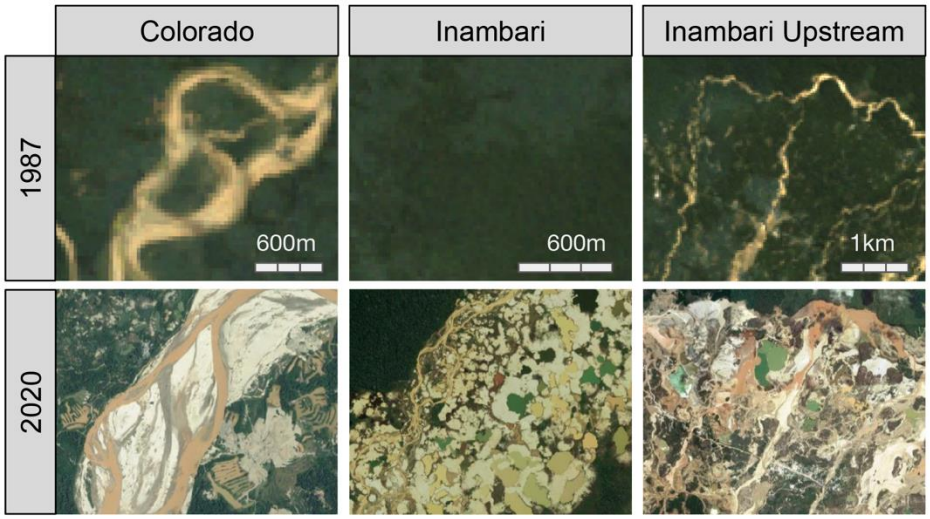

Figure 2.1: Comparison of historical (1987; Landsat) and current (2020; Google Earth from Maxar, Airbus, and CNES) landcover for mining-impacted locations. Locations along the Colorado River (left), adjacent to the Inambari River (middle), and in the Inambari headwaters (right) show the proliferation of mining ponds and deforestation. Specific locations can be seen in Appendix B: Figure S1. Top and bottom panels cover the same spatial extent. Note that in 1987, the Inambari area shown contained 100% forest cover

water (representing the summation of the dissolved and suspended fractions) and bulk sediment samples from a 200-km reach of the Madre de Dios River, its tributaries, and surrounding oxbow lakes and mining ponds. Sampling occurred in areas both upstream and downstream of ASGM activity to test its impact on the transport and fate of Hg. In each sample, we measured concentrations of total Hg and MeHg. We use MeHg concentrations as indicative of net Hg methylation, which represents both methylation and demethylation processes. Of the eight watersheds included in the study, mining operations have largely occurred in the Colorado and Inambari watersheds (Asner et al., 2013; Espejo et al., 2018). Three watersheds are located downstream of these two heavily mined watersheds (Co. - In West, Co. - In. East, and In. - Puerto), and three watersheds are located upstream (Upstream Manu, Reserve, and Manu - Co; Figure 2.2).

Section 2: Materials and Methods

Section 2.1: Sample Collection

All samples for Hg analysis were collected in July and August 2019 during the dry season (Appendix B: Figure S1). River samples were collected from the Madre de Dios River mainstem, upstream of a river confluence, downstream of a confluence, and from each tributary. One water sample was taken from near the water surface at each sampling point after the boat motor had been off for at least one minute. For oxbow lakes and mining ponds, one water sample was taken from the water surface. Water samples were collected using the clean hands-dirty hands protocol (EPA Method 1669) in new polyethylene terephthalate copolyester glycol (PETG) bottles and acidified to 0.4% with trace grade hydrochloric acid (HCl) within 24 hours of collection. Water samples were stored on ice in the field and then stored at 4°C until analysis. Note that all water samples are unfiltered, and all Hg values reported represent the concentration for the total water column. River sediment samples were collected underwater from the channel margins by compositing surficial sediment from at least five sampling points along a 30-meter transect using a shovel. These samples were taken during the dry season; during the wet season, the sampling locations are closer to the center of the channel since the width of the river increases by tens of meters. We therefore assume that the river sediment samples we collected are representative of well-mixed fluvial sediments. Oxbow lake and mining pond sediments were collected as channel margin sediment using a shovel (collected underwater as surficial sediment) and from three points in the center of the lake using an Eckman grab sampler. Sediment samples were collected using the clean hands-dirty hands protocol, double-bagged, frozen on dry ice in the field, and stored frozen until sample processing. Note that mining ponds were sampled in the La Pampa region, a watershed located adjacent to the Colorado watershed. La Pampa is an area that, until recently, contained widespread ASGM. It has been under military control since February 2019 (Operacion Mercurio) making it a safe area for field sampling. Due to logistical and safety concerns stemming from a

lack of police or military presence, it was not possible to sample mining ponds from the other actively mined watersheds examined in this study; however, mining practices in La Pampa are representative of those in the region.

Water samples for TSS were collected immediately after collecting water samples for Hg analysis. Water from just below the surface was pumped through a drill-operated pump with in-line glass fiber filter (pre-weighed), and the amount of water filtered was recorded. The filter was stored frozen until sample processing. A filter field blank was also taken and frozen for analysis.

Section 2.2 Laboratory Analyses

Unfiltered water samples were analyzed for total Hg via oxidation with bromine chloride for a minimum of 24 hours, purge and trap, cold vapor atomic fluorescence spectroscopy (CVAFS), and gas chromatographic (GC) separation (EPA Method 1631, revision E) on a Tekran 2600 Automated Total Mercury Analyzer. Calibration and continuous calibration verification (CCV) were performed using Brooks Rand Instruments Total Mercury Standard (1.0 ng/L) and initial calibration verification (ICV) was performed using SPEX Centriprep Inductively Coupled Plasma Mass Spectrometry (ICP-MS) Multi-Element in Solution Standard 2A. Instrument detection limit was 0.5 ng/L. All standards had average recoveries within 10% of the accepted values. The field blank, digestion blanks, and analysis blanks were below detection limit (BDL).

After lyophilization for at least five days, sediment samples were analyzed for total Hg on a Milestone Direct Mercury Analyzer (DMA-80) via thermal decomposition, catalytic reduction, amalgamation, desorption, and atomic absorption spectroscopy (EPA Method 7473). Calibration of the DMA-80 was performed using Brooks Rand Instruments Total Mercury Standard (1.0 ng/L). CCV and matrix spike (MS) were performed using NIST standard reference material 1633c (coal fly ash, 1005 ng/g), and QCS was performed using NIST certified reference material 2709a (San Joaquin Soil, 1100 ng/g). Instrument detection limit was 0.5 ng Hg. All samples were run in duplicate, with values accepted when the relative percent difference

between the two samples was within 10%. All standards and MS had average recoveries within 10% of the accepted values, and all blanks were BDL.

For MeHg, unfiltered water samples were extracted with trace grade sulfuric acid for a minimum of 24 hours (Munson et al., 2014). Samples were analyzed by aqueous ethylation with sodium tetraethylborate, purge and trap, CVAFS, GC, and ICP-MS on an Agilent 770 (EPA Method 1630) (Imura et al., 1971; Hintelmann and Evans, 1997). Calibration and CCV were performed using Brooks Rand Instruments Methylmercury Standard (1 ng/L). Method detection limit was 1 pg. All standards had average recoveries within 13% of the accepted values, and all blanks were BDL.

For TSS, filters were placed in the oven at 105°C for 48 hours. Filters were then reweighed. TSS was defined as the difference in filter mass before and after filtration divided by the volume of water that passed through the filter. The filter field blank had a negligible difference in mass.

Section 2.3: Surface Water Extent Analyses

Annual surface water extent for the study area was calculated using the JRC Global Surface Water Mapping Layers v1.1 (Pekel et al., 2016) in Google Earth Engine (Gorelick et al., 2017). This dataset includes global surface water masks at 30-meter resolution annually between 1984 and 2018. Due to gaps in the annual water masks caused by cloud cover, areas classified as seasonal and permanent water were overlaid in two-year intervals starting in 1985. The resulting yearly masks are therefore the maximum extent of surface water from the designated year and the year prior. Although this method may slightly overestimate water surface extent, it remains constant throughout the study, so proportional changes in lentic and lotic systems remain unaffected.

Lentic versus lotic environments were delineated by overlaying the annual surface water masks with the Global River Widths from Landsat (GRWL) database (Allen and Pavelsky, 2018). GRWL includes centerlines for all rivers wider than 30 meters globally. Lotic water pixels

located within river channels were identified using cumulative cost mapping with GRWL centerlines as source pixels (Yang et al., 2020). Cumulative cost mapping integrates the ‘cost’ of traversing given pixels out from a source node. By assigning water pixels a ‘cost’ of 0 and land pixels a ‘cost’ of 1, it is possible to effectively determine connectivity to the GRWL centerline. Morphological changes over time cause some adjacent ponds and oxbow lakes to sporadically overlap with river centerlines. This overlap may cause misclassification of lentic environments as lotic. As a result, our estimates of lentification are likely conservative. Similarly, to limit misclassification in heavily mined landscapes with significant connectivity between mining ponds and the river channel, cumulative cost mapping was limited to within 1,500 meters of the GRWL centerlines. Thus, some small gaps in the river channel mask exist where the river has moved laterally further than 1,500 meters from the historic centerline. As a final step, small gaps in the river channel mask along narrow river segments at the edge of satellite detectability were filled by dilating and then eroding the river channel mask by two Landsat pixels (60 meters). All surface waters outside of the river channel mask were considered lentic. Trends in annual changes in surface water extent for both lentic and lotic systems were calculated on a watershed basis using linear regression.

Deforestation within the study period was calculated using the Hansen Global Forest Change dataset v1.6 (Hansen et al., 2013), which contains 30-meter resolution global forest change annually between 2001 and 2018. Since all deforestation mobilizes soil and therefore creates opportunities for Hg transport, reported deforestation includes that caused by all sources (e.g., ASGM, natural river erosion, development), which potentially reduces the overall signal from deforestation directly linked to mining. Conversion rates to aquatic systems and barren soil were calculated by overlaying the water mask with the deforestation mask lagged by one year (i.e., delineated into areas that were water the year following deforestation versus land the year following deforestation). Total areas for both barren and aquatic conversion were then calculated for each watershed within the study area.

Section 2.4: Data Analyses and Statistical Analyses

All statistical analyses were performed using R version 3.6.0 statistical software. Statistical tests were performed using an alpha of 0.05. Since data were not normally distributed, comparisons were performed using the Kruskal-Wallis Analysis of Variance on Ranks followed by the Dunn's Test for pairwise comparisons. In all figures, we report statistically significant differences between groups ($p<0.05$) using letters, with groups sharing a letter having no statistically significant difference. Reported mercury concentrations in the manuscript represent the mean and standard error.

Section 3: Results

Section 3.1: Changes to the hydroscape

Our results highlight the 'lentification' (increased extent of slow-moving pond and lake ecosystems) of the Madre de Dios region that accompanies extensive ASGM activities, with lentic systems increasing by an average of 16 km^2 (670%) in heavily mined watersheds from the period 1985-1989 to 2014-2018, compared to only 0.83 km^2 (20%) in less impacted areas. Though we found that between 1985 and 2018, both lotic (all eight watersheds) and lentic systems (six of eight watersheds) increased overall in surface water extent ($p < 0.0001$), these changes vary by orders of magnitude between watersheds with and without extensive ASGM activity. In heavily mined watersheds, average surface extent of lakes and rivers over the 34 years increased by 0.53 $km^2\,yr^{-1}$ (6.63% yr^{-1}) and 1.22 $km^2\,yr^{-1}$ (2.13% yr^{-1}), respectively. Comparatively, in less heavily mined watersheds, the average change in lake area was roughly sixteen times smaller (0.02 $km^2\,yr^{-1}$, 0.41% yr^{-1}), and the rate of change in river surface area was substantially lower (0.39 $km^2\,yr^{-1}$, 1.06% yr^{-1}). Most of this increase in lake surface area was due to the proliferation of mining ponds after the year 2000 (Figure 2.2). This result parallels documented increases in AGSM activity, which were generally low from 1984 to 2000 and began to rise rapidly thereafter, with the largest increases following the 2008 global economic recession, and remaining consistently high since 2010 (Asner et al., 2013; Espejo et al., 2018).

The increase in river surface area in mined regions is primarily due to the expanded connectivity between the main channel and adjacent mining operations. These changes are likely similarly driven by ASGM operations on riverbanks. Although water classifications as lotic or lentic near riverbanks change between the two states due to seasonal changes in connectivity, these intra-annual changes are small relative to interannual trends in lentic area throughout the study period.

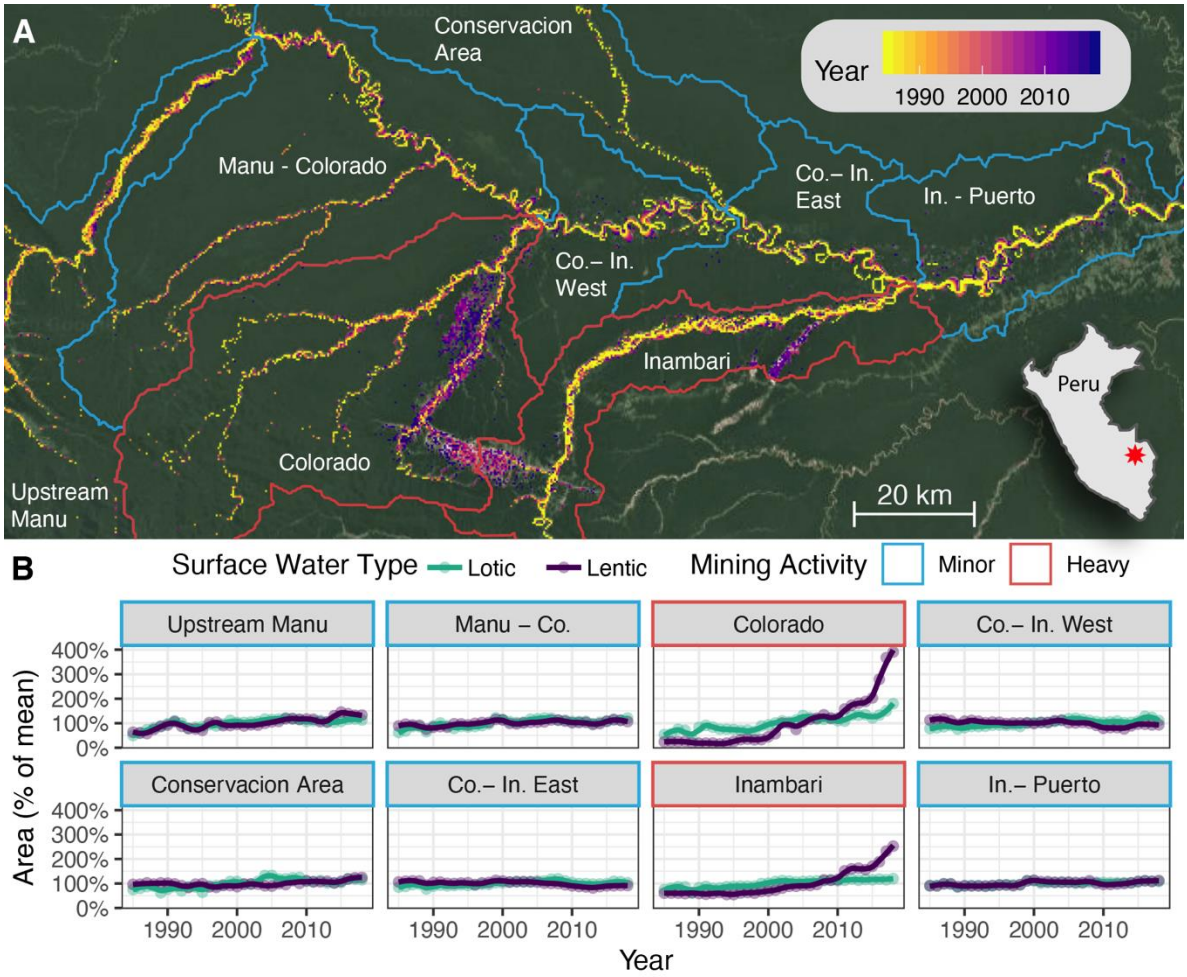

Figure 2.2: Spatial and temporal distribution of surface water extents in Madre de Dios, Peru. A) Map of the study area with historical surface water extent. Colors represent the first year a given area was detected as water. Historic river channels which pre-date satellite observations appear in yellow, while recent morphological changes and the expanse in mining ponds appear in magenta. B) Time series of normalized surface water extent broken down by watershed and lentic versus lotic environments. All water pixels connected to the main river channel for a given year are considered lotic; water pixels isolated from the main river channel are considered lentic. Basemap imagery from Google Earth (2020, from Landsat/Copernicus). See associated website for enhanced visualization of hydroscape changes. Sampling locations for mercury analysis are shown in Appendix B: Figure S1.

Previous studies have shown that ASGM leads to extensive deforestation of the landscape (Asner and Tupayachi, 2017; Espejo et al., 2018). To examine the extent of previously forested land that has been converted into aquatic systems, we partitioned deforestation into areas converted to barren ground and areas converted to aquatic systems for the year following the deforestation. We found that 66 km^2 of the 914 km^2 of deforested land in our study area (7.2% of previously forested areas) has been converted directly to lotic or lentic environments, with most of this conversion occurring in areas heavily impacted by mining (Appendix B: Figure S2). As deforestation mobilizes soil, it leads to increased sedimentation and Hg transport into surrounding water bodies (Diringer et al., 2020), potentially increasing net Hg methylation rates and disproportionately affecting aquatic organisms inhabiting areas directly converted from forested to aquatic landscapes.

Section 3.2: Landscape patterns in mercury concentration

We found that mercury loading was highest in river segments containing floodplain mining or downstream of significant ASGM activity (hereafter referred to as downstream rivers; $p < 0.0001$; Figure 2.3). Total Hg concentrations in these river waters were ~10 times that of other water bodies: 10.1 ± 2.8 ng Hg/L (n=12; reported as mean ± standard error), compared to 1.7 ± 0.4 ng Hg/L (n=12) in mining ponds and 1.3 ± 0.3 ng Hg/L (n=10) in downstream oxbow lakes. Average downstream river water total Hg concentration was 1,100 times the concentration of upstream river water and represented nine of the ten samples with the highest water column total Hg concentrations. Similar trends of elevated Hg concentration in rivers downstream of ASGM have previously been reported, including in Peru (Diringer et al., 2015; Gerson et al., 2018), but this is the first study to our knowledge that concurrently examines Hg trends from ASGM in both lake and river systems.

Given the correlation between total suspended solids (TSS) and water column total Hg concentration found in this study ($p < 0.0001$, $r^2=0.62$; Appendix B: Figure S3) and other studies (Maurice-Bourgoin et al., 2003; Biber et al., 2015; Moreno-Brush et al., 2016), as well as the

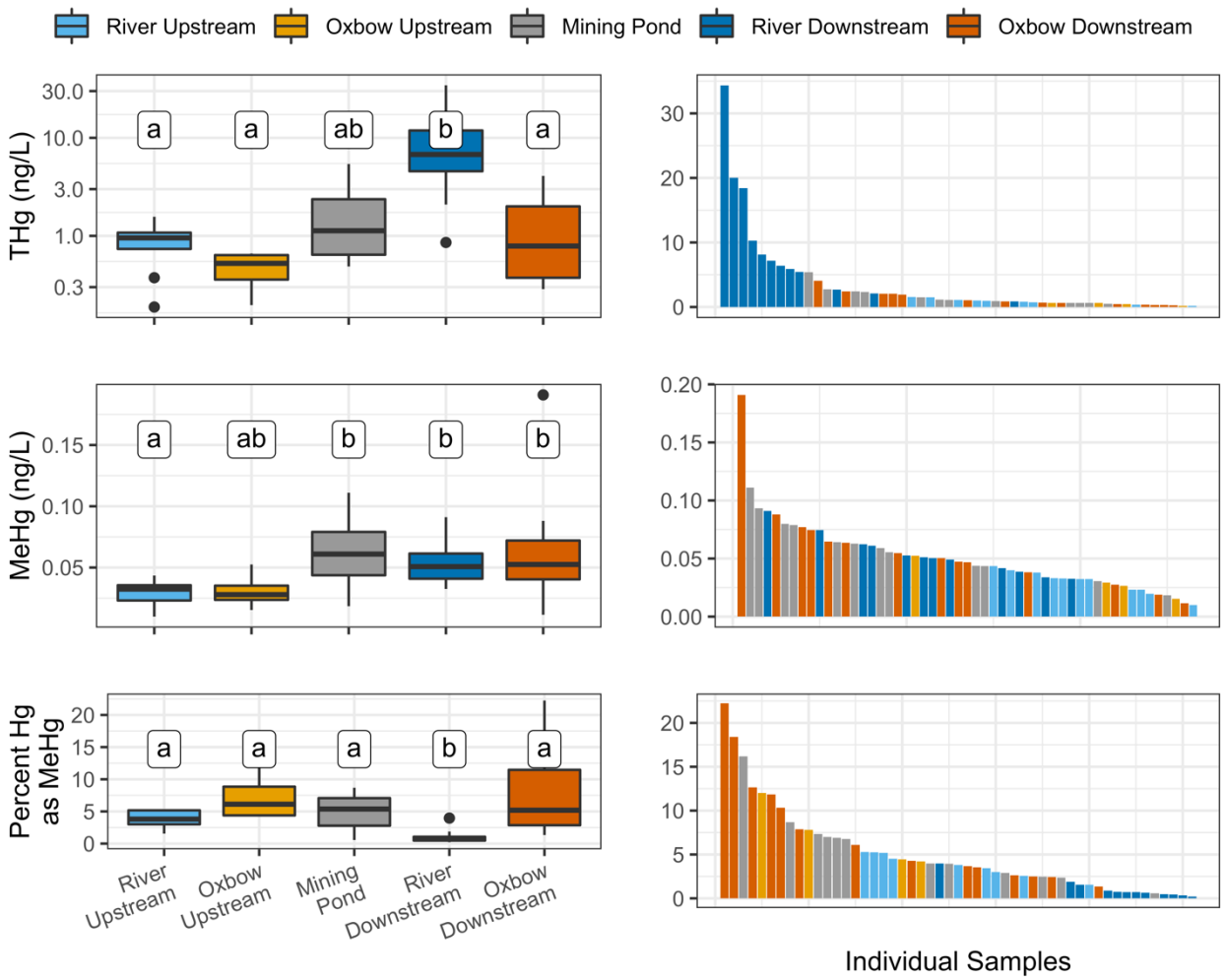

Figure 2.3. Concentration and distribution of water column total Hg (THg), methylmercury (MeHg), and percent Hg as MeHg across water bodies upstream and downstream of artisanal gold mining in Madre de Dios, Peru. Right column distribution data are observations shown in order of decreasing Hg values to highlight clustering among sampling locations. Letters represent statistically significant differences between values at each location according to a Kruskal-Wallis Analysis of Variance on Ranks followed by Dunn's Test.

higher concentration of TSS in downstream rivers compared to the other measured water bodies ($p < 0.0001$; Appendix B: Figure S4), we expect that Hg is transported bound to sediment particles (i.e., as particulate Hg) rather than in the dissolved fraction. Our finding of higher total Hg concentrations in oxbow lake sediments compared to downstream river sediments ($p = 0.030$; Appendix B: Figure S5) and the higher percent carbon content of oxbow lakes compared to other water bodies ($p < 0.005$) supports this assumption. Given this finding, it is important to note that sampling took place during dry season low flow conditions. During the

wet season (~Oct.-Apr.), precipitation increases 3-5 times, leading to meter-scale increases in river stage (Cañas and Waylen, 2012). While these increased flows historically created a highly seasonal flux of suspended sediment into the river, ASGM-driven erosion during the dry season is inverting historical seasonal patterns of suspended sediment concentrations in heavily mined areas of the watershed (Dethier et al., 2019), potentially exacerbating Hg transport and subsequent contamination of downstream aquatic environments.

Although water column total Hg concentrations were highest in downstream rivers, we found that the mining ponds and oxbow lakes were significantly more net efficient in converting Hg to the bioavailable form of MeHg (determined by the percent of Hg as MeHg; $p = 0.0032$, $p = 0.0003$, respectively). It is thus a combination of transport processes and residence times that is important for the fate of Hg in this landscape. On average, downstream river water contained 1.1 ± 0.3% of Hg as MeHg (n=12; reported as mean ± standard error), compared to 5.8 ± 1.2% (n=12) in mining ponds and 7.9 ± 2.1% in downstream oxbow lakes (n=10). Despite different total Hg loadings, downstream rivers, oxbow lakes, and mining ponds contained the same average concentration of MeHg ($p>0.05$). These trends are likely driven by the biogeochemical factors that promote methylation within lentic systems compared to lotic systems, as oxygen-limited systems generally have higher MeHg production than well-oxygenated systems (Todorova et al., 2009; Fleck et al., 2016). Note also that water column MeHg concentrations were not significantly correlated with TSS ($p=0.18$; Appendix B: Figure S3), suggesting that factors other than TSS are driving trends in MeHg. The combined effects of higher net methylation efficiency found in oxbow lakes and ponds and the 'lentification' of the hydroscape are highly likely to be increasing the risk of exposure to MeHg across ASGM-impacted regions beyond what might be anticipated based on the enhanced Hg loading alone.

Section 4: Discussion

ASGM within the Madre de Dios region of Peru creates a synergistic effect between Hg loading and landscape 'lentification' by expanding the systems that promote methylation of

inorganic Hg into MeHg. Between 1985-1989 and 2014-2018, the total surface area of lentic and lotic environments in heavily mined areas has increased by 670% and 98% respectively. Our results show that net MeHg production is 5-7 fold greater in lentic than in lotic systems within the study area. In combination, landscape 'lentification' and Hg loading are substantially increasing Hg bioavailability. This trend is likely to continue as long as gold prices remain high and ASGM activities remain a feasible livelihood for local populations living in less regulated areas. Increased Hg bioavailability in this global biodiversity hotspot poses a serious threat to local communities, including recently contacted indigenous groups, that consume high trophic-level fish (Gonzalez, 2015) as well as to endangered species like the iconic Giant Otter (*Pteronura brasiliensis*) that depend on lentic systems for habitat and foraging grounds (Gutleb et al., 1997).

To our knowledge, this is the first examination of interactions between Hg fate and transport and landscape hydrology associated with ASGM practices. Our results clearly show that the Madre de Dios region is vulnerable to the synergistic effects of lentification and Hg loading. Although this region is of particular concern due to its high levels of biodiversity, it is likely that Hg bioavailability is also increasing in other ASGM hotspots throughout the world. To determine whether this landscape lentification is a pervasive trend associated with ASGM, we examined the changing hydroscape in three additional ASGM hotspots around the globe (Figure 2.4). Watersheds with heavy mining activity in Venezuela (García-Sánchez et al., 2006), Ghana (Ferring and Hausermann, 2019), and Indonesia (Bruno et al., 2020) have all had three-to-eight-fold increases in the extent of lentic environments over the last 34 years. Assuming similar relative net methylation rates as in the Madre de Dios region, the ASGM-associated increase in lentic environments across the globe promotes net Hg methylation and bioaccumulation throughout the food chain. This process increases the threat from ASGM activities to vulnerable communities around the globe while simultaneously leading to severe ecological degradation. Thus, in evaluating the effects of Hg from ASGM, we need to consider not just the overall

loading of Hg into the aquatic ecosystem, but also how changes in the hydroscape might be influencing the processing of this Hg, particularly in global biodiversity hotspots.

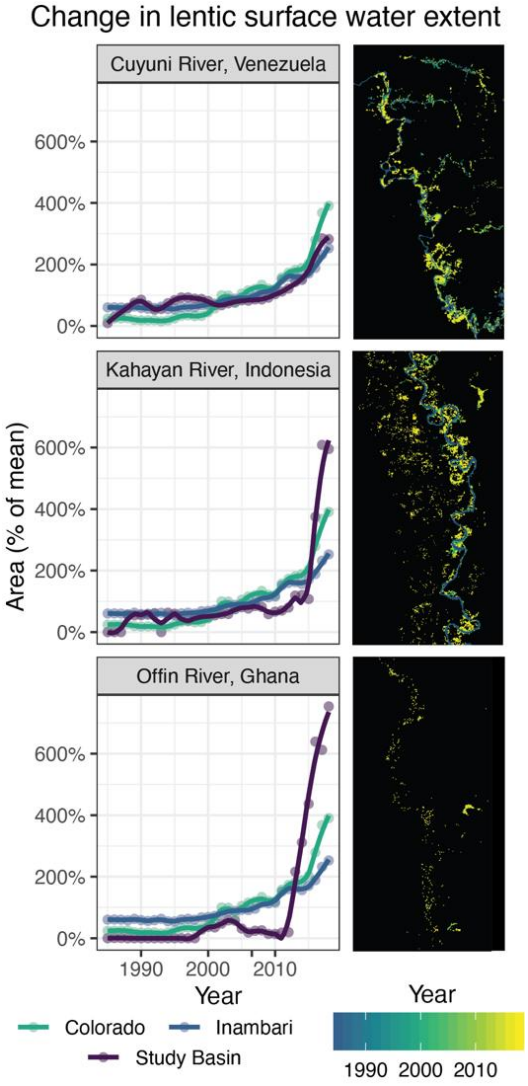

Figure 2. 4. Global examples of landscape lentification from three countries heavily impacted by ASGM. The left column shows the relative lentic surface area of the study country (in purple) compared to the heavily mined basins in Peru. The right column shows the historic water masks of the study country with colors denoting the first year a given pixel was classified as water. The main channel in the Offin River is smaller than 30 meters wide and below the remote sensing detection threshold; therefore, only surrounding mining ponds are measured. Black areas in the figures on the right represent pixels classified as land throughout the study period.

Chapter 3: Shifting patterns of lake color phenology in over 26,000 US lakes

Section 1: Introduction

Section 1.1: Summary

Lakes are often defined by seasonal cycles. The seasonal timing, or phenology, of many lake processes, such as primary productivity, are changing in response to human activities. However, long-term records exist for few lakes, and extrapolating patterns observed in these lakes to entire landscapes is exceedingly difficult using the limited number of in situ observations that are available. Limited landscape level observations means we do not know how common shifts in lake phenology are at macroscales. Here, we use a new remote sensing dataset, LimnoSat-US, to analyze U.S. summer lake color phenology between 1984 and 2020 across more than 26,000 lakes. Our results show that summer lake color seasonality can be generalized into five distinct phenology groups that follow well-known patterns of phytoplankton succession. The frequency with which lakes transition from one phenology group to another is tied to lake and landscape level characteristics. Lakes with high discharge and low variation in their seasonal extent are generally more stable while lakes in areas with high interannual variations in climate and catchment population density show less stability. Our research reveals previously unexamined spatiotemporal patterns in lake seasonality and demonstrates the utility of LimnoSat-US, which, with over 22 million remote sensing observations of lakes, creates novel opportunities to systematically examine changing lotic ecosystems at a national scale.

Section 1.2: Background

Lakes are critical freshwater resources that are highly sensitive to stressors such as climate change (Woolway et al., 2020) and altered land use (Martinuzzi et al., 2014). Globally, these stressors are shortening the duration of ice cover (Sharma et al., 2019), increasing rates

of lake carbon burial (Heathcote and Downing, 2012), increasing evaporative water loss (Wang et al., 2018), warming surface waters (O'Reilly et al., 2015), and changing mixing regimes (Woolway and Merchant, 2019; Maberly et al., 2020), all of which influence lake productivity and ecological state. These changes manifest themselves in the seasonality of lake processes. Just like a deciduous forest that comes to life in the spring, inland water bodies are characterized by a predictable seasonal succession of biological processes (Sommer et al., 2012). In the spring, many lakes experience a diatom bloom, followed by a 'clear-water' phase where zooplankton rapidly devour the newly plentiful phytoplankton (Matsuzaki et al., 2020). Summer algal biomass is constrained by nutrient availability, with nutrient-rich eutrophic lakes experiencing near-constant summer phytoplankton blooms, and nutrient-poor oligotrophic lakes experiencing relatively clear waters (Sommer et al., 1986). The difference between these states is visible to the naked eye, as the predominant color of a lake lies along a spectrum of blue (oligotrophic) to green (eutrophic); or as dissolved carbon concentrations increase, brown (dystrophic) (Webster et al., 2008).

The color of a lake reveals a lot about lake productivity and ecological state. A green lake will have a greater abundance of phytoplankton and a higher rate of carbon burial than a blue lake (Heathcote and Downing, 2012). Browning or greening of oligotrophic lakes may result in oxygen depletion and anoxic conditions (Müller et al., 2012; Knoll et al., 2018), which impacts nutrient cycling. Shifts in the magnitude and timing of annual color changes are indicators of short-term external (weather, nutrient, and carbon loading) and internal (biology) factors and/or long-term climate, watershed, and food web changes. These changes are not confined to single lakes, with landscape-level drivers impacting the color regimes of entire regions. For instance, shortened ice cover durations (Sharma et al., 2019) are shifting the spring-phytoplankton bloom earlier (Winder and Schindler, 2004), increases in dissolved organic carbon are browning lakes (Roulet and Moore, 2006; Monteith et al., 2007), and invasive zebra mussels are increasing water clarity (Binding et al., 2007), all at regional scales.

For a single lake, observing the annual pattern of lake color provides insight into the local ecosystem. At larger scales, simultaneously observing the annual patterns of many lakes provides evidence of the impacts of climate and land-use change and is critical in understanding the role of inland waters in carbon production and sequestration. Remote sensing enables this macroscale freshwater analysis because it captures a wide range of hydrologic conditions (e.g., Allen et al., 2020) with regular sampling intervals and global coverage. The Landsat series of satellites specifically provides over three decades of observations and can be used to accurately estimate water quality parameters such as chl-a and algal blooms (Dekker and Peters, 1993; Ho et al., 2019; Cao et al., 2020), colored dissolved organic matter (CDOM) (Griffin et al., 2018b; Olmanson et al., 2020), suspended sediments (Ritchie and Cooper, 1988; Dekker et al., 2001), water clarity (Olmanson et al., 2008; McCullough et al., 2013), and primary productivity (Kuhn et al., 2020). To infer water quality, these studies build models based on relationships between optically active constituent concentrations and their impact on water surface reflectance. These efforts are becoming increasingly accessible due to emerging datasets that match satellite observations with field measurements of water quality parameters for model training and development (Ross et al., 2019; Dethier et al., 2020; Spyrakos et al., 2020), as well as online processing and data storage platforms such as Google Earth Engine (Gorelick et al., 2017).

Here, we present a 36 year analysis of U.S. lake color phenology using LimnoSat-US, a new analysis-ready remote sensing dataset for inland waters. LimnoSat-US contains all cloud-free Landsat observations of U.S. lakes larger than 0.1 km^2 between 1984-2020. As either a stand-alone resource, or when combined with existing datasets such as AquaSat (Ross et al., 2019) and RiverSR (Gardner et al., 2020), LimnoSat-US provides opportunities for novel analyses of remotely sensed, macroscale patterns in U.S. freshwater resources. Through this initial application of LimnoSat-US, we attempt to identify the dominant phenology patterns in

U.S. lakes, how those patterns have changed over time, and what lake and landscape level characteristics control the stability of a given lake's seasonal cycle.

Section 2: Materials and Methods

Section 2.1: Database Development

We constructed the LimnoSat-US database (Topp et al., 2020b) by extracting USGS Tier 1 Landsat Surface Reflectance (T1-SR) (Rs) values over 56,792 lakes (HydroLAKES, Messager et al., 2016) across >328,000 scenes from Landsat 5 Thematic Mapper (TM), Landsat 7 Enhanced Thematic Mapper (ETM+), and Landsat 8 Optical Land Imager (OLI) sensors dating back to 1984. These observations include lakes throughout the conterminous United States and those directly adjacent to its border. While these surface reflectance products were originally developed for terrestrial applications, a growing body of research shows that they can be used to accurately estimate inland water quality parameters and perform on par with water-specific atmospheric correction algorithms (Griffin et al., 2018b; Kuhn et al., 2019; Olmanson et al., 2020). Within the T1-SR catalogues, Landsat 5 and Landsat 7 imagery are atmospherically corrected using the Landsat Ecosystem Disturbance Adaptive Processing System (LEDAPS) (Masek et al., 2006) while Landsat 8 images are corrected using the Landsat Surface Reflectance Code (LaSRC) (Vermote et al., 2016; Dwyer et al., 2018). We extracted reflectance values using an optimized workflow within Google Earth Engine (Gorelick et al., 2017) comprised of three key steps: 1) the calculation of the ‘deepest’ point (Chebyshev Center, Shen et al., 2015) for each lake within HydroLAKES; 2) water masking and extracting summary optical properties surrounding each deepest point; and 3) standardization of reflectance values across sensors (Appendix C: Figure S1).

Previous studies have used the centroids of lake polygons as representative locations for deep-water lake conditions (e.g., Soranno et al., 2017). However, there is no guarantee that the location of the centroid lies within the area defined by the polygon, nor that the centroid is necessarily the furthest point from the lake shore (Appendix C: Figure S2). Pulling satellite

reflectance values from centroids that fall within shallow littoral waters increases the likelihood of influence from the bed and nearshore land pixels (Volpe et al., 2011). To remedy this problem, we instead used the Chebyshev Center, or “deepest point”, of a lake polygon. The Chebyshev Center is defined as the center of the largest circle that can fit entirely within a given polygon’s boundary (Shen et al., 2015). We estimated the deepest point for each lake in Google Earth Engine (Gorelick et al., 2017) by identifying the location of the pixel that is furthest away from the lake shoreline (Yang, 2020)

Pixels within 120 meters of the deepest point were classified using the USGS Dynamic Surface Water Extent algorithm (DSWE) (Jones, 2015, 2019) and the USGS Landsat Tier 1 Surface Reflectance pixelQA band as derived by the CFMask cloud detection algorithm (Zhu et al., 2015). Observations were removed if any clouds, cloud shadow, snow, or ice were detected within the 120 meter buffer around the deepest point. Median values for all bands were subsequently calculated from high confidence water pixels as defined by DSWE (observations with less than 9 pixels of high confidence water were removed). While conservative, we assume the process of taking the median of only high confidence water pixels within 120 meters of the deepest point limits the impacts of adjacency effects, bottom reflectance, and possible noise due to wind-induced sun glint and surface or benthic macrophytes that may be prevalent in shallower waters. Final values are based solely on high confidence water pixels, but total counts of high confidence water pixels and partial surface water (vegetated) pixels were calculated in order to provide an indication of potential mixed pixels and/or noise in the final reflectance values. To address sensor variation and differences in atmospheric correction procedures, bands for each sensor were standardized following Gardner et al. (2020). Specifically, reflectance values were filtered to coincident time periods (1999-2011 for Landsat 5 and 7; 2012-2020 for Landsat 7 and 8) and Landsat 5 and 8 were standardized to Landsat 7 values through a second order polynomial regression of the 1-99th percentile values of each sensor

(Appendix C: Figure S3). Similar efforts focused on terrestrial applications have shown that statistical sensor correction can effectively improve multi-sensor continuity (Roy et al., 2016).

This process was optimized by iterating over Landsat WRS tiles and applying all necessary calculations in a single pass over each image/lake center. This approach dramatically speeds up computation on the Earth Engine servers by reducing the number of distinct image stacks generated and reducing the number of passes necessary to extract summary metrics from each lake within a given image. These performance operations become increasingly important as the size of analysis increases. While it varies with Earth Engine traffic, the optimized pipeline presented here decreases computation time for the >328,000 images in the analysis from approximately 30 days to 5 days for the contiguous U.S. when compared to pipelines using multiple passes and/or iterating by lake rather than WRS tile.

Section 2.2: Estimating Lake Color

Water color, as perceived by the human eye, is an intuitive measure of lake water properties. Color can be directly measured by any optical imager with bands in the visible spectrum and does not require knowledge of the inherent optical properties of water (Woerd and Wernand, 2015; Giardino et al., 2019b). We quantified lake color as the dominant wavelength (**λ**d) within the human visible spectrum by transforming surface reflectance into the chromaticity colorspace following Wang et al. (2015). Tristimulus values (X,Y,Z, Equation 1) were calculated from surface reflectance values (red, green, blue) and then converted into chromaticity coordinates (x, y, z, Equation 2).

$$X = 2.7689R + 1.7517G + 1.1302B$$

$$Y = 1.0000R + 4.5907G + 0.0601B$$

$$Z = 0.0565G + 5.5943B$$

(Equation 1)

$$x = \frac{X}{X+Y+Z} \qquad y = \frac{Y}{X+Y+Z} \qquad z = \frac{Z}{X+Y+Z}$$

(Equation 2)

Using these coordinates, the hue angle is calculated (Equation 3) and converted into **λ**d using the International Commission on Illumination (CIE) look-up tables.

$$\alpha = \left(arctan2\frac{x - 0.33}{y - 0.33}\right)\frac{180}{\pi}$$

(Equation 3)

In addition to dominant wavelength, which has known non-linearities in its distribution, we also calculated lake color within the Forel-Ule Color Index (FUI) space (Wang et al., 2015). The FUI is a discrete set of 21 colors that were developed specifically to identify water-color typologies (Barysheva, 1987). FUI values can be accurately calculated from multispectral imagery (Van der Woerd & Wernand, 2018; Wang et al., 2020) using either dominant wavelength or hue angle. Here, we use FUI values to more precisely show how we perceive various dominant wavelengths, the water-color typologies different wavelengths are associated with, and to assist in the visualization of color distributions.

Section 2.2: Seasonal lake color phenology

The development of the LimnoSat-US database provides novel opportunities for examining macrosystem patterns in U.S. lake dynamics. Clustering analysis is one common approach for extracting patterns from time series datasets that have no *a priori* assumptions about group membership (Liao, 2005) with successful applications in fields such as hydrology (Savoy et al., 2019; Brunner et al., 2020), ecology (Xue et al., 2014; Zhang and Hepner, 2017), and biogeochemistry (Byrnes et al., 2020). The overall goal of clustering analysis is to partition group membership based on within-group similarity and between-group dissimilarity. Here, we apply clustering analysis to time series of lake color to better understand the drivers of variation in lake seasonality over the past 36 years.

Lake color observations generated from the LimnoSat-US database were filtered to those between May and October to remove missing data caused by snow and ice. Observations

were broken into 6 distinct periods - (1984, 1990], (1990, 1996], (1996, 2002], (2002, 2008], (2008, 2014], (2014, 2020] - and were filtered to those with at least three observations per month per period, resulting in 26,607 lakes with enough data to calculate periodic seasonality for the analyses. Within each period, lake color phenology was calculated for both raw dominant wavelength and lake/period z-normalized dominant wavelength using a Nadaraya–Watson kernel regression (Watson, 1964; Nadaraya, 1964) implemented with the kmsooth function from the stats package in R (RCore Team, 2019). Application of the kernel regression allowed for the calculation of a weekly color value based on a gaussian weighted average of all observations within a window of 21 days from the point calculated. Extreme outliers (>4 standard deviations from the lake/period mean) were removed prior to the kernel regression for each series. The resulting time series consist of weekly estimates of lake color from May to October for each lake for each period (Figure 3.1).

Normalization of the time series is critical for accurately clustering lake phenologies using the dynamic time warping (DTW) method described below (Keogh and Kasetty, 2003; Mueen and Keogh, 2016). However, by standardizing the variance across time series, we artificially impose equal seasonal variation between lakes/periods that are relatively monotonic (i.e. aseasonal) and those that show true seasonality in the phenology of their color. Examination of the mean and standard deviation of dominant wavelength for the non-normalized time series shows that this is particularly problematic for end member lakes on either end of the color spectrum that show very little seasonal variation (σ < 5 nm, Appendix C: Figure S4). This can be seen in Figure 3.1, where oligotrophic Crater Lake shows minimal seasonality when compared to known eutrophic waterbodies (Lake Mendota and Lake Okeechobee). To address this issue while still following best practices of normalization for clustering analysis, those lakes/periods with a dominant wavelength standard deviation of less than 5 nm were classified *a priori* as aseasonal. This threshold guarantees that seasonal

variation within any remaining time series is at least ~10 nm around the mean color while effectively classifying aseasonal, monotonic, and end-member lakes as their own grouping.

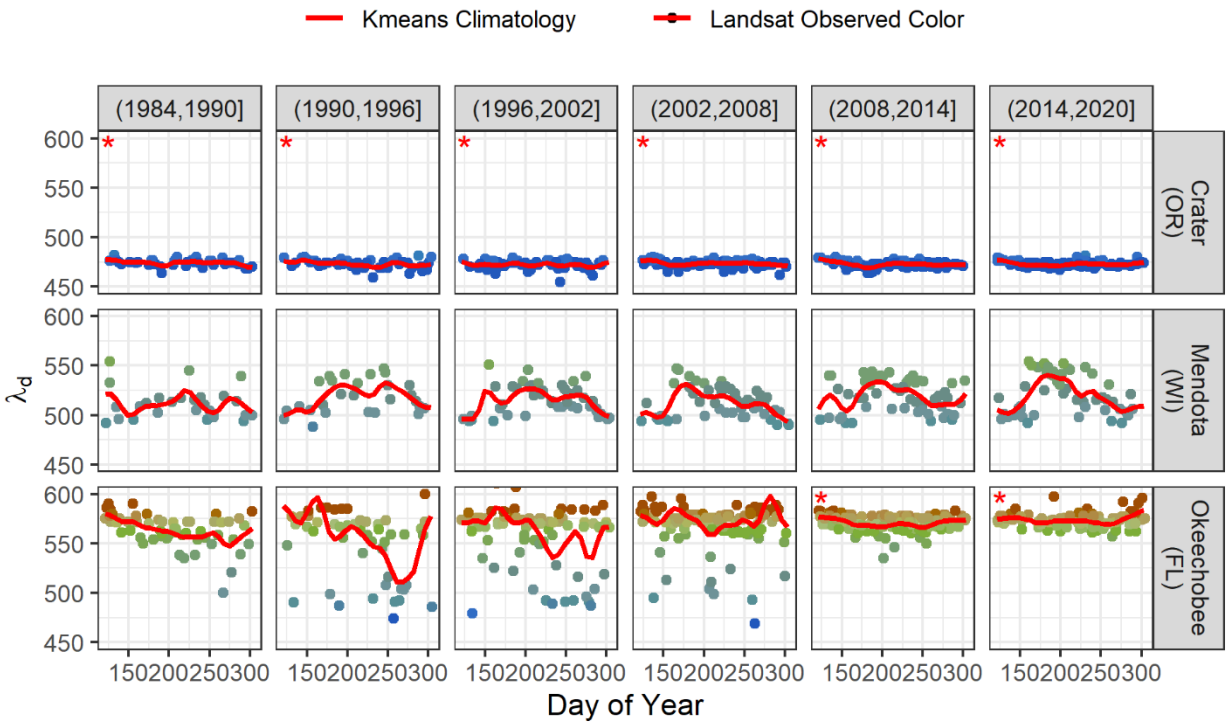

Figure 3.1. Examples of the calculated seasonal phenologies for three well studied lakes of different trophic states. Phenologies are composed of one observation per 7 days calculated by taking a gaussian weighted average of all points +/- 21 days from each calculated point. Lakes/periods marked by an asterisk were classified as aseasonal and placed in the a priori aseasonal cluster.

This process resulted in 109,643 individual time series available for cluster analysis and an additional 46,759 classified *a priori* as aseasonal. These time series were clustered using dynamic time warping (DTW) (Sakoa and Chiba, 1978) within a partitional clustering framework with barycenter averaging (Sarda-Espinosa et al., 2019). Dynamic time warping allows points within two time series to be compared within a user-defined window as opposed to using a one-to-one comparison found in traditional metrics like Euclidean distance. This elasticity reduces the impacts of noise, minor temporal shifts, and outliers, making it ideal for ecological systems with natural interannual variations (Xue et al., 2014; Zhang and Hepner, 2017; Savoy et al., 2019). The final number of clusters was determined by comparing the Davies-Bouldin (Davies and Bouldin, 1979) and Modified Davies-Bouldin (Kim and Ramakrishna, 2005) cluster validity

indexes (CVI) across iterations ranging from 2 to 8 clusters. The Davies-Bouldin and Modified Davies Bouldin were chosen because of their computational efficiency and strong performance when compared to other common CVIs (Arbelaitz et al., 2013).

One important validation of clustering analysis is how sensitive final clusters are to sample variations in their input, the idea being that stable, or 'universal', clusters will emerge across differing sampling schemes (Jain and Moreau, 1987). Here, we addressed issues of cluster stability using the Jaccard Similarity Index across 100 iterations of bootstrap sampling of our input time series. At each iteration, the original input time series were sampled with replacement, clustered, and the resulting clustering algorithm used to predict groupings for the original data. The Jaccard Similarity Index was then calculated based on how similar each new cluster was to the corresponding original cluster. The index ranges from 0 to 1, indicating that clusters share all or no members, with values greater than 0.5 generally indicating cluster stability and representativeness of true patterns within the data (Savoy et al., 2019). Significant differences in the distribution characteristics of the final clusters were identified using the non-parametric Kruskall Wallace Analysis of Variance on Ranks (Hollander and Wolfe, 1973) followed by Dunn's Test with a Bonferroni p-value correction (Dunn, 1961).

Finally, we examined the spatial autocorrelation of clusters and the overall stability of individual lake phenologies. Spatial autocorrelation was measured by randomly sampling 30% of the lakes, assigning them their most common cluster, and calculating the proportion of same cluster lakes versus different cluster lakes within 50 km windows moving outward from each lake in the subsample. Overall lake phenology stability was calculated by examining the number of times a given lake shifted between clusters throughout the 6 periods of study. Lakes were categorized on a scale from 0 (stable) to 5 (unstable) based on the total number of cluster transitions they made between 1984 and 2020. Lake and landscape level factors from HydroLAKES (Messager et al., 2016) and the Global Lake Area, Climate, and Population database (Meyer et al., 2020) were then used to assess lake characteristics that influence the

stability of a lake's seasonal phenology over time. Variables that potentially influence stability were identified through linear regression of lake stability (0-5) on the median value of the lake/climate attribute within each stability class. Those attributes with a coefficient p-value of less than 0.05 were further examined as correlates with lake stability.

Section 3: Results

The final LimnoSat-US database includes reflectance values spanning 36 years for 56,792 lakes across > 328,000 Landsat scenes. After initial quality control measures, the database contains over 22 million individual lake observations with an average of 393 +/- 233 (mean +/- standard deviation) observations per lake over the entire study period. While observations date back to 1984, the total number for any given year approximately doubles with the launch of Landsat 7 in 1999 (Figure 3.2).

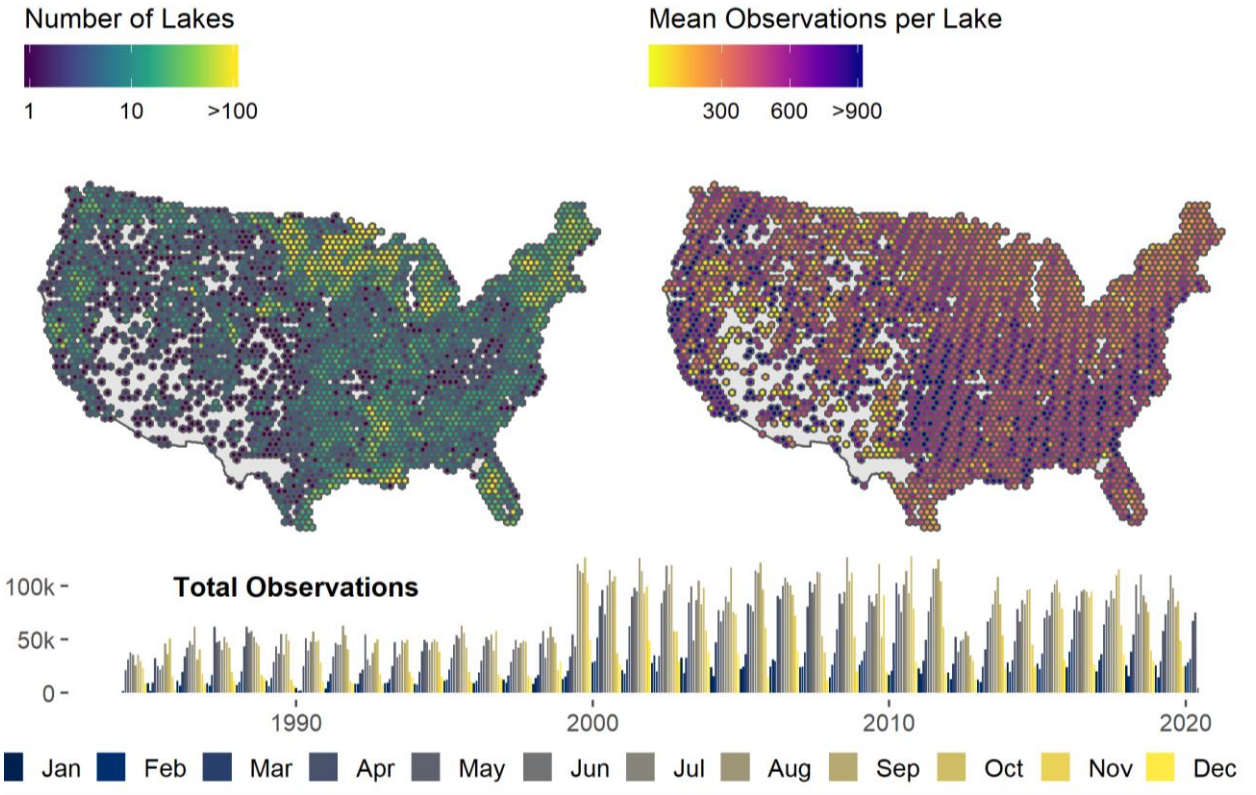

Figure 3.2. Temporal and spatial distributions of satellite observations contained within the LimnoSat-US database.

Section 3.1: Classes of lake color phenology.

Our final clustering partitions resulted in one of three membership classes for each lake/period that was not *a priori* classified as aseasonal (Figure 3.3). We describe these groups as Spring Greening, Summer Greening, or Bimodal. High mean Jaccard Similarity Indices across bootstrap sampling iterations (0.77, 0.80, 0.94 respectively) show these clusters are relatively universal, and that regardless of the initial sample, the same lakes are consistently clustered together. Within these clusters, we refer to red-shifted portions of the time series (increasing values) as greening or green-shifted and blue shifted portions of the time series (decreasing values) as blueing or blue-shifted. We highlight this terminology because even though red is the end-member of the upper wavelengths, the vast majority of the colors do not extend beyond the green portion of the spectrum. Descriptions of the summary attributes for each cluster are as follows:

1) Spring Greening (n = 55,378, 35.4%): Lake color is green-shifted in May/June and gradually moves towards the blue end of the spectrum throughout the summer and fall months. Median dominant wavelengths for these phenologies are significantly bluer ($p < 0.0001$) than those in the Summer Greening, Bimodal, or Aseasonal clusters (median $\lambda_d = 513$). They have the highest average coefficient of variation within each individual time series ($p < 0.0001$), with an average range of 37 nm for a given lake/period compared to 34 nm, 33 nm, and 12 nm for Summer Greening, Bimodal, and Aseasonal clusters, respectively. The distribution of colors within the cluster is concentrated around a mode 498 nm and skewed towards the greener portion of the spectrum.

2) Summer greening (n = 24,580, 15.7%): Lake color is characterized by gradual greening from May-August after which time it drops towards the blue end of the color spectrum. The distribution of colors shows a mode of 542 nm and a median of 524 nm with a blue-skewed distribution. On average, each individual time series within this class shows significantly less

variation than Spring Greening lakes/periods ($p < 0.0001$) but no significant difference from Bimodal lakes/periods.

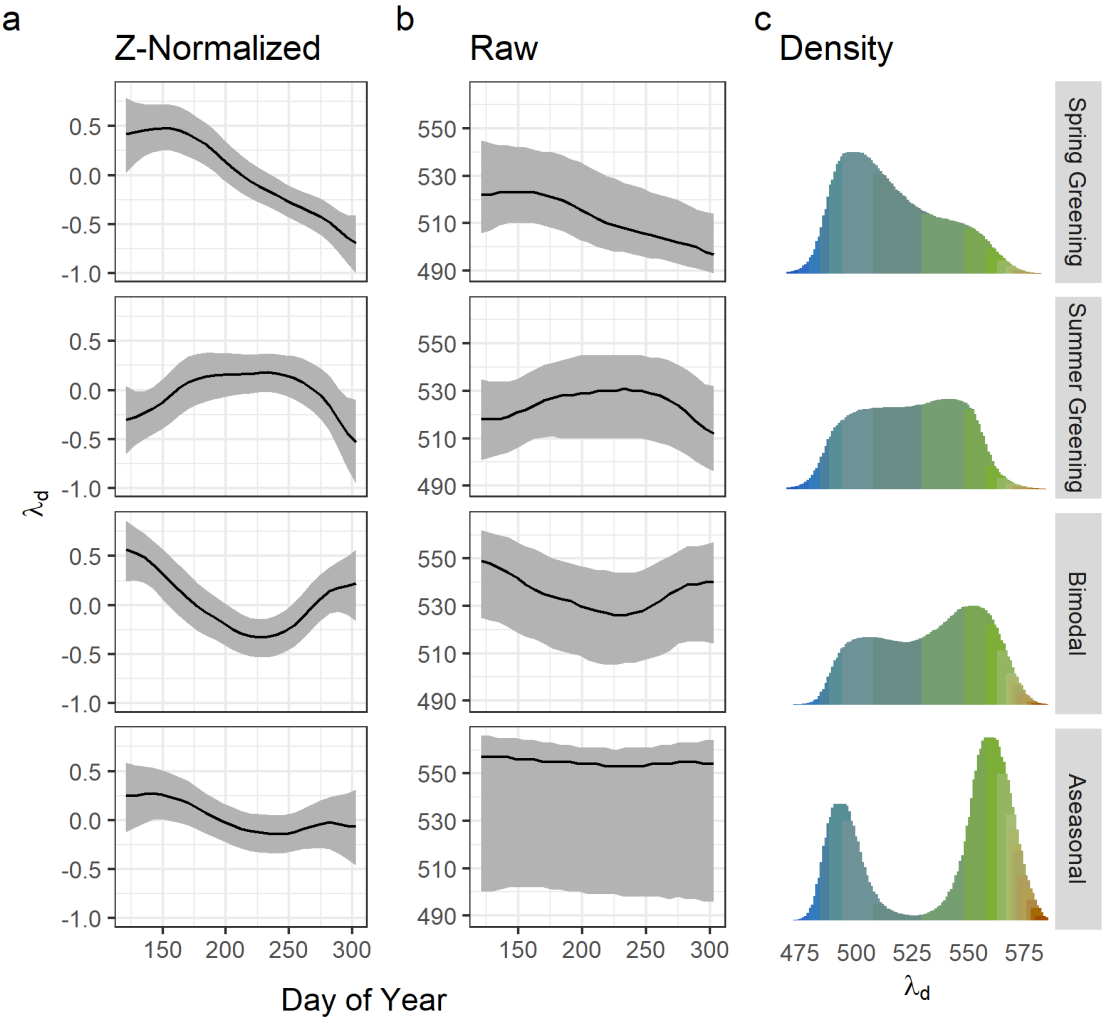

Figure 3.3. Results of cluster analysis for over 26,000 lakes and 156,000 seasonal time series. Black lines represent medians with grey ribbons representing the 1st-3rd quartile of each cluster. Clusters are shown both in their (a) z-normalized form used in the cluster analysis and (b) their raw dominant wavelength form. Distributions of color observations in each cluster are displayed using their associated Forel-Ule Index color. Note that the range of wavelengths associated with each Forel-Ule Index value varies.

3) Bimodal (n = 29,685, 19.0%): Lake color is most green-shifted in May/June and again in September/October, with a somewhat blue-shifted phase in the intervening months. Phenologies within this cluster are significantly more green-shifted ($p < 0.0001$) than lakes within either the Spring or Summer Greening clusters and show less variation ($p < 0.0001$) than

those in the Spring Greening clusters. The distribution of colors is concentrated around 553 nm with a much less pronounced peak at 507 nm.

4) Aseasonal (n = 46,759, 29.9%): The overall color distribution of this cluster is distinctly bimodal, with a primary mode at 559 nm and a secondary mode at 492 nm. This bimodal distribution, combined with the small variance in any given lake/period in the cluster, suggests it contains predominantly blue and predominantly green time series with very few observations in the intermediate green/blue space common within the three other clusters. The cluster also contains both the most green-shifted and most blue-shifted time series included within the analyses. Because of the crisp partition contained within the cluster and the ecological significance of blue versus green aseasonal time series, we further partition this cluster into Aseasonal (Blue) (n = 15,934) and Aseasonal (Green) (n = 30,825) lakes for the remainder of the analysis. Time series with a median dominant wavelength less than or greater than the anti-mode of the distribution (525 nm) are considered Aseasonal (Blue) and Aseasonal (Green) respectively.

Section 3.2: Lake stability over time

Aseasonal Green lakes showed the most stability over time, with an average of 73% +/- 6% (mean +/- standard deviation) of lakes remaining within the cluster between consecutive time periods. Aseasonal (Blue) and Spring Greening clusters showed similar retention rates of 57% +/- 17% and 57% +/- 9% respectively, while Bimodal and Summer Greening showed similar retention rates of 46% +/- 8% and 45% +/- 7%. However, of these, only the differences between Aseasonal (Green) and Bimodal/Summer Greening clusters were statistically significant at a 95% confidence interval. For Spring Greening, Aseasonal (Green), and Aseasonal (Blue) distributions, the number of lakes retained between each period was significantly higher than the number of lakes that transitioned to a different cluster ($p = 0.047$, $p = 0.007$, and $p = 0.0001$ respectively). Summer Greening and Bimodal clusters showed no significant difference between the proportion of lakes retained and lakes that transitioned to

other clusters, indicating less stability than the other three classes. However, these transitions showed distinct patterns, with lakes transitioning more commonly between similar clusters. As an example, on average 27% of Summer Greening lakes transitioned to Spring Greening lakes between periods, but only 4% of Summer Greening lakes transitioned to Aseasonal (Green) (Figure 3.4). Similarly, less than 0.2% of lakes in Aseasonal (Green) and Aseasonal (Blue) transitioned between the two clusters in any two consecutive periods indicating that state shifts between dominantly blue lakes and dominantly green lakes are very uncommon.

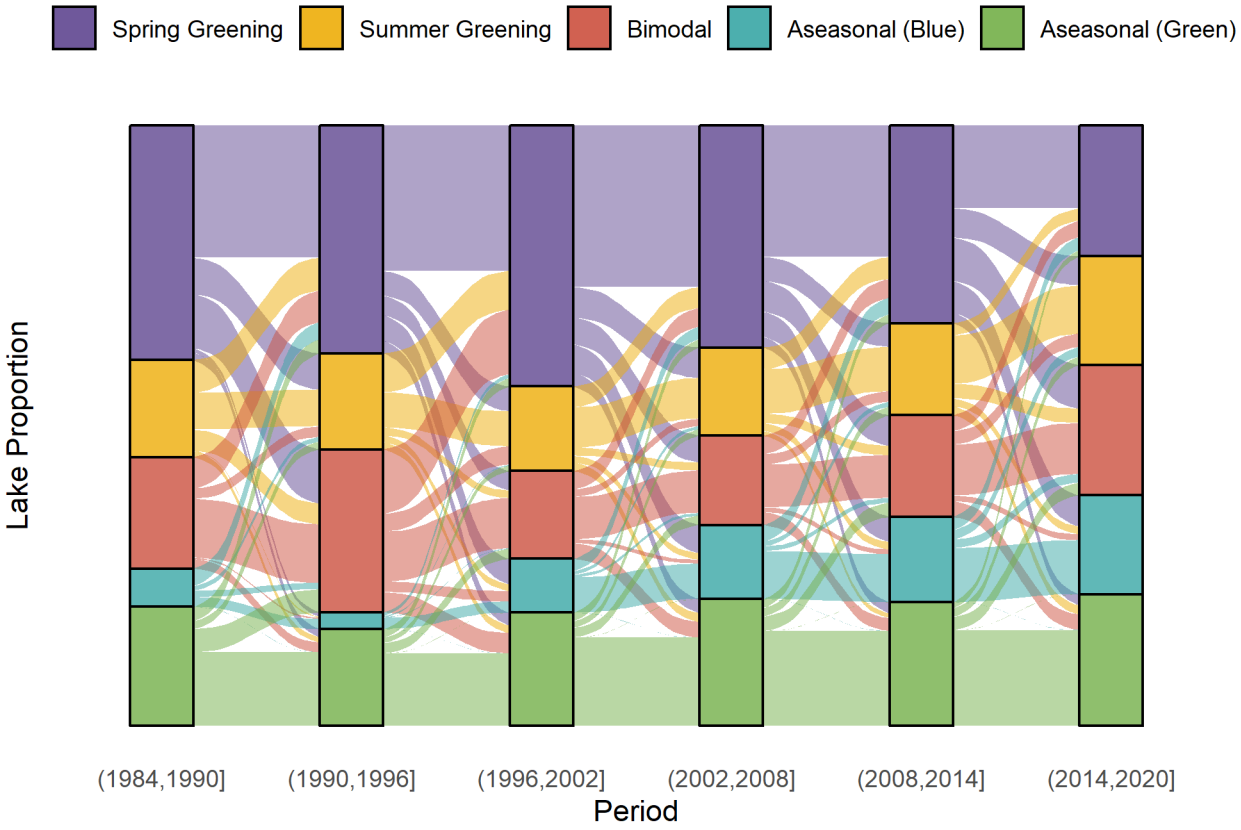

Figure 3.4. Sankey diagram showing the distribution of lake phenology transitions between periods. Each ribbon is proportional to the number of lakes that moved from one cluster class to another.

Lake stability, or the number of times a lake moved from one class to another (ranging from 0 transitions to 5), showed that lakes with three transitions were most common (n = 6,458) and lakes with five transitions least common (n = 1254) (Appendix C: Figure S5). We also calculated the number of unique clusters a lake occupied throughout its transitions. For

instance, a lake could change states between all five periods, giving it a stability score of five, but only be changing between two of the potential five clusters, giving it two unique states. Of the 26,067 lakes, 4,339 (16.6%) remained within the same cluster through all periods while only 21 (< 0.1%) occupied all five clusters at some point. For those lakes in between, lakes occupying two distinct states (n = 11,091; 42.5%) were most common followed by three states (n = 8,942; 34.3%) and four states (n = 1,674; 6.5%) respectively. Linear regressions between lake and landscape level metrics with overall lake stability showed significant relationships ($p < 0.01$) with 5 out of 26 possible metrics (Appendix C: Table S1), although some of these metrics have significant cross-correlation (Appendix C: Figure S6).

Section 4: Discussion

Section 4.1: Lake seasonal phenology types

Existing paradigms regarding the seasonality of lake color are generally derived from individual lakes with rich sampling histories of water quality observations; however these long-term field records are rare and limited to a small subsample of lakes (Stanley et al., 2019). While these data-rich study lakes are essential for understanding fine-scale ecosystem processes, they lack the spatial coverage to generalize across entire landscapes (Soranno et al., 2014; Collins et al., 2019). Within our clustering analysis, we found that lake color phenology can largely be categorized as Aseasonal, Spring Greening, Summer Greening, or Bimodal. These phenologies show distinct regional patterns and spatial auto-correlation, with the probability of two lakes being in the same cluster showing a significant relationship to the distance between those two lakes ($p < 0.0001$) up to a distance of ~1,500 km (Figure 3.5b).

Each cluster has a unique distribution of dominant wavelengths (Figure 3.5), which suggests that the timing of seasonal variation in color is connected with lake biogeochemistry. This conclusion is supported by long-standing models of freshwater phytoplankton succession (Sommer et al., 1986) and observations of annual cycles of chlorophyll-a, a proxy for phytoplankton biomass (Winder and Cloern, 2010). Oligotrophic temperate lakes often show the

archetypal pattern of a spring phytoplankton bloom followed by low summer concentrations. This was the dominant phenology in our observations (35.4%), which is in-line with a study of 125 aquatic systems that found that nearly half of the sites displayed a dominant 12-month cycle with one phytoplankton peak per year (Winder and Cloern, 2010). As nutrient availability increases, eutrophic lakes tend to experience discrete phytoplankton blooms in the spring and late-summer/fall (Marshall and Peters, 1989). This pattern is captured in our Bimodal cluster, where the raw dominant wavelength values are significantly greener than those in any other cluster except for Aseasonal (Green). The summer-greening cluster captures eutrophic to hyper-eutrophic lakes featuring prolonged summer blooms with highly variable summer algal concentrations (Huisman et al., 2018; Carpenter et al., 2020). The characterization of Bimodal and Summer Greening lakes/periods as eutrophic is further supported by the low levels of variation we observe in dominant wavelengths when compared to Spring Greening lakes/periods. Dominant wavelength saturates with high amounts of suspended matter, chl-a, and/or CDOM (Bukata et al., 1997), meaning that highly productive, algae-filled lakes with significant amounts of these constituents would show low variation as dominant wavelength saturates. It is also possible that lakes in these categories are dystrophic CDOM-dominated lakes, as they include some of the most red-shifted (brown) waterbodies within the study.

The proportion of lakes that fall within different clusters does not show an overall trend over time; however, since the 1996-2002 period, the number of lakes classified as either Bimodal or Aseasonal (Blue) have increased while the number classified as Spring Greening have been decreasing (Figures 3.4, 3.5). Much of the increase in Aseasonal (Blue) lakes is concentrated in the Pacific Northwest and occurred prior to 2008, whereas the decrease in Spring Greening Lakes has predominantly occurred in higher-latitude lakes that may be more sensitive to changes in snowmelt and ice cover regimes which control nutrient and sediment fluxes that influence lake productivity (Gerten and Adrian, 2002; Sharma et al., 2019). Patterns in the Aseasonal (Green) cluster show much less variation both spatially and temporally, being

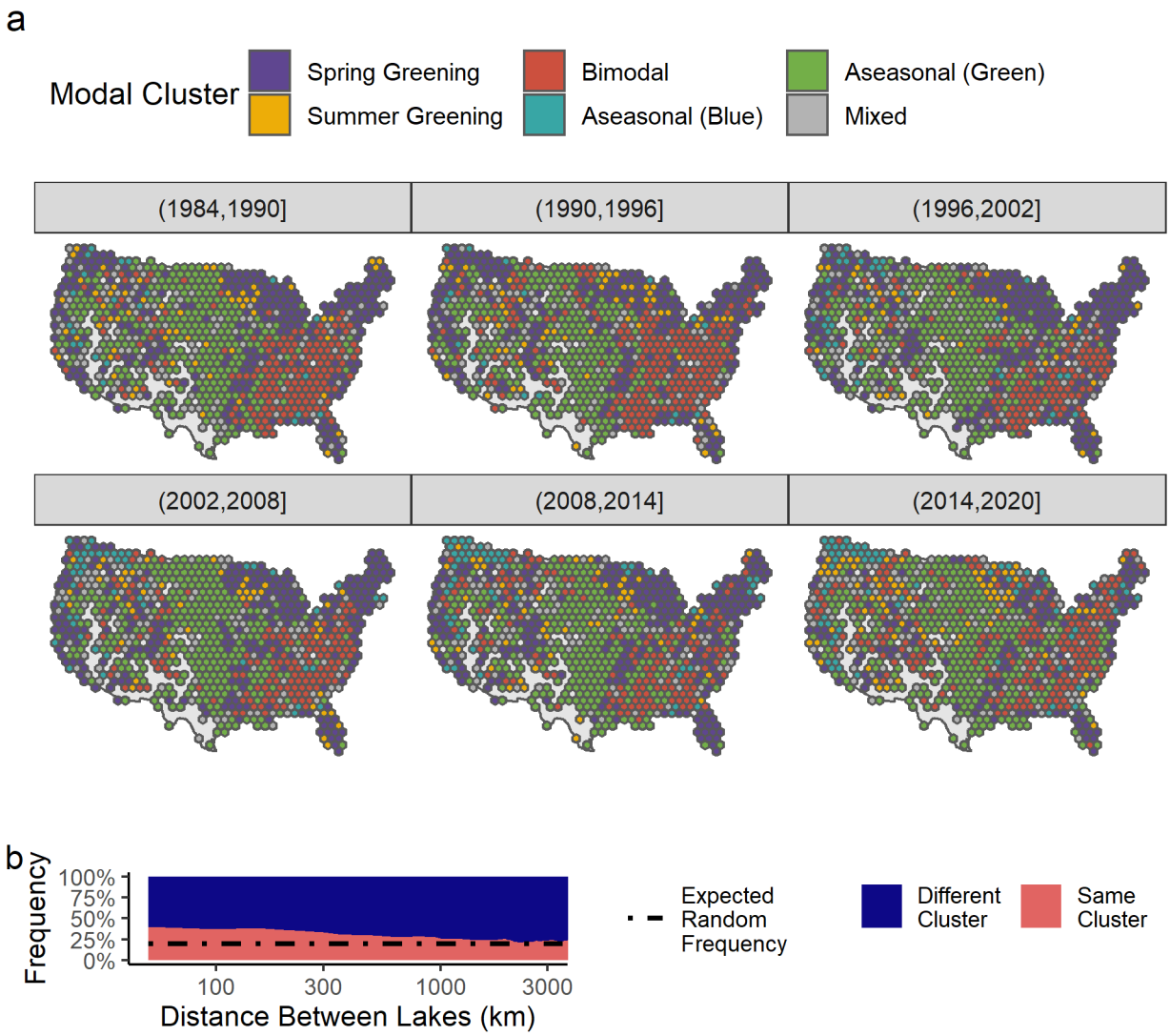

Figure 3.5. a) The modal cluster within each 100 km x 100 km grid across time periods. Mixed grids are those where there is no dominant cluster (i.e. two or more clusters are equally prevalent). b) The frequency of same cluster pairs to different cluster pairs using each lake's modal cluster. The frequency distributions were calculated within 50 km windows for a random sample of 30% of the study lakes. The dotted line represents the expected frequency if the distribution was random without any spatial autocorrelation.

largely concentrated in the agriculturally dominated central and northern plains and showing no distinct temporal pattern in quantity. While the increase in Aseasonal (Blue) lakes is potentially indicative of reduced sediment and nutrient inputs in certain parts of the country, the increase in Bimodal lakes, when taken with its close match to eutrophic phytoplankton succussion patterns, indicates increases in lake productivity across portions of the U.S. since the mid 1990s. This

pattern supports recent research showing a transition from bluer lakes to murky chlorophyll-a and CDOM-dominated lakes throughout the US between 2007 and 2012 (Leech et al., 2018). However, dominant wavelength, and optical water color more generally, is controlled by a variety of optically active water color constituents in addition to phytoplankton (Mobley, 1994; Gholizadeh et al., 2016), and partitioning these optical components is beyond the scope of this analysis. The result does, however, merit further research using a database like LimnoSat-US to examine country wide trends in lake chlorophyll-a content.

Section 4.2: Factors influencing lake stability over time

Lake stability, or the number of times a lake moved between clusters during the study period, showed significant relationships with multiple lake and landscape level metrics from HydroLAKES and the Global Lake, Climate, and Population database (GLCP) (Figure 3.6, Appendix C: Table S1). These relationships can generally be categorized as either hydrological properties or landscape properties. Important hydrological properties related to stability include lake size and discharge (both positively correlated with stability). This result supports existing research suggesting that larger water bodies are less reactive to perturbations than smaller, shallower lakes that can fluctuate among multiple productivity regimes (Scheffer and van Nes, 2007). We also find that hydrologically dynamic lakes are consistently less stable, with lakes showing large interannual variations in seasonal surface extent exhibiting less stability. It is likely that these hydrologically dynamic lakes are more sensitive to seasonal variations in runoff and resuspension of lakebed sediments leading to large interannual variations in nutrient and sediment load.

The landscape level metrics that showed the strongest relationship with lake stability were catchment population and elevation ($p < 0.01$) followed by mean temperature and mean monthly precipitation ($p < 0.05$). Similarly, for the subset of these variables where we had observations at annual timescales, we found that high coefficients of variation between years (interannual variation) of these metrics showed strong linear relationships to stability. The

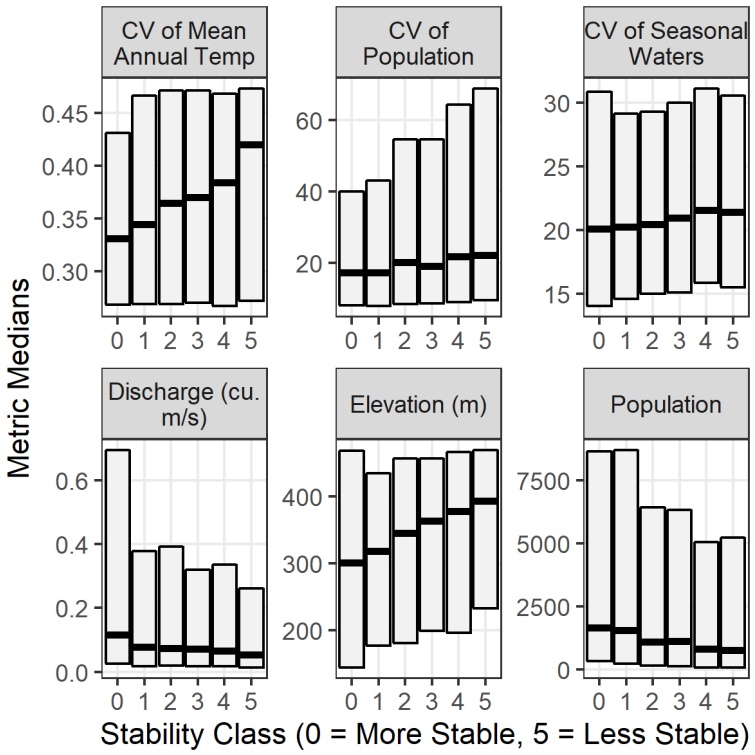

Figure 3.6. Lake and landscape level metrics that showed the most significant relationships with stability, or the number of times a given lake moved from one cluster to another between periods ($p < 0.01$ with the exception of discharge, $p = 0.019$). Center bars represent median values while boxes span the 1st-3rd quartiles.

impact of these landscape-level metrics on stability supports work showing that lakes integrate surrounding climatic and land cover changes (Rose et al., 2017). These results are of particular interest for relatively pristine high-elevation lakes that will be disproportionately impacted by changing precipitation and temperature regimes through climate change (Oleksy et al., 2020b, 2020a). Finally, we found that lakes in catchments with higher populations were generally more stable; however, lakes in catchments with high variation in population (likely increasing urban areas) showed less stability. Overall, our examination of landscape level metrics shows that the stability of a lake often follows the stability of its environment, with lakes subject to interannual variations in climate or anthropogenic stressors generally showing less stability in their overall seasonal phenology.

Section 5: Conclusion

Remote sensing has the capability to substantially increase our understanding of macroscale aquatic ecosystem processes. Here, we contribute to a growing body of inland

water remote sensing resources with LimnoSat-US, which contains >22,000,000 remotely sensed lake observations. Prior to this study, large-scale analyses of lake phenologies were limited to dozens to hundreds of waterbodies (Marshall and Peters, 1989; Winder and Cloern, 2010; Ho et al., 2019). Here, we were able to analyze U.S. summer lake color phenology across more than 26,000 lakes over 36 years, showing both temporal and spatial patterns and trends, as well as linking phenology to lake and landscape-level metrics. Better understanding the full distribution of lake phenology will allow for more accurate scaling of global nutrient and carbon cycling. While the analysis presented here relies simply on lake color, combining LimnoSat-US with databases such as AquaSat (Ross et al., 2019), RiverSR (Gardner et al., 2020), and LIMNADES (Spyrakos et al., 2020), will allow for more explicit modelling and analysis of specific water quality components, allowing researchers to partition the patterns observed here into optically active water quality components including chlorophyll-a, suspended sediments, and CDOM.

Chapter 4: Multi-Decadal Improvement in U.S. Lake Water Clarity

Section 1: Introduction

Section 1.1: Summary

Across the globe, recent work examining the state of freshwater resources paints an increasingly dire picture of degraded water quality. However, much of this work either focuses on a small subset of large waterbodies or uses *in situ* water quality datasets that contain biases in when and where sampling occurred. Using these unrepresentative samples limits our understanding of landscape level changes in aquatic systems. In lakes, overall water clarity provides a strong proxy for water quality because it responds to surrounding atmospheric and terrestrial processes. Here, we use satellite remote sensing of over 14,000 lakes to show that lake water clarity in the U.S. has increased by an average of 0.52 cm yr^{-1} since 1984. The largest increases occurred prior to 2000 in densely populated catchments and within smaller waterbodies. This is consistent with observed improvements in water quality in U.S. streams and lakes stemming from sweeping environmental reforms in the 1970s and 1980s that prioritized point-source pollution in largely urban areas. The comprehensive, long-term trends presented here emphasize the need for representative sampling of freshwater resources when examining macroscale trends and are consistent with the idea that extensive U.S. freshwater pollution abatement measures have been effective and enduring, at least for point-source pollution controls.

Section 1.2: Background

Recent large-scale studies of the aquatic ecosystems have been facilitated by a growing number of easy to use to global (Filazzola et al., 2020) and sub-continental (Fölster et al., 2014; Soranno et al., 2017; Read et al., 2017) datasets of field water quality measurements. However,

research into one of the largest such datasets (Soranno et al., 2017) suggests that historical field samples tend to be biased towards larger, problematic waterbodies and often lack the temporal continuity necessary for detecting long term trends (Stanley et al., 2019). Using this unrepresentative data to understand regional to national scale lake dynamics can lead to significantly different results when compared to statistically-representative samples (Paulsen et al., 1998; Peterson et al., 1999). While this problem of representativeness is increasingly acknowledged in sampling efforts (e.g., the U.S. National Lake Assessment; NLA) (Pollard et al., 2018) systematic sampling programs are costly, can have limited temporal resolution and continuity, and require compromise between scientific rigor and logistical practicality (Hughes and Peck, 2008). No such sampling program is available at continental scales over multiple decades.

One response to the challenges represented by field studies is to use remote sensing to estimate water quality parameters. Over the past decade, inland water quality remote sensing research has increasingly focused on larger spatial and temporal domains in order to address challenging science questions (Olmanson et al., 2008; Ho et al., 2019; Topp et al., 2020a). Here, we use remote sensing to conduct the first multi-decadal, national-scale assessment of U.S. lake water clarity by developing a carefully validated data-driven model that is generalizable across more than three decades for the entire contiguous U.S. We calculate regional summer lake water clarity trends from 1984-2018 across nine U.S. ecoregions in two different samples of lakes: a statistically stratified sample (n = 1,029 lakes) defined by the 2012 NLA (Peck et al., 2013) and a large random sample (n = 13,362 lakes) from the National Hydrography Dataset (NHDPlusV2) (McKay et al., 2019). We compare the overarching trends from these remotely-sensed estimates to each other and to the entirety of the available *in situ* data from the Water Quality Portal (WQP) (Read et al., 2017) and LAGOS-NE (Soranno et al., 2017), which jointly have over 1 million field observations of U.S. lake clarity dating back to 1984. In doing so we observe the impact of different sampling approaches and illustrate the

biases that exist when using historical field samples to identify long term trends. To complement the ecoregion analysis and compare our work to existing studies focusing on larger lakes (Ho et al., 2019), we add all U.S. lakes larger than 10 km^2 to our NLA and random samples and examine trends in lakes with over 25 years of observations (n = 8,897) to identify how lake-specific trends vary with lake size and population density.

Section 2: Materials and Methods

Section 2.1: Data Processing and Acquisition

Figure S1 (Appendix D) depicts a summary of the project workflow. Data for model training and validation was derived from a variant of the AquaSat database (Ross et al., 2019) which combines historical water quality measurements from the Water Quality Portal (Read et al., 2017) and LAGOS-NE (Soranno et al., 2017) with coincident (+/- 1 day) satellite images from the USGS tier 1 surface reflectance collections for Landsat 5, 7, and 8. While the atmospheric corrections used to generate these surface reflectance products were originally developed for terrestrial applications, a growing body of research shows that they can be used to accurately estimate inland water quality parameters and perform on par with water-specific atmospheric correction algorithms (Griffin et al., 2018b; Kuhn et al., 2019; Olmanson et al., 2020). Site IDs from AquaSat were spatially joined to lake polygons from NHDPlusV2 (McKay et al., 2019) (NHD) and then linked to catchment level metrics from the LakeCat database (Hill et al., 2018). From the initial AquaSat database, observations were removed if:

- they did not coincide with a lake polygon from NHDPlus V2
- over half of the water pixels within 120 meters of the sample site were classified as anything other than high confidence water by the USGS Dynamic Surface Water Extent water mask (Jones, 2019)
- the Landsat scene contained over 50% cloud cover

- one or more Landsat bands was beyond a reasonable reflectance for water (0-0.2)
- the Fmask (Zhu et al., 2015) indicated the presence of clouds, cloud shadows, or ice over the sample site
- the observation was impacted by topographic shadow
- recorded field water clarity (measured as Secchi disk depth) was < 0.1 meters or > 10 meters (the limits used for the NLA field sampling).
- two identical clarity observations occurred on the same day within the same lake as a result of duplication between WQP and LAGOS-NE (WQP observations were kept while LAGOS-NE observations were removed in these circumstances)

Similarly, reflectance values for analyzing national clarity trends were calculated using the same filters and methodology described above using the lake center as the sample point and taking the median value of high confidence water pixels within 120 meters for all study lakes. As an additional test, the predictions using lake center median values were compared with predictions using whole lake median values for the 2012 NLA lake sample. The two sets of predictions showed strong agreement (R^2 = 0.95, Appendix D: Figure S2), so lake centers were used for consistency with AquaSat's point based method. All reflectance values were extracted from Google Earth Engine (Gorelick et al., 2017) for the three samples of interest within the study: the statistically stratified NLA 2012 sample (n = 1,038), a large random sample of 2,000 lakes per ecoregion (n = 18,000), and all lakes greater than 10 km^2 (n = 1,170).

Each subsample contained a portion of lakes that were ultimately removed through the quality control measures described above. Spot checking of the removed waterbodies revealed that the most common cause for removal was lack of Landsat visible pure water pixels caused by either irregular waterbody shape (long and narrow), surface vegetation on the waterbody, overhanging vegetation along the shoreline, or a misclassification of a lake within NHD.

Removal of these waterbodies led to total lake counts of 1,029 for the NLA sample, 13,362 for the random sample, and 1,105 for lakes over 10 km^2 (for a total of 14,971 unique lakes). While conservative, this filtering approach ensured minimal error from mixed pixels, sun glint, and surrounding adjacency effects from nearby land.

Reflectance values from the differing Landsat sensors were normalized following Gardner et al. (2020). For each satellite pair (Landsat 5/7 and Landsat 7/8), the reflectance values observed over the entirety of the NLA sample of lakes were first filtered to coincident time periods when both sensors were active (1999-2012 for Landsat 5 and 7 and 2013-2018 for Landsat 7 and 8). We assume that the distribution of collected reflectance values for a given band should be identical given a sufficient number of observations over the same array of targets regardless of sensor. Based on this assumption, we calculated the 1^{st}-99^{th} reflectance percentiles for each sensor/band during periods of coincident satellite activity. Since Landsat 7 spans the time periods of both Landsat 5 and Landsat 8, each band in 5 and 8 was corrected to Landsat 7 values through a 2^{nd} order polynomial regression of the 1^{st}-99^{th} percentiles of reflectance values between the two sensors for the overlapping time period (Appendix D: Figure S3). The resulting regression equations were then applied to all Landsat 5 and 8 values within AquaSat as well as for all the included study lakes. Ultimately, applying these corrections to the reflectance values reduced the final model mean absolute error by 0.2 meters, suggesting that standardizing the reflectance values between sensors successfully reduced errors from sensor differences.

Application of the above quality control measures for AquaSat resulted in a model training and testing database of 250,760 observations of Secchi Disk depth, associated Landsat reflectance, and site specific lake and catchment properties for an optically diverse sample of waterbodies across the United States dating back to 1984 (Appendix D: Figure S4). Reflectance values for specific bands and band ratios within the training dataset were analyzed for correlations with atmospheric optical depth derived from the MERRA2 reanalysis data (Randles

et al., 2017). Correlations were examined both over the entire study period and between 1991 and 1993, when aerosol optical depth values were particularly high due to the eruption of Mt. Pinatubo. Optical parameters that showed the least correlation to atmospheric optical depth ($r < 0.15$ during 1992 and 1993 and $r < 0.1$ for the study period) were then chosen for inclusion in the modelling pipeline. These included Blue/Green and Nir/Red ratios and the dominant wavelength as described by Wang et al. (2015).

Of the non-optical parameters from the LakeCAT database, we included those that could impact water clarity and were mostly static over time (Appendix D: Table S1). Static 2006 values for catchment level percent impervious surfaces, percent urban landcover, percent forested landcover, percent cropland, and percent wetland landcover were included despite potentially being unrepresentative of the entire study period in some catchments. These variables were deemed important based on existing research (Lottig et al., 2017; Rose et al., 2017), domain expertise, and various preliminary empirical tests of feature importance, and therefore were included in the modelling pipeline. All lake and landscape-level variables were rounded to the nearest tenth or whole number, depending on the variable scale, in order to prevent certain variables from acting as location identifiers and to avoid overfitting during model training. This initial reduction in the feature space of the training dataset resulted in three optical variables and 27 static lake/landscape variables for each AquaSat matchup observation.

Section 2.2: Model Development and Validation

Non-parametric, supervised machine learning algorithms are increasingly popular within the remote sensing community due to their robustness, ease of use, and relatively low computational requirements (Li et al., 2016). Among these algorithms, extreme gradient boosting (Xgboost) has been shown to outperform similar non-parametric classification and regression schemes for urban land cover classification (Georganos et al., 2018), determining aerosol optical depth (Just et al., 2018), and modeling solar radiation (Fan et al., 2018). Xgboost classifiers are ensemble models that combine a suite of ‘weak’ classifiers in order to minimize

overall error. Within each iteration, estimates with large errors from the previous iteration are weighted in order to force the model to maximize its performance on the most challenging calibration data. The iterations are additive, meaning that the final model is the sum of the previously weighted regressions.

Here, we use the generalized linear module of Xgboost as it was found to outperform the tree based module for low values of water clarity. This implementation of Xgboost creates a generalized linear model using elastic net regularization (Zou and Hastie, 2005) and coordinate descent optimization (Friedman et al., 2010). To better understand the structure of the final model, as well as the influence of each input feature on model predictions, we calculated the feature importance and accumulated local effects (ALE) (Apley and Zhu, 2020) for all model inputs (Appendix D: Figure S5). ALE values represent the average marginal impact of a feature on final predictions as the feature value increases or decreases within a 'local' window of values. Examining ALE values is an effective method for interpreting machine learning models that are otherwise opaque in their structure (i.e. black boxes) (Molnar, 2020).

In order to avoid model overfitting and limit the final number of input variables, we incorporated forward feature selection (FFS) (Meyer et al., 2018) with target oriented leave-location-leave-time out cross validation (LLLTO-CV) (Meyer et al., 2019) into our Xgboost model development. FFS and LLLTO-CV effectively reduce overfitting by cross-validating the model on locations and times not used for model training and removing variables with high spatial or temporal correlations with observed clarity. We set aside 20% of the training dataset (n = 50,153) to use for post-development model testing and trained our initial model with the remaining 80% (n=200,607) using FFS and LLLTO-CV. This process reduced the overall number of input variables from 30 to 11 (3 optical properties and 8 static lake/landscape variables) (Appendix D: Table S1). Finally, the hyperparameters of the model were tuned using a grid search approach with conservative hyperparameter values.

Section 2.3: Annual Lake Water Clarity Predictions

Lake observations downloaded from Google Earth Engine were limited to those between May and September in order to remove the influence of snow and ice while maximizing the number of cloud free images captured. For any given lake and year, the median of all cloud free predictions was taken as representative of summer lake clarity. These summer clarity predictions were then averaged across the nine ecoregions defined within the NLA to generate estimates of annual regional water clarity. For the NLA sample of lakes, this process led to an average of 883 observations spread across 103 lakes being averaged for each regional estimate of summer water clarity. The NLA provides weights for lakes used in analyses at the state and national scale; however, no ecoregion scale weights are provided, and therefore regional means calculated here represent the unweighted regional means of the 2012 NLA sample lakes.

Model error was propagated into the mean regional estimates through 1000 iterations of bootstrap sampling. Within each iteration, annual lake median values within each region were sampled with replacement, and the new subsample was used to calculate the annual mean for the region. This bootstrapping procedure effectively propagates a different amount of model noise into each estimate of mean summer clarity by incorporating a different sample of lakes into each iteration of the regional estimate. This resampling results in a distribution of 1000 estimates of clarity for each year/region. We take the mean +/- the standard deviation of these distributions to generate 90% confidence bounds for each annual estimate of clarity.

In order to analyze overarching regional trends, we calculated Thiel-Sen Slopes for each of the generated time series based on the mean of the bootstrap sampling procedure. Thiel-Sen Slope is a nonparametric measure of the magnitude of monotonic trends that is insensitive to outliers within the dataset (Sen, 1968). It determines overall trends by calculating slopes between each pair of points in a time series and then taking the median of all slopes. It is often used in conjunction with Mann-Kendall trend analysis to quantify the more binary Mann-Kendall

tau statistic (Kendall, 1948). The trends presented here are based on the full remote sensing time series; however, we also calculated trends excluding the years in which atmospheric optical depth was potentially impacted by the Mt. Pinatubo eruption (1991-1993). Overall trends using the filtered timeseries showed only minor differences from the full-time series (Appendix D: Figure S6) indicating that the reported patterns observed here are not artefacts of the abnormal atmospheric conditions in the early 1990s. Trends for the field data were analyzed using the same method as the remote sensing predictions by first taking the summer median of each sampling point, averaging the median values by year/region, and calculating Thiel-Sen slopes from the resulting regional estimates.

Finally, we identified lakes with more than 25 years of observations to conduct lake-scale analysis (n = 8,897). We calculated Thiel-Sen Slopes for each individual time series of median summer clarity to examine the distribution of trends at the lake scale. Individual lake trends were binned by lake size and catchment population density to analyze the impact of these lake characteristics on overall clarity trends. The resulting distributions across size classes and catchment population density showed longer tails towards positive trends and were therefore analyzed using non-parametric Mann-Whitney tests rather than the more common parametric t-test. While we did not explicitly propagate model error into these individual lake time series, we attempt to reduce the impact of model noise by examining distributions rather than individual lakes and calculating the median trend for each binned distribution.

Section 3: Results

Section 3.1: Model Validation

Validation of our data-driven remote sensing model (Figure 4.1, Appendix D: Figure S7) indicates that it performs on par with existing regional remote sensing models developed using either traditional regression methods or semi-analytical modelling (Olmanson et al., 2008; Ren et al., 2018; Page et al., 2019). However, unlike previous regional models that are only applicable to a specific scene, sensor, or area, the model presented here is generalizable for

over three decades for the entire contiguous United States. Model error was calculated using the hold-out data (n=50,153) not used in model training. Error metrics were calculated at the observation level as well as at the aggregated ecoregion level used in the final analysis. Examination of the model residuals shows a consistent normal distribution over time. This is important both because it reaffirms the sensor correction procedure described above and because it leads to more accurate regional estimates, as over and underpredictions cancel each other out. Observation level error metrics for the final model include a mean absolute error of 0.71 meters (mape = 38%) and bias of < 0.01 meters. Regional/annually aggregated error

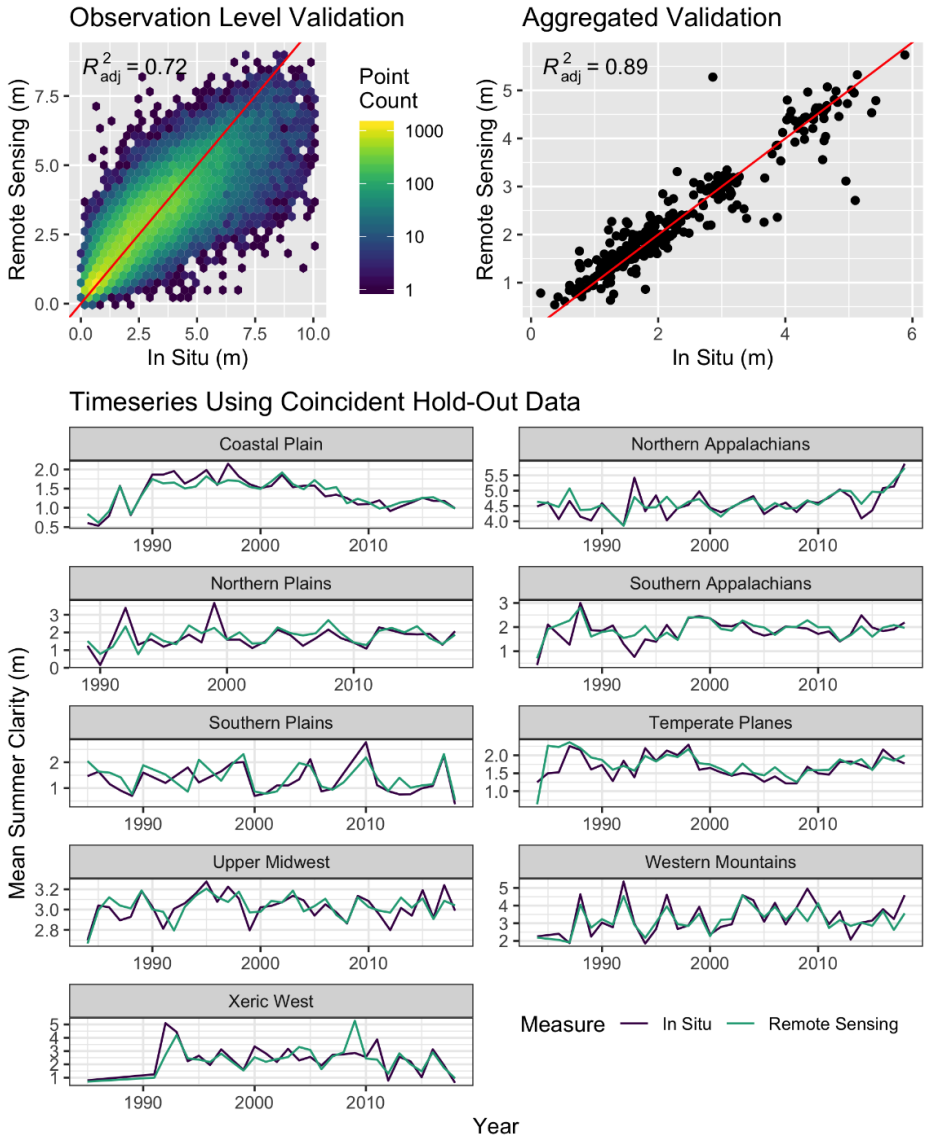

Figure 4.1. Model validation based on hold-out data not used in model development. Clockwise from the upper left: Point based model performance, model performance aggregated by year and region, and regional timeseries of aggregated validation. Note that the time series shown only include hold-out estimates coincident with field measurements used for validation and do not represent the final time series of the study. They are provided to illustrate that the validation captures regional temporal patterns seen in the field data.

metrics include a mean absolute error of 0.25 meters (mape = 14%) and a bias of -0.02 meters. The distributions of estimates generated through the bootstrap sampling procedure have an average standard deviation of 0.09 meters around the mean estimate. As each re-sampling propagates varying amounts of model error into the final mean annual value for a region, this low standard deviation suggests that the bootstrapping procedure likely further reduces the uncertainty of our annual regional estimates.

Feature importance, measured as gain (i.e. the improvement in accuracy when a given feature is included), shows that optical variables, especially the dominant wavelength, contribute the most predictive capability to the model (Appendix D: Figure S5). To further validate the contribution of optical variables to the model, we validated a second, purely optical model on the same training and testing data which resulted in an RMSE of 1.3 m. The purely optical model was able to explain 50% of the total variance (R^2) within the validation dataset compared to 72% from the combined landscape model. This difference indicates that the optical parameters contributed up to 70% (0.50/0.72) of the explained variance within the final combined landscape model, with the static lake and landscape variable characteristics contributing at least 30%. The calculation of ALE values provides additional detail on the underlying structure of the model as well as evidence that the model is capturing many of the physical relationships we would expect. For example, we see that as the dominant wavelength of an observation moves from 475 nm (within the blue spectrum) to 560 nm (within the green spectrum) the impact on clarity predictions goes from a 50 cm increase to a 75cm decrease. This difference likely captures decreased clarity as algae and suspended sediment increases.

Model performance was also broken down by lake size, satellite, data source, and time to ensure that predicted trends were not artefacts of lake or sensor characteristics (Appendix D: Figure S7). While variations in model fit across lake sizes, sensors, and data sources are nominal, the validation did show a slight increase in bias over time, with clarity in earlier years being slightly overpredicted on average and clarity in later years being slightly underpredicted.

However, if anything, this small change in bias over time makes our trend predictions conservative as later years are generally underpredicted. We included a breakdown by data source because LAGOS-NE field measurements are all geolocated to lake center points while WQP uses explicit sampling site coordinates (Ross et al., 2019). For observations recorded in both, we deferred to WQP because of the spatial specificity. However, validation results from both datasets show strong agreement, likely because the vast majority of lakes are small enough that there is minimal variation between lake center points and nearby sampling locations. This similarity also supports the above stated decision to predict clarity based on median center point reflectance values rather than median whole lake reflectance values.

As an additional check, we conducted two comparisons of model performance against known benchmarks in the field. First, we compared our regional estimates of lake water clarity to those of the 2007 and 2012 National Lake Assessments and found strong agreement between the reported field values and our model predictions (mape = 17.7%) (Appendix D: Figure S8). Second, we generated mean summer predictions for the individual lakes included in LakeBrowser (Olmanson et al., 2008), a well-validated water clarity remote sensing project focused on over 10,000 lakes in Minnesota (https://lakes.rs.umn.edu/). Comparison of the predictions from the two modelling approaches show agreement when comparing annual estimates at the ecoregion level used by LakeBrowser (R^2 = 0.82) and when compared to field data from the WQP and LAGOS-NE (Appendix D: Figure S9).

Section 3.2: Trends in U.S. Lake Water Clarity

Time series generated for the NLA sample of lakes show that, on average, water clarity in U.S. lakes increased at a rate of 0.52 cm yr^{-1} from 1984-2018. Seven of the nine NLA ecoregions show significant positive trends ($p < 0.05$) that varied from 0.23 cm yr^{-1} ($p = 0.040$) in the Coastal Plains to 1.00 cm yr^{-1} ($p < 1e^{-5}$) in the Northern Appalachians (Figure 4.2). Significant trends were absent in the Southern Appalachian and Southern Plains regions, but no

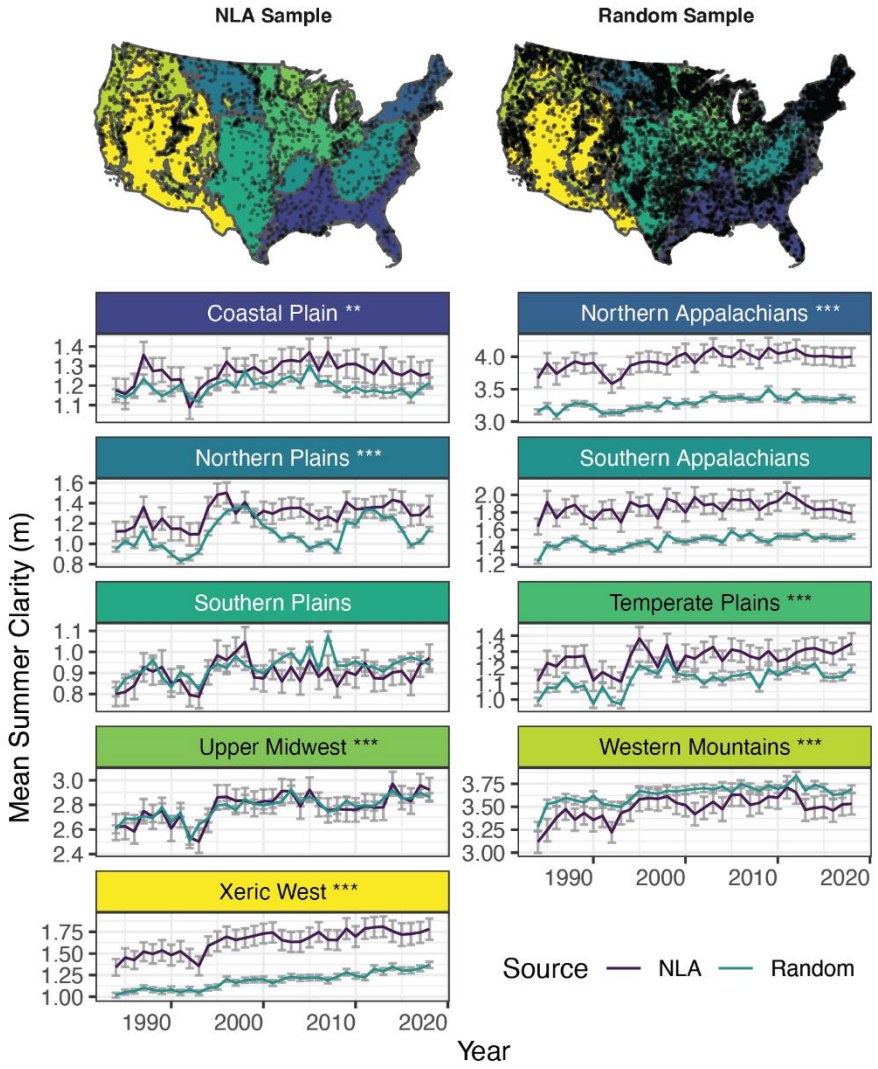

Figure 4.2. Regional modelled trends in water clarity for the statistically stratified sample of NLA lakes that are Landsat visible and a large random sample of Landsat visible lakes. Trends and their associated confidence intervals represent the mean and standard deviation of values calculated through 1000 iterations of bootstrap sampling of the NLA and random sample lakes respectively. Points on maps represent individual lakes included in the sample. Asterisks indicate significance levels of trends determined by Thiel-Sen slopes at 90% (*), 95% (**), and 99% (***) confidence levels for the NLA sample of lakes.

region had a significant decline in clarity. All regions with significant trends show clarity shifts throughout the study period that are greater in magnitude than their mean confidence interval.

Interannual variations in percent clarity change between ecoregions are significantly correlated ($p < 0.05$) in 24 of the 36 (67%) possible region pair combinations (Appendix D: Figure S10). Additionally, during 29% (n=10) of the observed years, at least eight of the nine

ecoregions showed synchronous increases or decreases in clarity compared to the previous year. While some of these years line up with discrete events (e.g., 1987 was heavily impacted by the Pacific Decadal Oscillation), ascribing this synchrony to specific climatological or anthropogenic drivers is difficult due to the multiscale controls on lake water clarity (Soranno et al., 2014; Rose et al., 2017). However, the scale of the changes suggests that drivers of water clarity function at national scales for at least some parts of the study period.

Section 3.3: Impacts of lake size and population

Recent studies of large-scale drivers of inland water quality suggest both that 1) a variety of anthropogenic and climate forcings are leading to an increase in algal blooms and concomitant decreases in water clarity in many lakes (O'Neil et al., 2012; Ho et al., 2019), and that 2) nutrient loading of U.S. rivers, particularly near urban areas, is decreasing (Keiser and Shapiro, 2019; Stets et al., 2020), a trend that should translate to decreased algal growth in downstream waters, particularly if these receiving systems have relatively short mean water residence times or are isolated from non-point sources of nutrient inputs (Jeppesen et al., 2005; Schindler, 2010). These contradictory narratives may reflect limited use of representative samples at large spatial scales, with most studies systematically under-sampling smaller waterbodies despite their numerical dominance and ecological significance (Downing et al., 2006).

To better compare our analysis to previous work focusing on larger lakes and river systems, we generated annual water clarity time series for all U.S. lakes larger than 10 km^2 (n = 1,105) in addition to our NLA and random samples to create a full dataset of 14,971 unique lakes. From this sample, we selected only those lakes with at least 25 years of cloud-free remote sensing observations (n_{lakes} = 8,897 lakes, $n_{observations}$ = 2,727,021) and binned them by size class (<1, 1-10, 10-100, and >100 km^2) and catchment population density (20% quantiles) to compare how trends differed by lake size and examine potential links to improving stream water quality in urban areas. The resulting distributions of trends show that the most significant

clarity improvements are occurring in smaller waterbodies and in densely populated areas (Figure 4.3). Lake size and population density are not significantly correlated, nor are these results related to differences between natural lakes and reservoirs, which show no significant difference in their distribution of trends (p = 0.69). For lake size, median trends for lakes in the smallest to largest size classes are 0.28, 0.19, 0.08, and 0.02 cm yr^{-1}, respectively, with all but

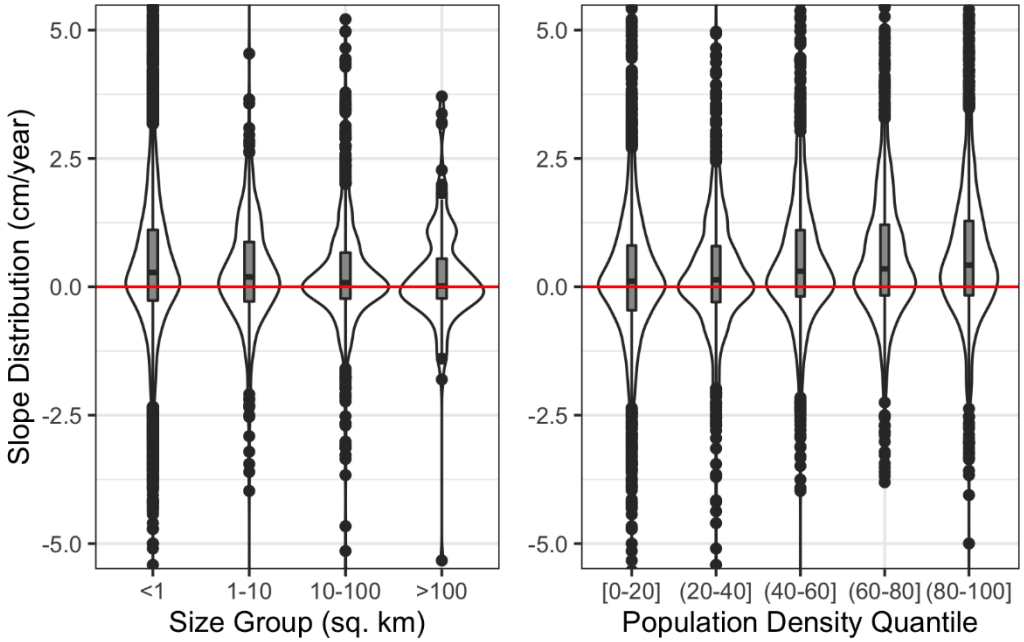

Figure 4.3. Distribution of modelled trends in lakes with greater than 25 years of observations by (left) lake size class (<1 km2, n= 7,339; 1-10 km2, n=509; 10-100 km2, n= 925; >100 km2, n=124) and (right) 2010 catchment population density quantiles. Actual values for quintiles in terms of people per km2: [0-1], (1-3], (3-11], (11-43], (43, 3,970]. Y-axis limits set to -5 to 5 for visualization.

the last class significant at a 99% confidence level. Trends for lakes in catchments within the lowest population density quintile (20%) were approximately four times smaller than for lakes in the most urban upper quintile ($p = 2.2e^{-16}$). Given these trends and the important controls of population density and lake size, research focusing primarily on large lakes may accurately find that water clarity is not increasing. However, the more systematic analysis presented here provides a more complex story in which clarity dynamics are dependent on lake-specific limnological and geographic attributes.

Section 3.4: Sampling impact on patterns of water clarity

To examine the effect of lake sampling on observed patterns in water clarity, we replicated our NLA analysis using: 1) remote sensing estimates for a large random sample of lakes (n = 13,362, Figure 4.2), and 2) the entirety of field data from both LAGOS-NE and WQP, two of the largest national field databases of water quality in the U.S (n = 1,296,659 observations between 1984 and 2018). Results of this comparison show that the NLA sample of lakes accurately reflects temporal patterns of lake clarity across ecoregions compared to a random sample, with some minor geographical exceptions (Figure 4.2). Regardless of these differences, regional temporal patterns in water clarity are highly correlated between the NLA and random samples, with Pearson's Correlation Coefficients ranging from 0.55 ($p = 5.4e^{-4}$) in the Southern Plains to 0.91 in the Upper Midwest ($p = 1.0e^{-5}$). These high correlations between

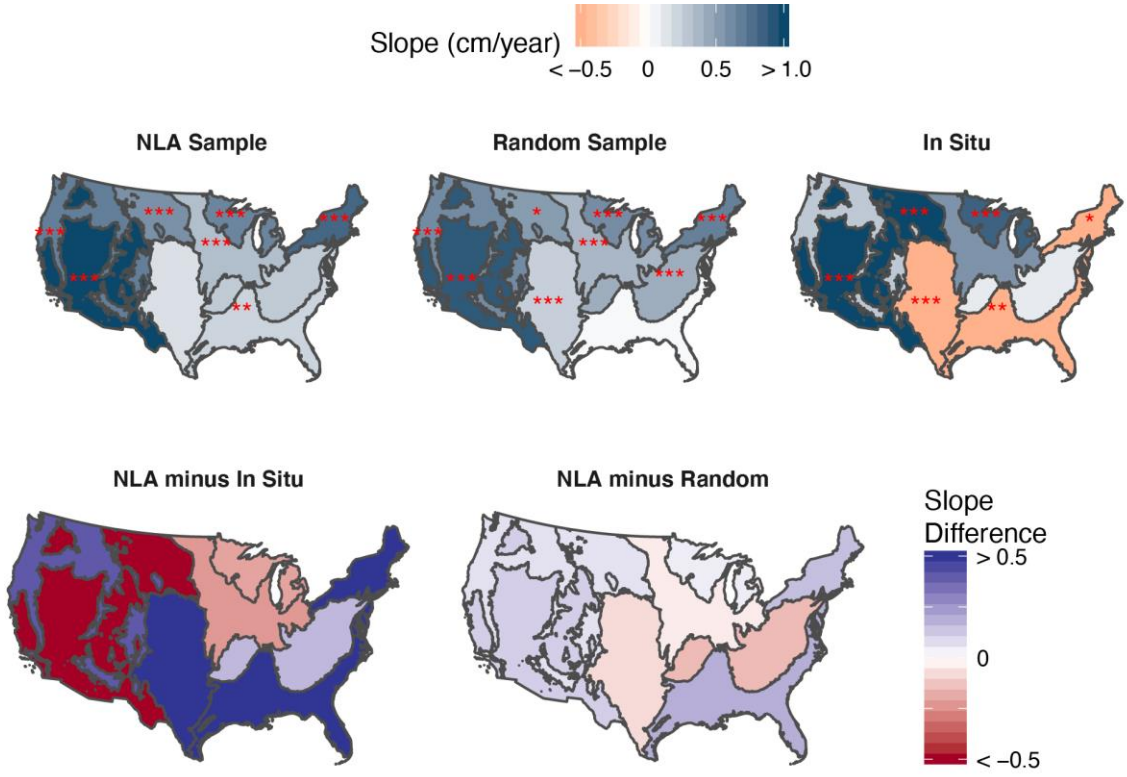

Figure 4.4. Differences in observed ecoregion trends *when conducting the analysis with all the in situ samples from the WQP/LAGOS-NE and the modelling results from the NLA lake sample and a large random sample. Asterisks indicate significance levels of trends determined by Thiel-Sen slopes at 90% (*), 95% (**), and 99% (***) confidence levels.*

samples suggest that the NLA sample is representative of a larger random sample of lakes and that observed trends are insensitive to lake sampling given a large enough sample size and regular sampling intervals.

Conversely, comparison of the remotely sensed NLA and large random samples to historical field observations from LAGOS-NE and WQP reveals substantial discrepancies in overall trends (Figure 4.4). Time series of historical regional clarity calculated with the full set of field data lack significant correlations ($p < 0.01$) with the time series from the NLA sample in seven of the nine study regions. Slopes differ by orders of magnitude from the closely-matched random and NLA samples, in some cases with significant trends in the opposite direction. These results emphasize that conducting an identical analysis with spatiotemporally inconsistent and potentially *ad hoc* field sampling leads to substantially different trends in water clarity compared to the same analysis using representatively sampled remote sensing estimates.

Section 4: Discussion

Our analysis of long-term trends in lake water clarity across the United States highlights that:

- Overall clarity in U.S. lakes increased between 1984 and 2018. This increase was concentrated largely in lakes smaller than 10 km^2 and in more urban areas.
- A systematic understanding of national patterns in lake water clarity requires a representative sample of lakes. These macrosystem-level patterns are not reflected in aggregated historical field data.

By applying our model across both the NLA sample of lakes and a larger random sample, we successfully capture long-term patterns in U.S. lake water clarity that are unobservable in historic and contemporary field sampling efforts. The NLA represents the current best-practice in large scale field monitoring across the U.S.; however, we show that lake clarity nationally has distinct temporal patterns that are not fully captured with the 5-year return period of the NLA field sampling efforts. High correlations between trends observed with

different lake samples, high correlations in time series among regions, and periods of uniform change at the national scale all point to the influence of one or more drivers of lake water clarity operating at a national scale or larger. We examined relationships between observed water clarity patterns and potential forcing variables (temperature, precipitation, sulfate deposition, and the Pacific Decadal Oscillation, Appendix D: Figure S11) and found that the regional impacts of these correlations varied, likely due to complex, cross-scale interactions that lead to variable regional influences as different drivers interact with each other (Soranno et al., 2014; Rose et al., 2017; Read et al., 2017). However, while more difficult to quantify, the period analyzed here begins directly after a round of sweeping environmental legislation in the 1970s and 1980s. These major national level policies include the Clean Water Act (CWA 1972; amended 1977 and 1987), the National Environmental Policy Act (NEPA 1969), the Clean Air Act (CAA 1963, amended 1965, 1966, 1967, 1969, 1970, 1977, 1990), the Safe Water Drinking Act (SWDA 1974, amended 1986,1996), and the Endangered Species Act (ESA 1973), all of which targeted freshwater resources and habitat to varying extents.

Our results are consistent with recent studies showing regional (Wong et al., 2018; Ator et al., 2019) and national (Keiser and Shapiro, 2019; Stets et al., 2020) improvements to U.S. streams and rivers (Wong et al., 2018; Ator et al., 2019; Keiser and Shapiro, 2019; Stets et al., 2020) and lakes (Keiser and Shapiro, 2019) directly attributable to the CWA. Specifically, they show declining nutrient concentrations in urban areas caused by reductions in point source pollution and improved stormwater management emphasized by the CWA. Although agricultural streams have not undergone significant changes in nutrient loads, they have shown declines in suspended sediments, consistent with improved sediment management practices (Stets et al., 2020). These recorded improvements in streams and rivers provide a mechanism for increasing lake water clarity, as changes in fluvial systems often equate to changes in sediment and nutrient inputs to lakes (Fraterrigo and Downing, 2008). This argument assumes that the observed improvements in clarity can be attributed to declining suspended sediment and

nutrient concentrations rather than the other contributor to water clarity – 'colored' dissolved organic matter (cDOM) because where cDOM patterns exist in lakes, they are predominantly positive (Monteith et al., 2007) and therefore not contributing to increases in clarity.

Evaluating long-term nutrient dynamics is more challenging because of limitations in data availability over the period of study at the national scale. An analysis of the 17-state region represented by the LAGOS database revealed that total nitrogen decreased while total phosphorus concentrations have neither decreased nor increased in the vast majority of lakes sampled during summer months between 1990 and 2013 (Oliver et al., 2017). While this nutrient decrease alone potentially contributed to increased lake clarity in nitrogen-limited waterbodies, the study lacks lake water quality data that corresponds to the period of greatest change observed in streams, which was steepest from 1982-1992 within urban areas (Stets et al., 2020). The diminishing improvements in stream water quality after this period are likely because investment in municipal and industrial water pollution control efforts began to gradually taper off in the mid-1990s (Keiser et al., 2019). Even allowing for a delay in water quality response to phosphorus reductions (Jeppesen et al., 2005), these funding patterns are consistent with the greatest gains in water clarity occurring over the first two decades of the CWA within lakes in densely settled areas and smaller waterbodies that tend to be more responsive to management activities because of their shorter average water residence times. Our results support this conclusion, with smaller lakes showing over three times the median increase in clarity than larger lakes ($p = 4.7e^{-8}$), with lakes in catchments with higher population density showing over four times the median increase in clarity than lakes in low population density catchments ($p = 2.2e^{-16}$) (Figure 4.3), and a slowdown of clarity improvements after 2000 due to diminishing returns of reduced point source pollution. This slowdown was likely exacerbated due to difficulties reducing nonpoint sources of pollution, particularly in some regions of the country where changes in the precipitation regime are exacerbating nutrient loading to surface waters (Ballard et al., 2019).

Comparison of observed trends across the NLA sample of lakes, a large random sample, and historical field records provides both empirical support for the representativeness of the NLA and evidence for the shortcomings of relying solely on potentially biased historical field samples for systematic monitoring of freshwater resources. Examining trends at the lake and regional level highlights the potential for an unrepresentative sample of lakes to inaccurately depict system-wide patterns. Specifically, when we restrict analysis to larger waterbodies, we find only nominal change in U.S. lake clarity, but the more inclusive analysis presented here suggests that overall lake water clarity within the United States has increased over the past 35 years. While this is the first study of trends in lake water clarity at a national scale, it extends regional studies throughout the northeast that have found water quality in lakes is either largely stable or improving (Peckham and Lillesand, 2006; Binding et al., 2015; Canfield et al., 2016; Oliver et al., 2017), as well as work in China and Sweden indicating that national management policies are decreasing eutrophication rates (Fölster et al., 2014; Ma et al., 2020; Wang et al., 2020). While more work is required to understand the multiscale drivers of water clarity, the results presented here bring us closer to realizing research goals dating back more than 20 years emphasizing that representative sampling is required for effective monitoring of freshwater resources (Paulsen et al., 1998; Peterson et al., 1999).

APPENDIX A: SUPPLEMENTARY MATERIAL FOR CHAPTER 1

This Appendix includes:

Tables S1:S4

Link to the inland water quality remote sensing index in its entirety here:

https://docs.google.com/spreadsheets/d/1GMka4B-E16FmXBWjv0lhBN0T-07oeZT4riepMMHvZz4/edit?usp=sharingusp=sharing

Table S1. Summary of the optically active water quality indicators measured through inland water remote sensing studies. Specific studies, sensor information, and modelling approaches focusing on the listed parameters and included in the review can be accessed through the inland water quality remote sensing index linked to in Appendix A. For a more detailed, technical discussion of specific algorithms and spectral responses for each parameter see Matthews (2011), Gholizadeh et al. (2016), and Giardino et al. (2019)

Parameter	Parameter Description	Measurement Purpose	Dominant Spectral Response	Number of Studies Reviewed
Chlorophyll-a	Photosynthetically active compounds found in plants, algae, and cyanobacteria that convert light into energy for photosynthesis	Lake productivity/trophic state, harmful algal bloom detection	Fluorescents - 680 nm; Absorption - 450-475 nm and 670 nm; Backscattering: ~550 nm and ~700 nm	132
Total Suspended Solids	Inorganic and organic particles held in suspension throughout a water column	Inorganic sediment flux, biogeochemical cycling, light conditions	Reflectance peak between ~500 and ~800 depending on concentration	94
Colored Dissolved Organic Matter	Colored portion of total dissolved organic carbon	Carbon production and cycling, light conditions	Highly absorptive, especially below 500 nm	30
Water Clarity	Measure of total light penetration into a waterbody, typically measured as Secchi Disk Depth or turbidity	Lake productivity/trophic state, light conditions, sediment concentrations, harmful algal bloom detection	Highly dependent on the composition of the previous parameters with generally higher reflectance across the spectrum at lower values	89

Table S2. Summary of the common approaches to algorithm development for remote sensing of inland waters studies.

Modelling Approach	Description	Benefits	Limitations	Number of Studies Reviewed
Empirical	Algorithms involving empirical relationships between spectral bands and band ratios and the water quality parameter of interest, typically through linear regression.	Transparent, easily interpretable, no a priori assumptions required	Non-generalizable beyond the range and setting of the training data, unable to handle complex non-linear interactions	279
Semi-Empirical	Spectral band-ratio algorithms based on the physical properties of the water quality constituent of interest	Easily interpretable, more generalizable than empirical approaches	Unable to handle non-linear interactions, requires site-specific calibration and validation	15
Semi-Analytical	Analytical inversion-based models calibrated using field observations	Theoretically generalizable, mechanistic, potential for cross-sensor transferability	Requires representative field data for calibration and validation, computationally more expensive	61
Machine Learning	A subset of empirical methods which leverage large amounts of data and iterative learning to extract relationships between spectral properties and water quality parameters	Capable of handling non-linear relationships, no a priori assumptions required, generalizable depending on training data	Prone to overfitting, opaque, computationally expensive	29

Table S3. Summary of collected information for the detailed literature review index.

Index Parameter	***Parameter Description***
Identifying information	Composed of an index number, author(s), journal, title, year of publication, DOI, and total citation count pulled from SCOPUS.
Locational Information	Country of focus and central latitude and longitude of the study area.
Study Scale	The order of magnitude of the study area in km2. The surface area of the waterbody for single waterbody studies, total area of all waterbodies for spatially discontinuous studies, or the total area of the entire region if the study area was contiguous. Represented as 10^1 km2, 10^2 km2, 10^3 km2, etc.
Study Period	The duration of the study. If no temporal analysis was conducted than the period was marked na. Total study length was determined as the date of the first image to the date of the final image.
Sensor Information	Satellite and/or airborne sensors utilized and the spectral resolution of each sensor (hyperspectral or multispectral)
Atmospheric Correction	A binary yes/no regarding the application of an atmospheric correction for the final model.
Parameters	The water quality parameters included in the study.
Waterbody Type	The waterbody of focus (Rivers, Lakes/Reservoirs, Estuaries, or Deltas)
Modeling Approach Information	The model inputs, chosen modelling methodology, and total number of models used. Also included is information on if different modelling approaches were compared (i.e. empirical vs semi-analytical approaches).
Number of Methodology Figures	The total count of figures focused on background information. These include study area maps, flow charts, tables with input data, and other figures depicting the theory or method behind the modelling approach.
Number of Validation Figures	The total count of figures focused on model validation. These include tables of error metrics and actual vs. predicted plots.
Number of Trend, Impact, and Driver Figures	The total count of figures and tables depicting some spatial or temporal trend. These include maps, timelines, figures depicting correlations between water quality parameters and climatic or anthropogenic drivers, and figures or tables examining the impacts of changing water quality parameters on ecological or anthropogenic systems.
Paper Category	The final classification of the paper based on total figure counts and proposed hypothesis/science questions.
Model Fit Error	Reported error metrics for model fit.
Model Validation Error	Reported error metrics for model validation based on data not used in model development.

Table S4. Summary of studies using remote sensing to analyze impacts and drivers of water quality and classified as water quality science papers within the analysis.

	Author	Scale (km^2)	Duration	Water body	Approach	Constituent	Analysis Summary
Anthropogenic Drivers	(Ren et al., 2018)	10^3	1-5 Years	Lakes	Empirical	SDD	Examines spatiotemporal variations in water clarity and sediment discharge connected to the Three Gorges Dam. Finds that certain areas have inversely corelated clarity driven by surface flow dynamics.
	(Hou et al., 2017)	10^5	>10 Years	Lakes	Empirical	TSS	Examines the spatiotemporal response of TSS in the Yangtze River Basin to the construction of the Three Gorges Dam. Found that the reservoir construction drove varying regional effects, and that recent improvements in TSS are likely correlated with increased NDVI in the area.
	(Cui et al., 2013)	10^3	5-10 Years	Lakes	Empirical	TSS	Examines the spatiotemporal trends of TSS in a Chinese lake and how it correlates with dredging activities and climactic drivers.
	(McCullough et al., 2012)	10^4	>10 Years	Lakes	Empirical	SDD	Utilizes Landsat data to examine water clarity in Maine over 15 years. Finds that decreased clarity is somewhat correlated to the presence of timber harvesting in a watershed.
	Cui, Wu, and Liu, 2009	10^3	1-5 Years	Lakes	Empirical	SDD	Examines the interactions between elevated TSS levels driven by river backflow into Poyang Lake (China) and lake dredging. Finds that the combined impact is greater than either event by itself.
	(Wu et al., 2007)	10^3	5-10 Years	Lakes	Empirical	SDD	Utilizes Landsat and MODIS data to measure the effect of dredging on water clarity.
Climatic Drivers	Lymburner et al., 2016	10^5	>10 Years	Lakes	Semi Analytical	TSS	Examines interactions between decadal climate variations (ENSO) and TSS concentrations in optically heterogenous lakes across western Australia.
	(Robert et al., 2017)	10^2	>10 Years	Lakes	Empirical	TSS	Examines climactic drivers of TSS extremes and seasonal cycles in Mali lakes.
	(Huang et al., 2015)	10^3	< 1 Month	Lakes	Empirical	TSS, Chl-a, TP	Examines how the provision of phosphorous from sediment resuspension controls TSS and chl-a dynamics in a shallow lake.
	Zhang et al., 2016	10^3	5-10 Years	Lakes	Empirical	TSS	Analyzes spatiotemporal dynamics of river plumes in a shallow lake and their correlation with rainfall magnitude.
	Zhu et al., 2014	10^3	1-5 Years	Lakes	Semi Empirical	Algal Blooms	Examines how typhoon induced sediment resuspension and nutrient mixing impact the development dynamics of algal blooms.

	Author	Scale (km^2)	Duration	Water body	Approach	Constituent	Analysis Summary
	Curtarelli et al., 2015	10^2	< 1 Year	Lakes	Empirical	Chl-a	Combines remote sensing with hydrodynamic modelling to examine the role of thermal stratification and mixing on chl-a dynamics.
	Matthews, 2014	10^3	>10 Years	Lakes	Empirical	Chl-a	Identifies long term trends in chl-a and cyanobacteria blooms across 50 lakes in South Africa. Discusses how clustering of overarching trends and lake trophic state follow biogeophysical landscape properties.
	Huang et al., 2014	10^3	>10 Years	Lakes	Semi Empirical	Chl-a	Examines the role of wind, precipitation, decadal climate signals, and resuspension driven nutrient availability on the presence/dynamics of algal blooms.
	(Duane Nellis et al., 1998)	10^2	< 1 Year	Lakes	Semi Analytical	TSS	Examines the impacts of a flood event on sediment concentration, pool size, and water quality dynamics in a Kansas reservoir.
	(Wang et al., 2012)	10^3	5-10 Years	Multiple	Empirical	Turbidity	Examines the role of hurricanes in controlling turbidity levels in Florida's Lake Okeechobee and two connected estuaries.
	Ng et al., 2011	10^2	< 1 Year	Lakes	Semi Empirical	Chl-a	Incorporates remote sensing data into a 3D hydrological model to analyze dinoflagellate dispersion within a lake ecosystem. Finds that bloom growth is controlled by stratification while dispersion is driven by wave forces.
	(Sass et al., 2008a)a	10^3	>10 Years	Lakes	Empirical	Chl-a	Examines variations in trophic state within boreal lakes driven by climactic variables. Finds that growing season length and May temperatures are key drivers.
	(Bayley et al., 2007)	10^2	>10 Years	Lakes	Empirical	Chl-a	Tests the 'stable states' hypothesis regarding trophic status for boreal lakes and finds that most lakes in the study area have one dominate state rather than two.
	(Feng et al., 2015)	10^4	5-10 Years	Lakes	Semi Empirical	Chl-a	Identifies high risk eutrophication areas and their relationship to connectivity and precipitation.
	(Duan et al., 2017)	10^2	>10 Years	Lakes	Machine Learning	Chl-a	Analyzes spatiotemporal distributions of phycocyanin and chl-a and develops a hazard assessment map to identify safe areas for drinking water outlets.
Landscape Level Drivers	(Dvornikov et al., 2018)	10^2	Snapshot	Lakes	Empirical	CDOM	Analyzes landscape level drivers of CDOM in arctic lakes and finds significant relationships between thermocirque presence and elevated CDOM levels.
	(Sass et al., 2008b)	10^3	>10 Years	Lakes	Empirical	Chl-a	Examines connectivity, wetland area, and concentrations of Ca and Mg that control the trophic state of boreal lakes.

	Author	Scale (km^2)	Duration	Water body	Approach	Constituent	Analysis Summary
	(Rose et al., 2017)	10^5	>10 Years	Lakes	Empirical	SDD	Examines how watershed and riparian zone characteristics drive water clarity and finds that during wet years, watershed scale drivers dominate while for dry years riparian characteristics are more important.
Forecasting	(Qin et al., 2015)	10^3	1-5 Years	Lakes	Empirical	Chl-a	Develops a dynamic forecasting model incorporating wind, precipitation, and remotely sensed chl-a concentration to predict algal bloom development in Lake Taihu, China. The applied model helped remove over 1,000,000 tons of algal scum from the lake.
	(Imen et al., 2015)	10^3	1-5 Years	Lakes	Machine Learning	TSS	Utilizes remotely sensed TSS data to construct a real-time forecasting model for predicting degraded water quality near drinking water outlets in Lake Mead.
	(Zhang et al., 2013)	10^3	< 1 Month	Lakes	Mixed	Chl-a	Develops forecasting model capable of predicting algal blooms 3-5 days in advance in shallow Lake Taihu in China.
Water Quality Impacts	(Sandström et al., 2016)	10^3	5-10 Years	Lakes	Product	Chl-a	Utilizes remotely sensed water quality parameters to identify and explain variations in fish habitat and species composition. Found that habitat was highly correlated with CDOM and chl-a levels.
	Torbick et al., 2014	10^5	1-5 Years	Lakes	Empirical	Chl-a	Examines distribution of algal blooms in relation to reported cases of amyotrophic lateral sclerosis (ALS) to identify high risk areas for the disease.
	(Potes et al., 2012)	10^2	1-5 Years	Lakes	Empirical	Turbidity	Incorporates remotely sensed turbidity into a two-layer bulk model to predict surface water temperature.
	(Finger et al., 2014)	10^3	5-10 Years	Lakes	Product	Chl-a	Incorporates remotely sensed chl-a data into a model examining the dynamics and drivers of cholera outbreaks in the Democratic Republic of Congo.
	Pavelsky and Smith, 2009	10^3	< 1 Year	Lakes/ River	Empirical	TSS	Utilizes remotely sensed TSS concentration to examine river velocity, flow reversal, and hyrodologic recharge of floodplain lakes in the Peace-Athabasca Delta.
	(Telmer et al., 2006)	10^5	>10 Years	Rivers	Empirical	TSS	By using the correlation between TSS and mercury, the authors present a remote estimation of mercury concentrations, which they use to examine likely drivers of increased mercury concentrations from gold-mining.
	(Overeem et al., 2017)	10^4	>10 Years	Rivers	Empirical	TSS	Examined flux of suspended sediment from Greenland ice sheet, highlighting disproportionately high global contribution of sediment.

	Author	Scale (km^2)	Duration	Water body	Approach	Constituent	Analysis Summary
Water Quality Dynamics	(Griffin et al., 2011)	10^4	5-10 Years	Rivers	Empirical	CDOM	Used remote sensing of CDOM and DOC to highlight the interannual variability of both, while also highlighting that the spatial and temporal variability likely causes underestimates of DOC flux from Kolyma River.
	(Walker, 1996)	10^5	1-5 Years	Estuaries	Semi Analytical	TSS	With remote sensing estimates of suspended sediments, Walker explores causes of plume variability in the Mississippi River.
	(Falcini et al., 2012)	10^4	< 1 Year	Rivers	Product	TSS	Used remote estimates of TSS to examine sedimentation in wetlands and link them to hydrodynamics with implications for wetland restoration

APPENDIX B: SUPPLEMENTARY MATERIAL FOR CHAPTER 2

This Appendix includes:

Figures S1-S5

Table S1

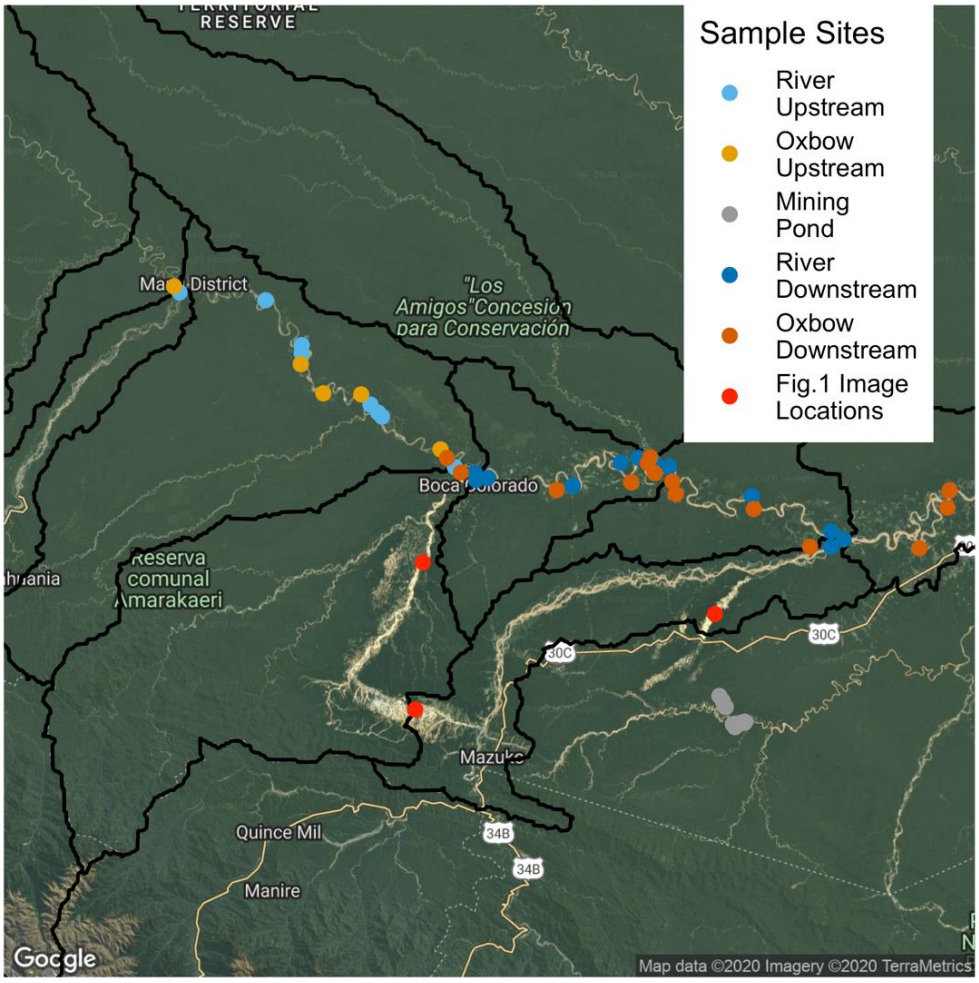

Figure S1: Map of sampling locations for Hg analysis. Black lines indicate the study basins, as displayed in Figure 2.2. Mining ponds within the study basins themselves were inaccessible due to safety limitations. However, samples were obtained at La Pampa, an area which recently experienced heavy mining but was taken over by the Peruvian military in 2019. Mining practices at La Pampa are representative of those throughout the region.

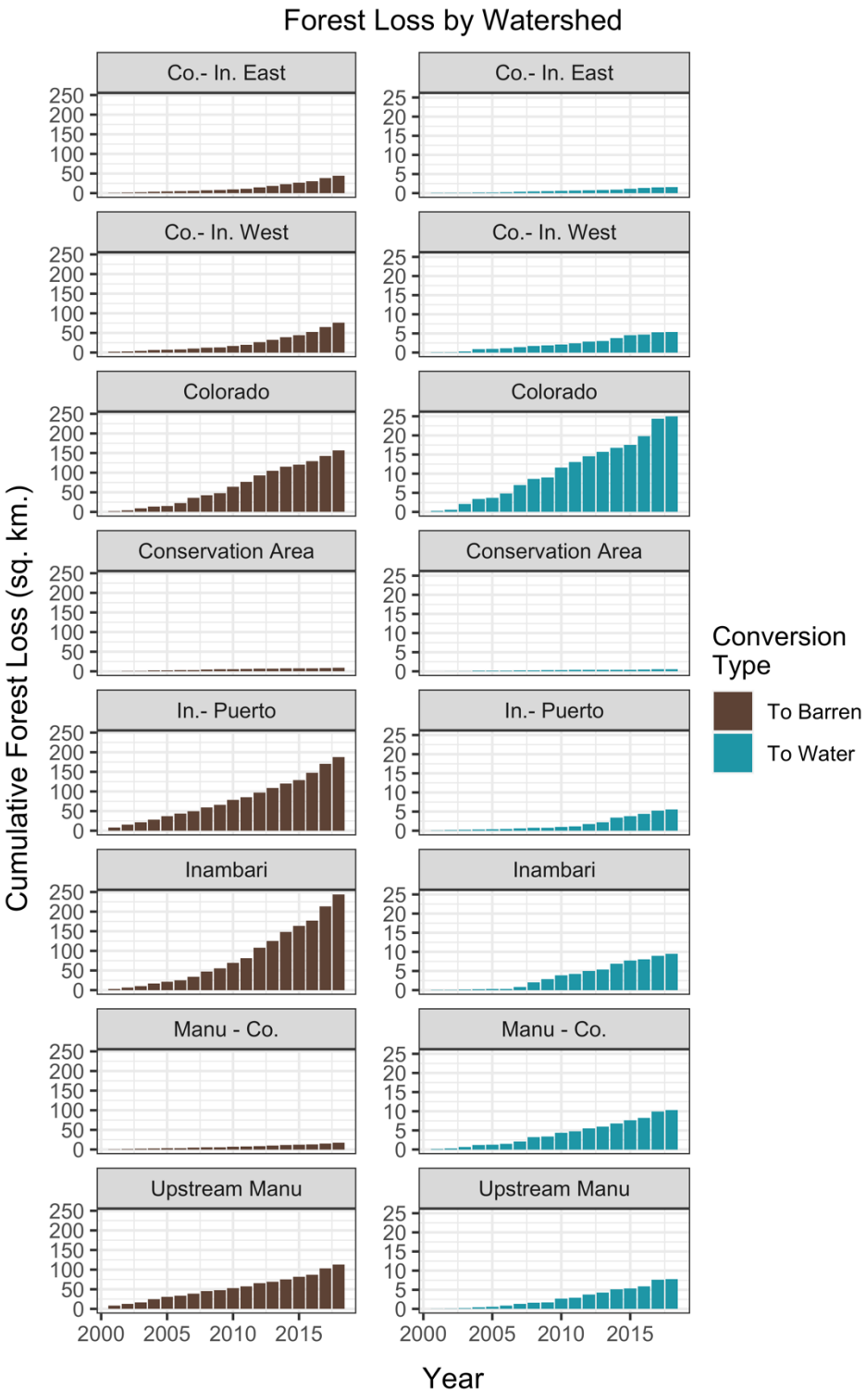

Figure S2: Cumulative forest loss by watershed and conversion type from any cause between 2000 and 2018.

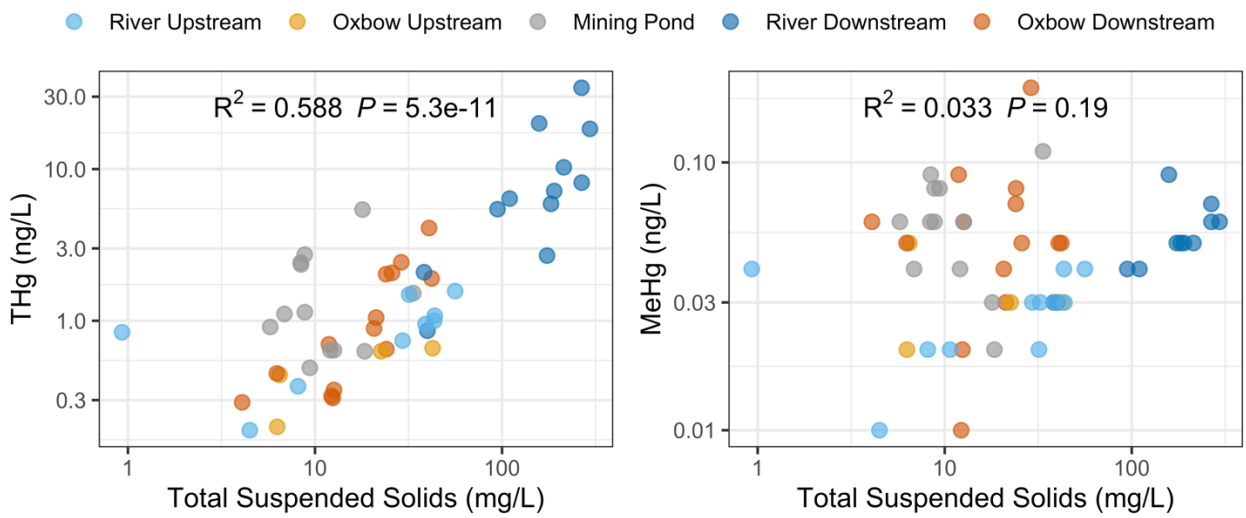

Figure S3: Relationship between water column total Hg (left), MeHg (right), and total suspended solids (TSS) across water bodies upstream and downstream of artisanal gold mining in Madre de Dios, Peru. Note that the axes are in log-log scale.

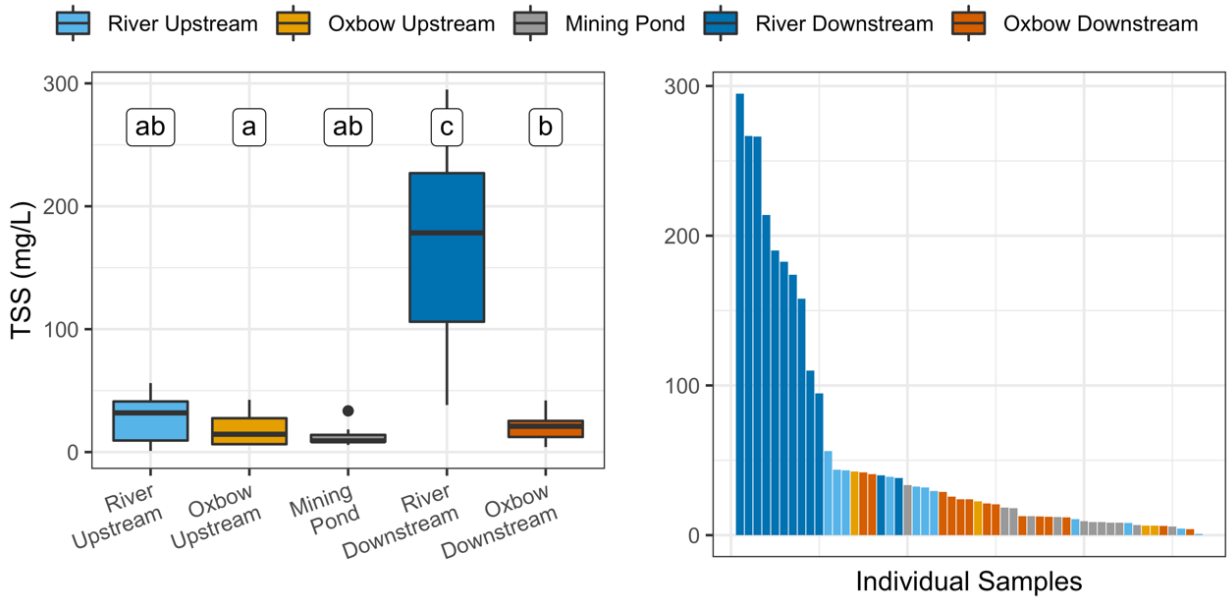

Figure S4: Concentration and distribution of water column total suspended solids (TSS) across water bodies upstream and downstream of artisanal gold mining in in Madre de Dios, Peru. Letters represent statistically significant differences ($p < 0.05$) between values at each location, according to a Kruskal-Wallis Analysis of Variance followed by Dunn's Test.

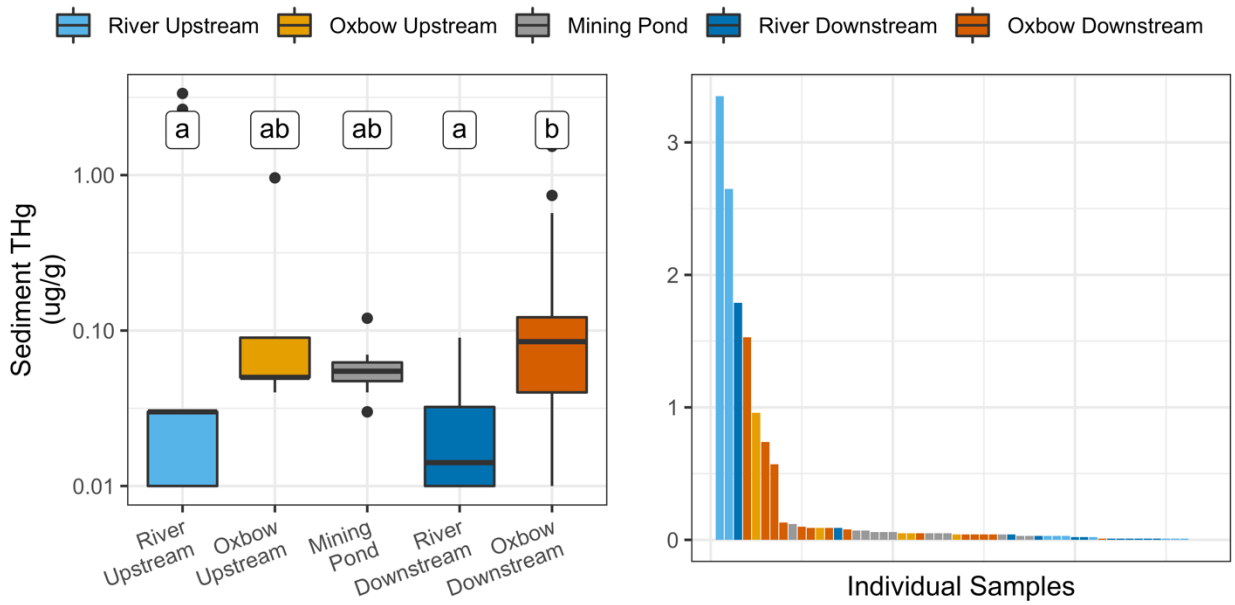

Figure S5: Concentration and distribution of sediment total Hg (THg) across water bodies upstream and downstream of artisanal gold mining in in Madre de Dios, Peru. Letters represent statistically significant differences ($p < 0.05$) between values at each location, according to a Kruskal-Wallis Analysis of Variance followed by Dunn's Test.

Table S1: Total mercury (THg), methylmercury (MeHg), total suspended solids (TSS) and percent carbon (%C) data for water and sediment samples collected in rivers, oxbow lakes, and mining ponds in Madre de Dios, Peru in summer 2019.

Site ID	Site Type	Latitude	Longitude	[THg] water (ng/L)	[MeHg] water (ng/L)	%MeHg water	Average [THg] sediment (μg/g)	[TSS] (mg/L)	%C sediment
R1	river.downstream	-12.71525	-69.73079	18.41	0.06	0.34	0.03	294.96	0.12
R2	river.downstream	-12.72855	-69.75352	34.35	0.07	0.22	0.09	266.18	0.86
R3	river.downstream	-12.70092	-69.75365	8.14	0.06	0.75	0.01	266.67	0.18
R4	river.downstream	-12.639	-69.897	10.27	0.05	0.48	0.01	213.84	0.12
R5	river.downstream	-12.57847	-70.0741	2.09	0.03	1.56	0.01	38.26	0.04
R6	river.downstream	-12.58666	-70.0468	7.17	0.05	0.71	0.02	190.09	0.25
R7	river.downstream	-12.57132	-70.10258	2.69	0.05	1.87	0.04	174.03	0.86
R8	river.downstream	-12.58002	-70.13416	6.39	0.04	0.65	1.79	109.85	0.07
R9	river.downstream	-12.62084	-70.22094	5.44	0.04	0.71	0.01	94.62	0.15
R10	river.downstream	-12.61061	-70.39618	20	0.09	0.46	0.01	157.89	0.04
R11	river.downstream	-12.59836	-70.39838	0.86	0.03	3.96	0.02	39.91	0.44
R12	river.downstream	-12.6071	-70.37541	5.9	0.05	0.89	0.01	182.68	0.06
R13	river.upstream	-12.58797	-70.43443	1.08	0.03	3	0.03	43.69	0.93
R14	river.upstream	-12.4986	-70.56638	1.49	0.02	1.55	0.03	31.88	0.96
R15	river.upstream	-12.49175	-70.57346	0.19	0.01	5.29	0	4.48	0.08
R16	river.upstream	-12.47754	-70.5872	1.57	0.04	2.55	0.01	56.14	0.15
R17	river.upstream	-12.3868	-70.71183	0.84	0.04	5.17	0.03	0.93	0.87
R18	river.upstream	-12.40611	-70.71347	1	0.04	3.8	0.02	43.35	0.15
R19	river.upstream	-12.37264	-70.71174		0.03		2.65	32.43	0.07
R20	river.upstream	-12.29333	-70.77677	0.95	0.03	3.45	0.01	38.99	0.13
R21	river.upstream	-12.27949	-70.93287	0.37	0.02	5.24	3.35	8.12	0.2
R22	river.upstream	-12.26895	-70.94278	0.74	0.03	4.51	0	29.41	0.04
R23	river.upstream	-12.26912	-70.94264		0.02		0.01	10.68	0.26
OL1	oxbow.lake.downstream	-12.59852	-70.07249	2.43	0.19	7.87	0.1	28.92	1.48
OL2	oxbow.lake.downstream	-12.61479	-70.11527	0.65	0.08	11.84	0.57	24.06	1.39
OL3	oxbow.lake.downstream	-12.62844	-70.2504	4.09	0.05	1.33	0.13	40.69	0.76
OL4	oxbow.lake.downstream	-12.57176	-70.4486	1.05	0.03	2.63	0.09	21.23	0.27
OL5	oxbow.lake.upstream	-12.55659	-70.46041	0.63	0.03	4.2	0.96	22.54	1.03
OL6	oxbow.lake.upstream	-12.45771	-70.67259	0.66	0.03	4.45	0.05	42.53	1.85
OL7	oxbow.lake.upstream	-12.40622	-70.71348	0.2	0.02	7.8	0.05	6.28	1.46
OL8	oxbow.lake.upstream	-12.26912	-70.94264				0.04		0.87
OL9	oxbow.lake.upstream	-12.45953	-70.604	0.44	0.05	12	0.09	6.47	1.56
OL10	oxbow.lake.downstream	-12.59755	-70.4237	0.89	0.04	4.29	0.08	20.69	0.57

OL11	oxbow.lake.downstream	-12.61335	-70.04083	0.31	0.02	6.09	0.09	12.44	4.4
OL12	oxbow.lake.downstream	-12.66187	-69.8934	0.45	0.05	10.34	0.74	6.25	2.42
OL13	oxbow.lake.downstream	-12.62909	-69.53897	0.7	0.09	12.65	0.04	11.87	0.67
OL14	oxbow.lake.downstream	-12.659388	-69.542938	2.07	0.05	2.43	0.01	25.81	0.8
OL15	oxbow.lake.downstream	-12.73096	-69.59354	1.9	0.05	2.49	0.04	42.01	0.62
OL16	oxbow.lake.downstream	-12.72838	-69.79144	2.03	0.07	3.67	0.05	23.98	0.62
OL17	oxbow.lake.downstream	-12.58058	-70.08558	0.35	0.06	18.4	0.04	12.63	1.21
OL18	oxbow.lake.downstream	-12.57036	-70.08096	0.32	0.01	3.55	0.04	12.25	2.26
OL19	oxbow.lake.downstream	-12.63518	-70.03457	0.29	0.06	22.25	1.53	4.08	4.03
MP1	mining.pond	-13.04659	-69.92761	2.73	0.06	2.35	0.07	8.81	0.34
MP2	mining.pond	-13.0416	-69.93137	0.64	0.06	8.69	0.03	12.62	0.53
MP3	mining.pond	-13.04051	-69.92562	5.41	0.03	0.56	0.05	17.95	0.50
MP4	mining.pond	-13.04005	-69.91745	0.91	0.06	6.89	0.06	5.76	0.84
MP5	mining.pond	-13.03922	-69.9162	0.49	0.08	16.18	0.12	9.38	0.45
MP6	mining.pond	-13.03837	-69.91466	2.35	0.09	3.98	0.03	8.42	0.39
MP7	mining.pond	-13.03691	-69.90986	0.64	0.04	6.77	0.04	12.07	0.52
MP8	mining.pond	-13.03893	-69.90997	2.42	0.06	2.45	0.06	8.38	0.88
MP9	mining.pond	-12.04069	-69.91524	1.14	0.08	6.99	0.05	8.82	0.53
MP10	mining.pond	-13.01114	-69.94402	1.52	0.11	7.33	0.07	33.53	0.96
MP11	mining.pond	-13.00044	-69.94968	1.11	0.04	3.93	0.05	6.86	0.22
MP12	mining.pond	-12.99166	-69.95575	0.63	0.02	2.91	0.06	18.44	0.29

APPENDIX C: SUPPLEMENTARY MATERIAL FOR CHAPTER 3

This Appendix includes:

Figures S1-S6

Table S1

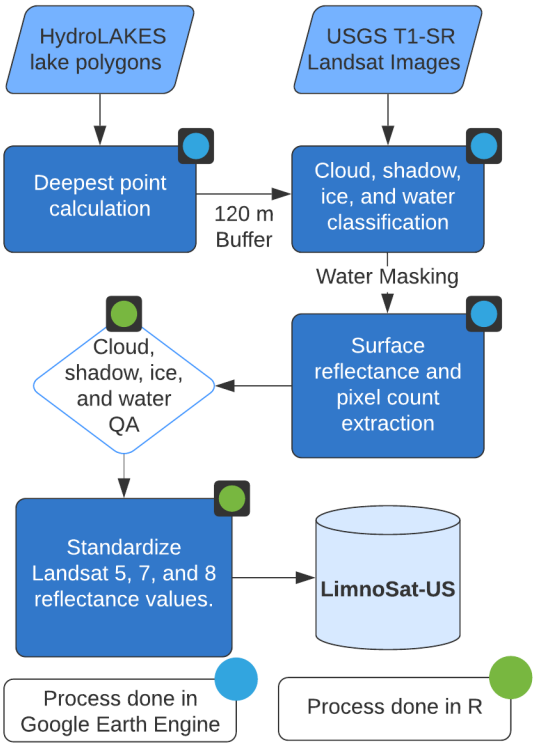

Figure S1. Workflow diagram of key steps in the LimnoSat-US database production.

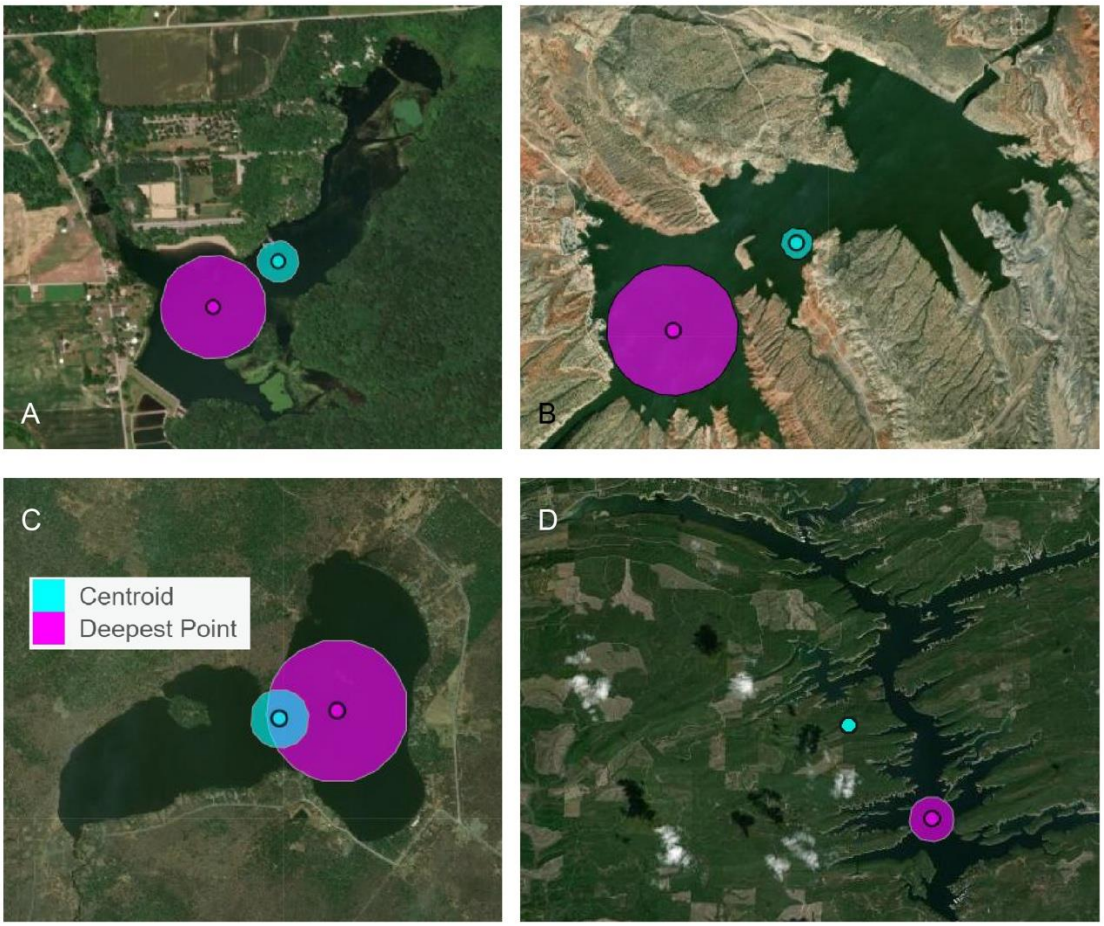

Figure S2. Examples of comparisons between lake centroids and the deepest point calculated using the Chebyshev Center method in (A) Indiana, (B) Wyoming, (C) Maine, and (D) Arkansas. For (D), the centroid doesn't fall within the lake's surface.

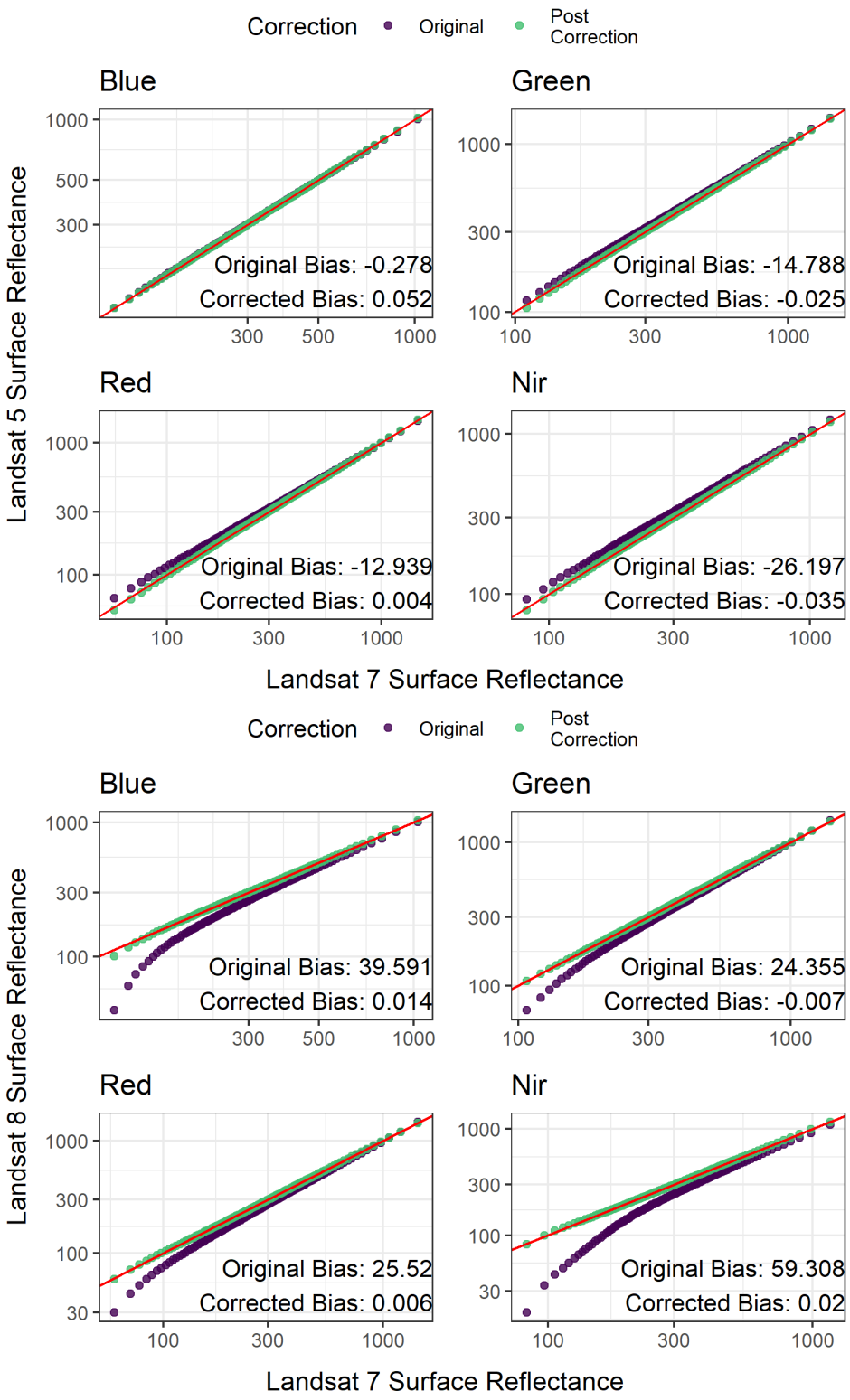

Figure S3. Examples of the distributions of satellite reflectance values between sensors before and after the described correction procedure. Red lines indicate 1:1 lines. Note that plots are in log-log scale.

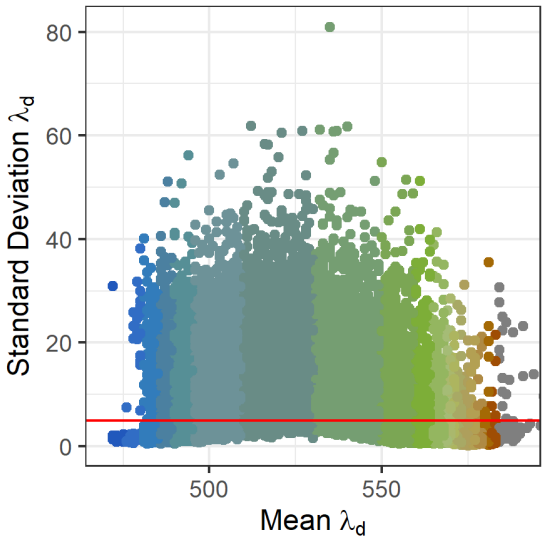

Figure S4. Mean and standard deviation of dominant wavelengths for each non-normalized lake/period time series. Red line represents the cut-off point for the a priori aseasonal cluster. Colors represent associated Forel-Ule Indexes (grey points are outside the forel-ule range).

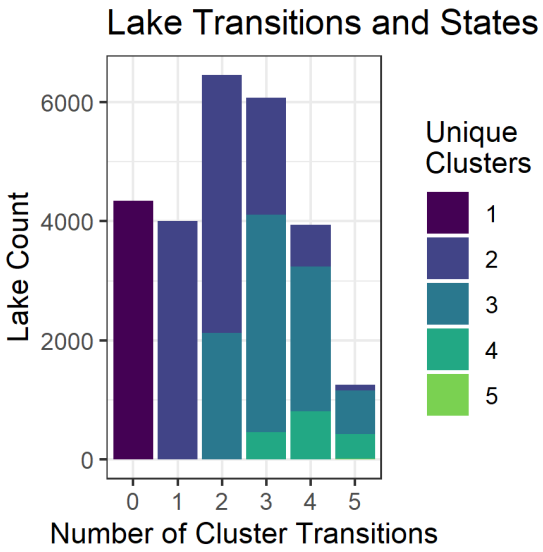

Figure S5. Total counts for lake stability classes (x-axis) colored by the number of unique states each lake occupied throughout the course of the study period.

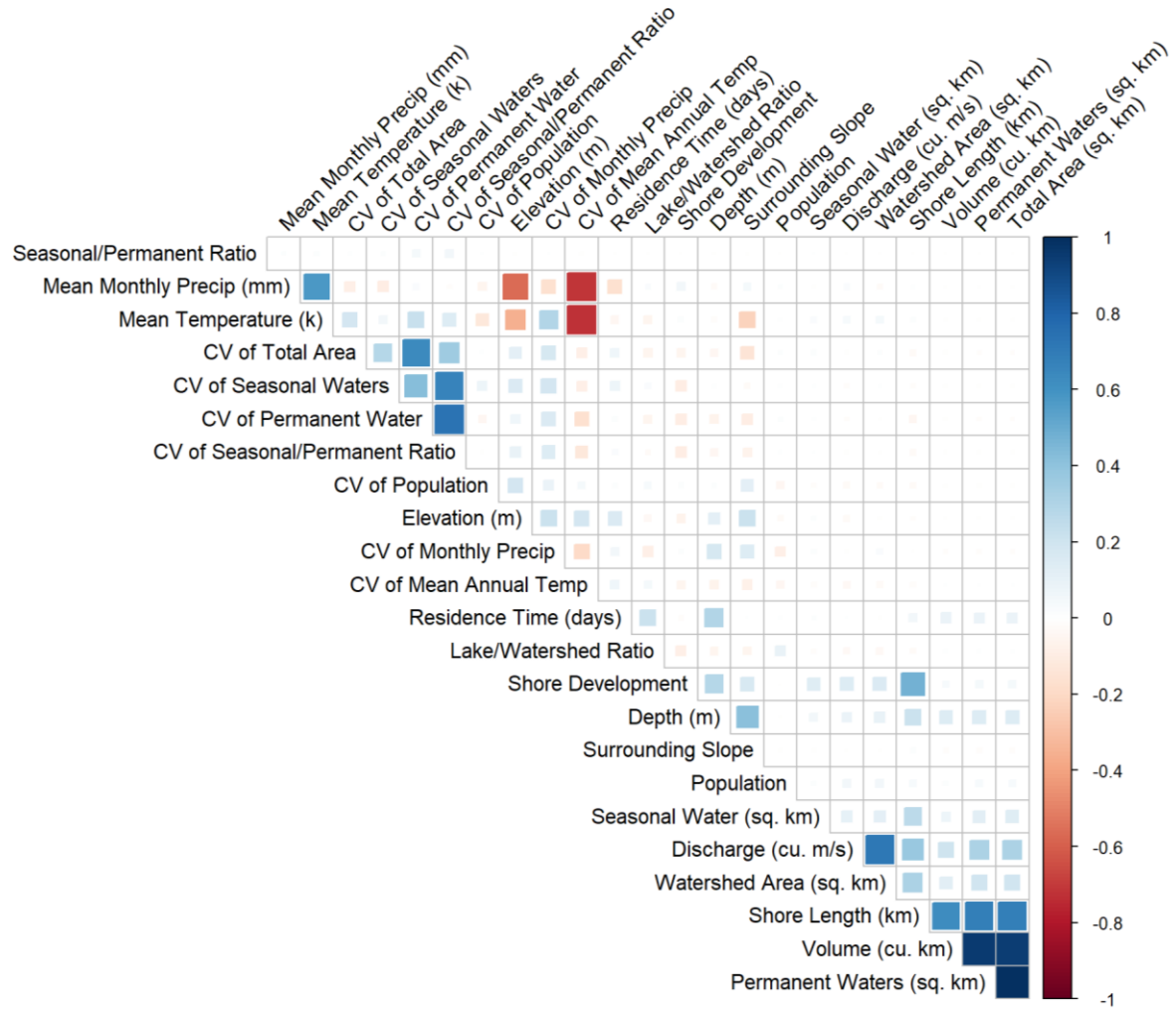

Figure S6. Correlation matrix for variables from HydroLakes and GLPC used to analyze drivers of lake phenology stability.

Variable	Coefficient	Std.Error	p.value
Elevation (m)	0.052	0.003	0.000
CV of Mean Annual Temp	57.610	6.937	0.001
Population	-0.005	0.001	0.002
CV of Seasonal Waters	2.865	0.450	0.003
CV of Population	0.815	0.172	0.009
Discharge (cu. m/s)	-77.415	20.245	0.019
Mean Temperature (k)	-1.460	0.400	0.022
Residence Time (days)	0.047	0.013	0.023
Seasonal Water (sq. km)	-130.614	38.787	0.028
Permanent Waters (sq. km)	-46.695	14.328	0.031
CV of Seasonal/Permanent Ratio	1.872	0.579	0.032
Lake/Watershed Ratio	169.832	53.717	0.034
Shore Length (km)	-8.727	2.784	0.035
Surrounding Slope	11.141	3.672	0.039
Total Area (sq. km)	-33.516	11.478	0.043
Mean Monthly Precip (mm)	-0.514	0.178	0.045
Depth (m)	31.034	11.013	0.048
Volume (cu. km)	-13.772	5.039	0.052
Watershed Area (sq. km)	-0.403	0.156	0.061
Seasonal/Permanent Ratio	-74.721	36.562	0.110
CV of Monthly Precip	-3.867	1.920	0.114
CV of Total Area	-12.886	7.689	0.169
CV of Permanent Water	-2.921	5.279	0.610
Shore Development	-50.000	101.550	0.648

Table S1. Results from regressions of lake and landscape metrics with lake stability ordered by level of statistical significance.

APPENDIX D: SUPPLEMENTARY MATERIAL FOR CHAPTER 4

This Appendix includes:

Figures S1-S11

Table S1

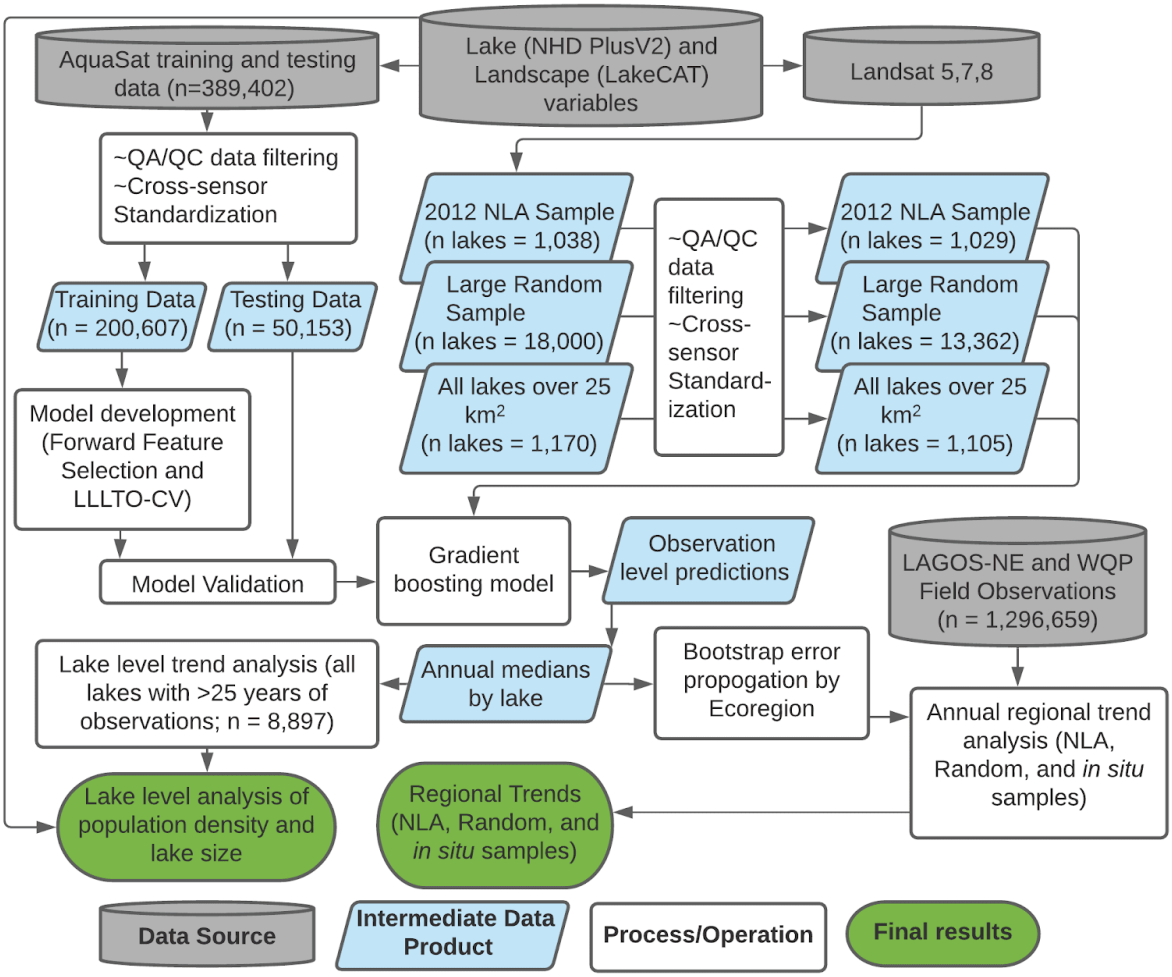

Figure S1: A summary of the project workflow including data sources, lake samples, and intermediate processing steps.

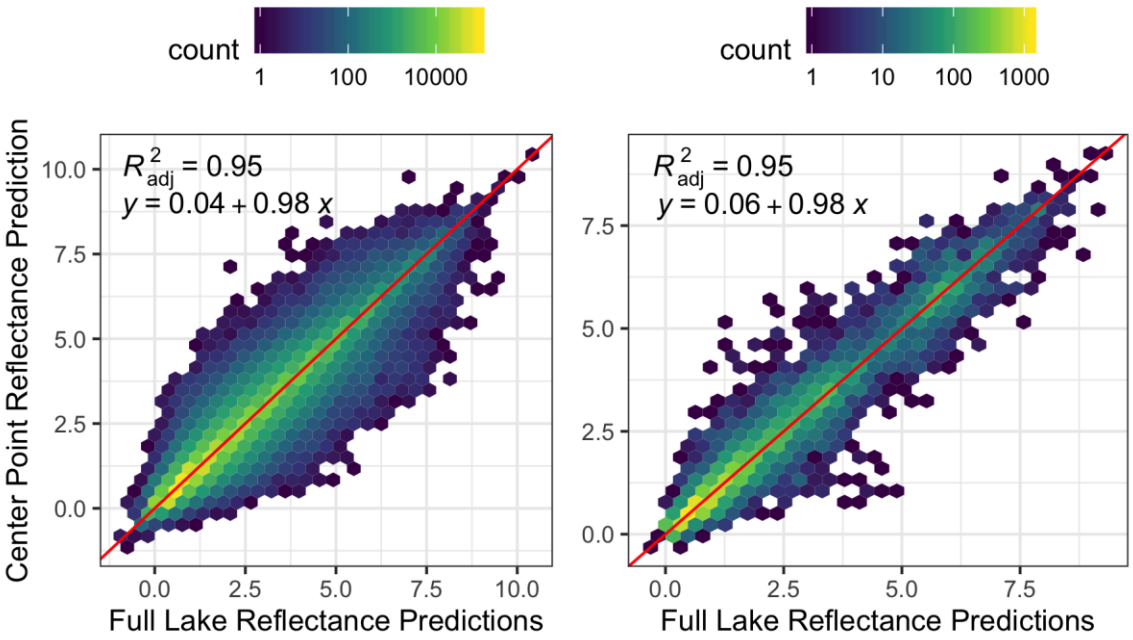

Figure S2. Comparison of predictions using median reflectance values from a buffered lake center point and median reflectance values from the entire lake polygon for (left) the full NLA 2012 sample of lakes and (right) NLA lakes over 10 km2 where there is the highest potential difference for variation between center point and full lake reflectance values. Red line indicates 1:1 while the color indicates the density of points for a given location.

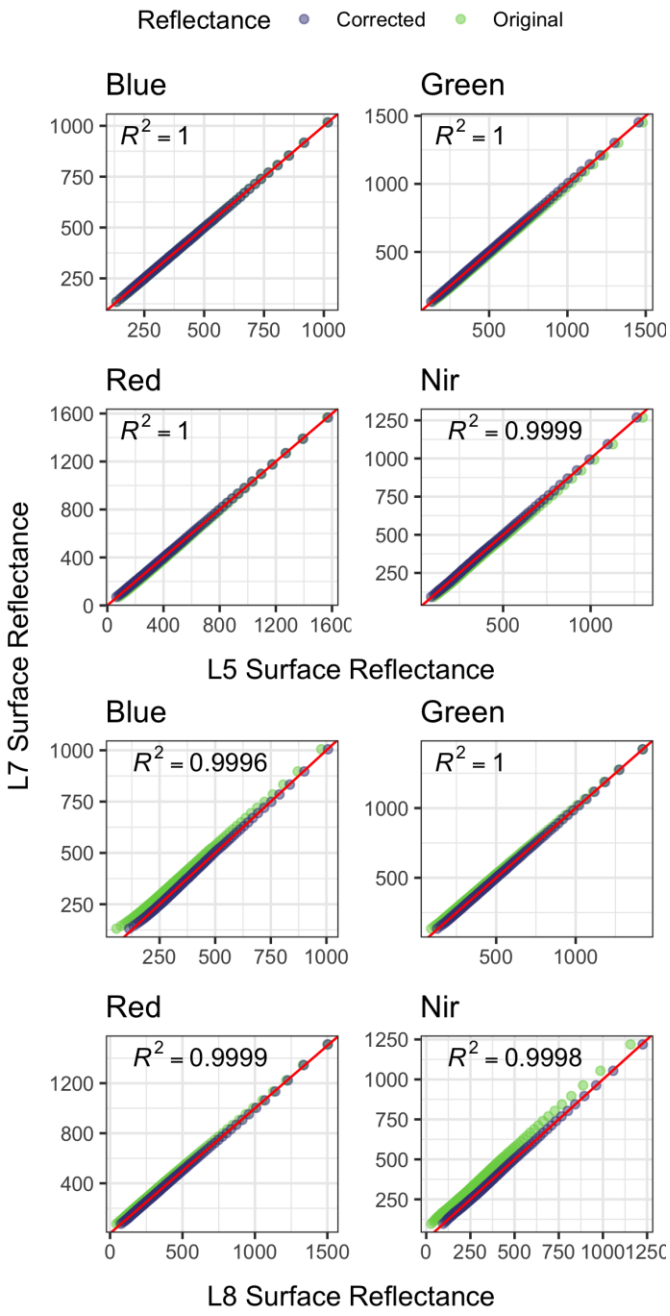

Figure S3. Results of sensor corrections for Landsat 5 and Landsat 8 to Landsat 7 values. Reflectance values from the 1st-99th percentile were taken from the distributions of values during coincident flight years over the entirety of the NLA dataset (n = 1,029 lakes) and corrected to Landsat 7 values through second order polynomial regression. Red lines are 1:1 lines and R2 values are for corrected reflectance and Landsat 7 reflectance.

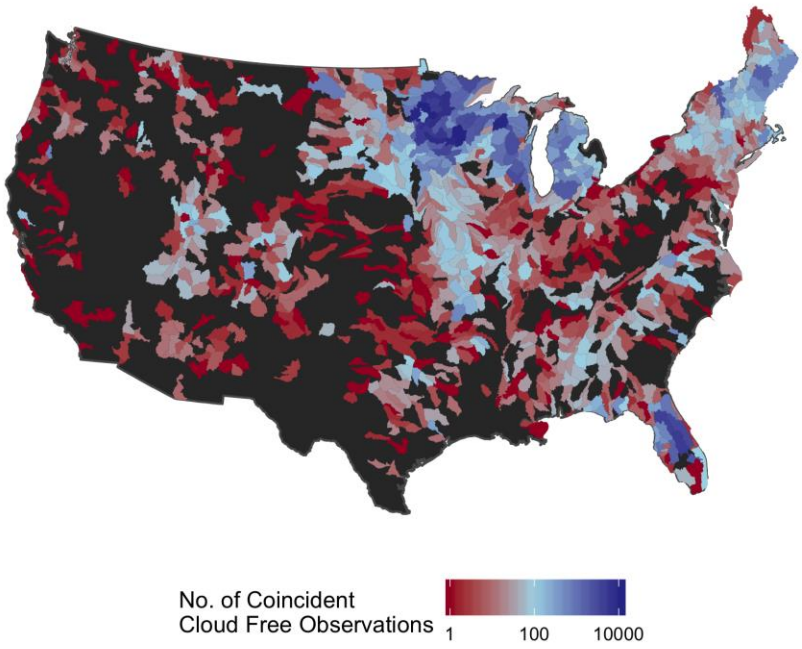

Figure S4. Distribution of coincident satellite and field observations used for model training and validation aggregated by HUC 8 watershed. Distributions largely follow the geographical concentration of lakes. Areas shown as dark grey contain no coincident observations.

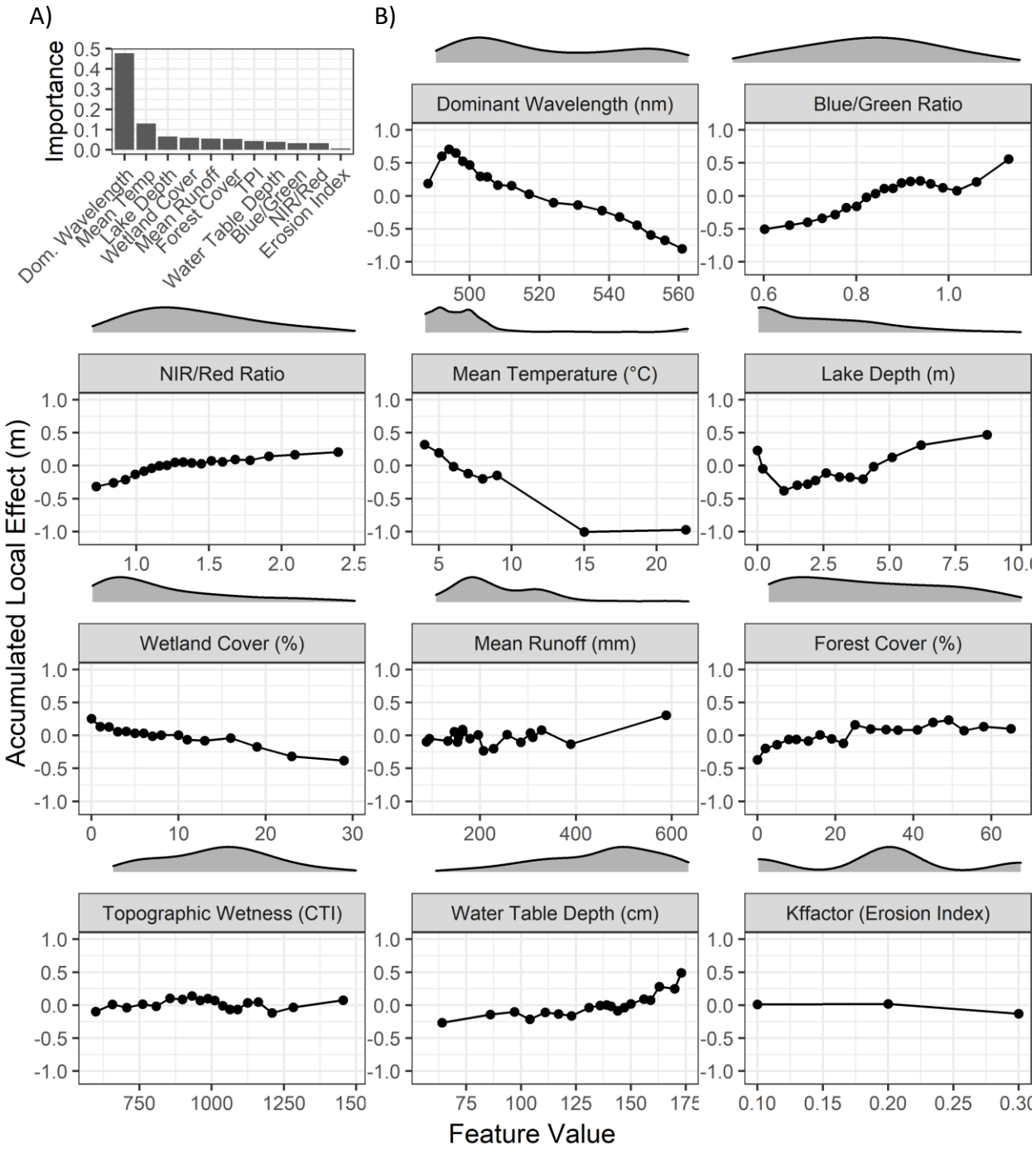

Figure S5. A) Feature importance as measured by model gain for all the model inputs. B) Accumulated local effects (ALE) for each feature. Values along the y-axis represent the average impact to model predictions as you move along a localized window of feature values. Values along with x-axis are the feature values within the training dataset. Density distribution plots above the ALE plots show the distribution of each feature (5th-95th percentile) within the training set.

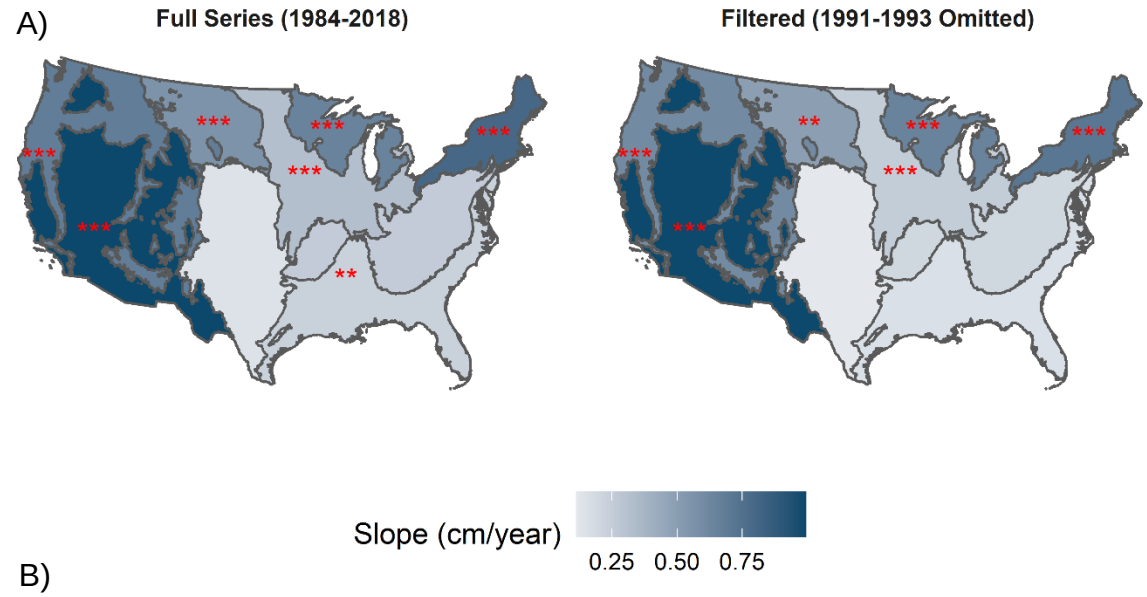

B)

Full Validation

Red line is 1:1

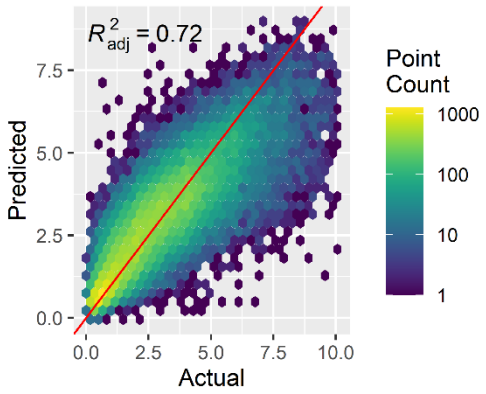

mae	mape	bias
0.714	0.38	0.004

1991-1993 Validation

Red line is 1:1

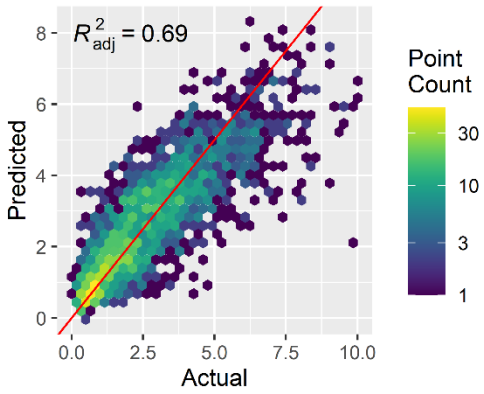

mae	mape	bias
0.751	0.389	0.043

Figure S6. A) Comparison of estimated Sen Slopes for the 2012 NLA sample of lakes for the full timeseries and omitting years with high atmospheric optical depth due to the Mt. Pinatubo eruption. Trends for all regions remain positive within the filtered timeseries and only one region, the Coastal Plains, is no longer statistically significant at a 95% confidence interval. B) Hold-out validation metrics for the full timeseries compared to 1991-1993. Bias is ~4 cm higher in 1991-1993, indicating that if anything clarity is slightly underpredicted for the years in question compared to the full time period.

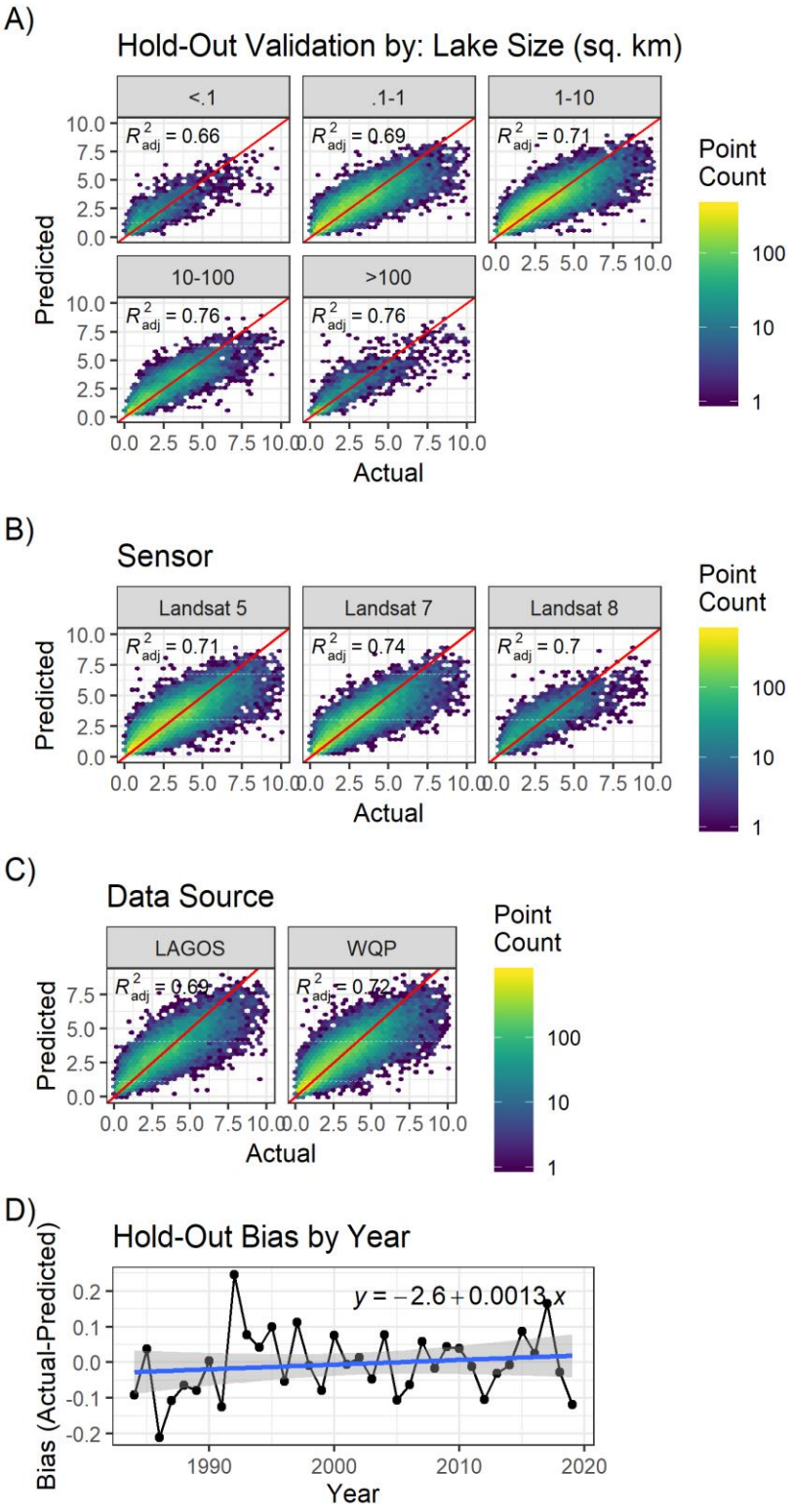

Figure S7. Breakdown of model validation by (A) lake size, (B) sensor, (C) data source, and (D) time. Red lines represent 1:1 lines.

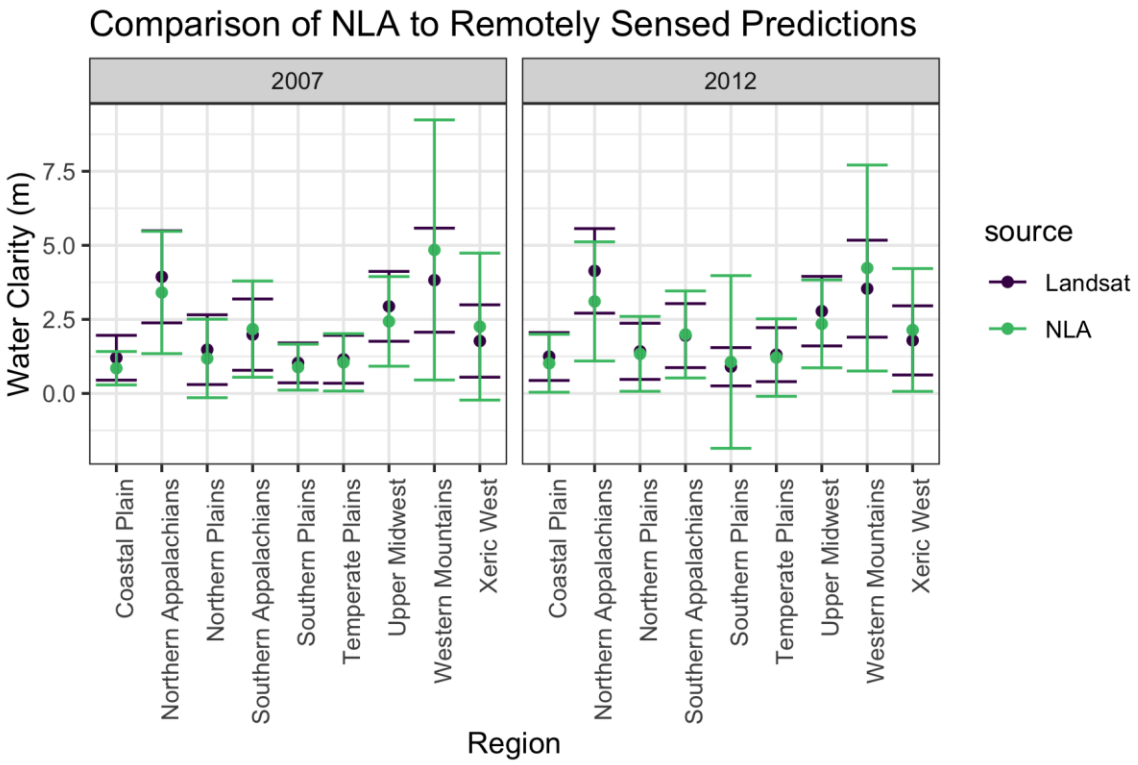

Figure S8. Comparison of predicted regional summer water clarity values with field measurements from the 2007 NLA (left) and 2012 NLA (right). Points represent regional means and error bars represent one standard deviation.

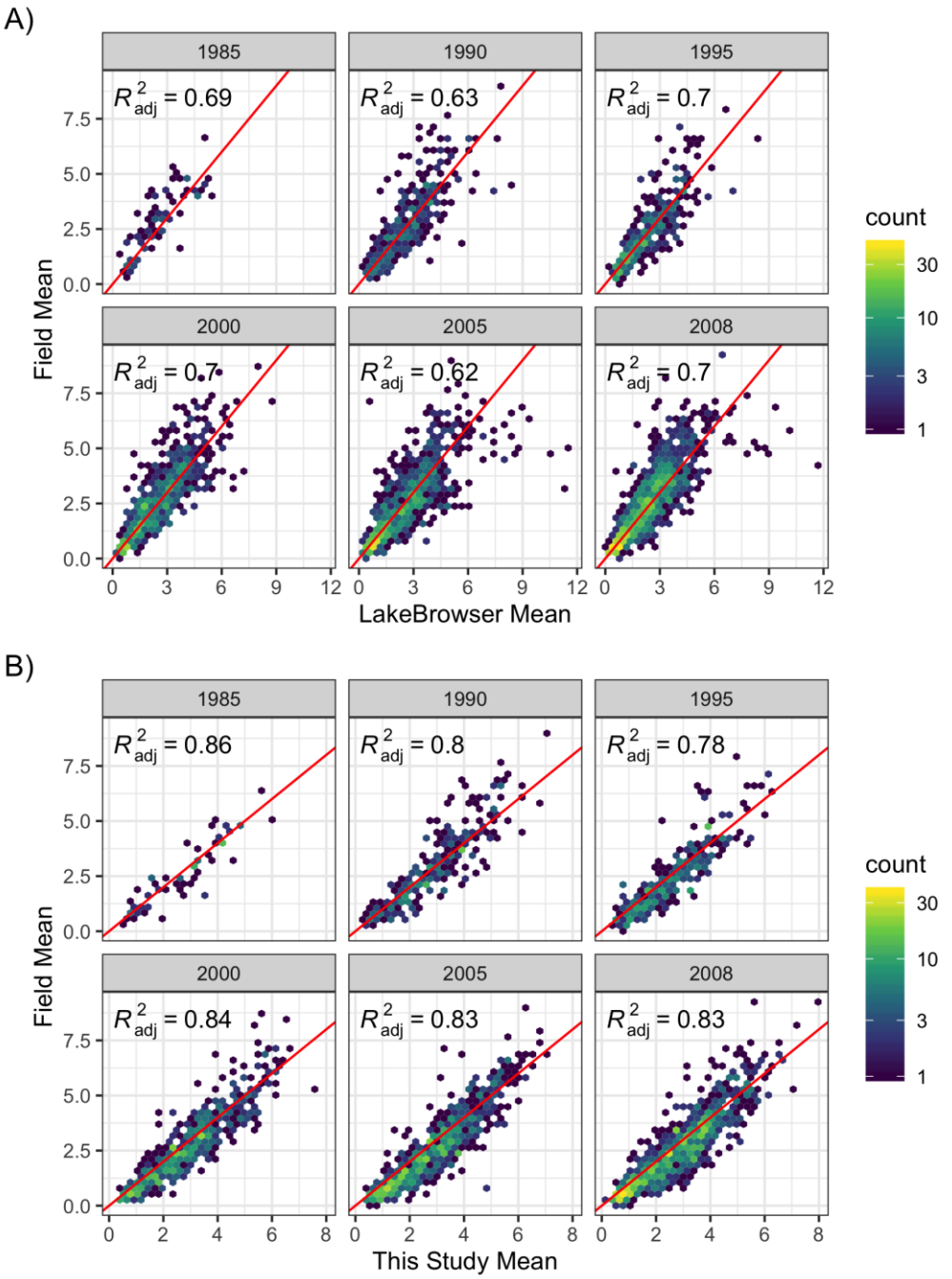

Figure S9. Comparison of predicted mean annual clarity for individual lakes from (A) LakeBrowser and (B) this study for those lakes/years with field data from the Water Quality Portal or LAGOS-NE. Predictions from LakeBrowser are those available from their data portal and represent the mean clarity estimate from 1-2 Landsat scenes per year. This study's predictions were derived by filtering cloud free Landsat scenes for each year down to only those months considered by LakeBrowser; however, since specific source scene data is unavailable from LakeBrowser, our summer estimates are the mean of all available scenes in the coincident time period (generally 2-4 scenes per lake per year), and therefore do not exactly match those from LakeBrowser.

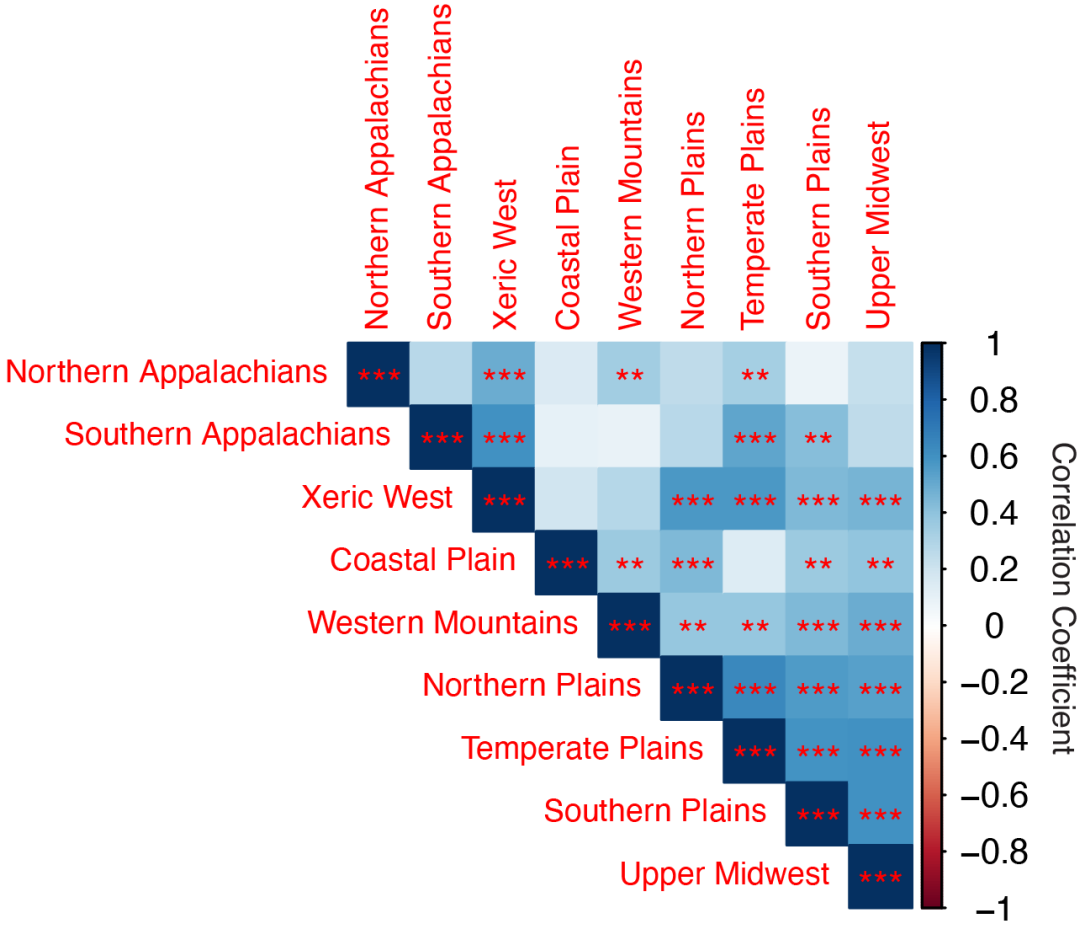

Figure S10. Pearson's correlation matrix for time series between regions using the NLA sample of lakes. One, two, and three asterisks represent significance at the 90th, 95th, and 99th percent confidence intervals respectively.

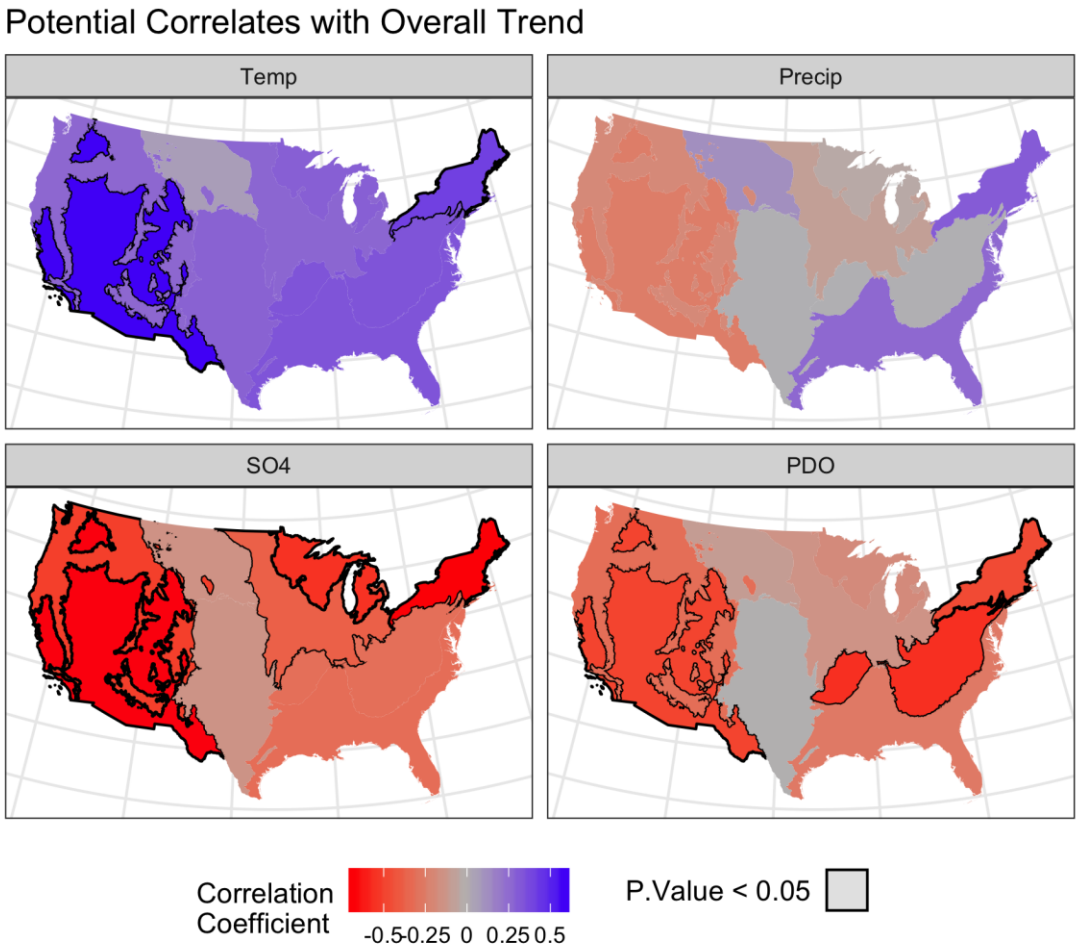

Figure S11. Ecoregion scale correlations. Clockwise from the top left: Ecoregion mean annual summer temperature from PRISM, Ecoregion mean annual summer precipitation from PRISM, Pacific Decadal Oscillation, and mean regional SO4 deposition from the National Atmospheric Deposition Program.

Variable	Description
Lake Area	Lake area from NHD v2 (sq. km)
Lake Depth	**Mean lake depth from NHD v2 (m)**
NIR/Red	**Band Ratio**
Blue/Green	**Band Ratio**
Forel-Ule Index	**Dominant Color Wavelength as defined by Wang et al. (2015)**
Network Status	Binary on/off network status for lake based on NHD flowlines
Percent Carbonate	Percent of catchment area classified as lithology type: carbonate residual material
Mean Precipitation	PRISM climate data - 30-year normal mean precipitation (mm): Annual period: 1981-2010 within the catchment
Mean Temperature	**PRISM climate data - 30-year normal mean temperature (C°): Annual period: 1981-2010 within the catchment**
Runoff	**Mean runoff (mm) within catchment**
Percent Clay	Mean % clay content of soils (STATSGO) within catchment
Percent Sand	Mean % sand content of soils (STATSGO) within catchment
Percent Organic Matter	Mean organic matter content (% by weight) of soils (STATSGO) within catchment
Soil Permeability	Mean permeability (cm/hour) of soils (STATSGO) within catchment
Bedrock Depth	Mean depth (cm) to bedrock of soils (STATSGO) within catchment
Water Table Depth	**Mean seasonal water table depth (cm) of soils (STATSGO) within catchment**
Base Flow Index	Base flow is the component of streamflow that can be attributed to ground-water discharge into streams. The BFI is the ratio of base flow to total flow, expressed as a percentage, within catchment
Elevation	Mean catchment elevation (m)
Atmospheric Optical Depth	Atmospheric Optical Depth over observation pulled from MERRA 2 reanalysis data
Kffactor	**Mean of STATSGO Kffactor raster within catchment. The Universal Soil Loss Equation (USLE) and represents a relative index of susceptibility of bare, cultivated soil to particle detachment and transport by rainfall**
Catchement Area	Area of local catchment (square km)
Percent Agriculture	% of catchment area classified as ag land cover (NLCD 2006 classes 81-82) occurring on slopes > 10%
NPDE Density	Density of permitted NPDES (National Pollutant Discharge Elimination System) sites within catchment (sites/square km)
Hydraulic Conductivity	Mean lithological hydraulic conductivity (micrometers per second) content in surface or near surface geology within catchment
Percent Impervious Surface	Mean imperviousness of anthropogenic surfaces within catchment (NLCD 2006)
Percent Urban	Percent of catchment classified as either medium or high density urban (NLCD 2006)
Percent Forest	**Percent of catchment classified as either deciduous, coniferous, or mixed forest (NLCD 2006)**
Percent Crop	Percent of catchment area classified as crop land use (NLCD 2006 class 82)
Percent Wetland	**Percent of catchment classified as woody or herbaceous wetland landcover (NLCD 2006)**
Topographic Wetness Index	**Mean Composite Topographic Index (CTI)[Wetness Index] within catchment**

Table S1. Variables included in modelling pipeline. Variables included in the final model after FFS with LLLTO-CV procedure are indicated in bold.

REFERENCES

Adamo, M., Matta, E., Bresciani, M., Carolis, G. De, Vaiciute, D., Giardino, C., and Pasquariello, G., 2013, On the synergistic use of SAR and optical imagery to monitor cyanobacteria blooms: The Curonian Lagoon case study: European Journal of Remote Sensing, v. 46, p. 789–805, doi:10.5721/EuJRS20134647.

Adrian, R. et al., 2009, Lakes as sentinels of climate change: Limnology and Oceanography, v. 54, p. 2283–2297, doi:10.4319/lo.2009.54.6_part_2.2283.

Alikas, K., and Reinart, A., 2008, Validation of the MERIS products on large European lakes: Peipsi, Vänern and Vättern: Hydrobiologia, v. 599, p. 161–168, doi:10.1007/s10750-007-9212-0.

Allen, G.H., and Pavelsky, T.M., 2018, Global extent of rivers and streams: Science, v. 361, p. 585–588, doi:10.1126/science.aat0636.

Allen, G.H., Yang, X., Gardner, J., Holliman, J., David, C.H., and Ross, M., 2020, Timing of Landsat overpasses effectively captures flow conditions of large rivers: Remote Sensing, v. 12, p. 1510, doi:10.3390/rs12091510.

Alvarez-Berríos, N., Campos-Cerqueira, M., Hernández-Serna, A., Delgado, C.J.A., Román-Dañobeytia, F., and Aide, T.M., 2016, Impacts of small-scale gold mining on birds and anurans near the Tambopata Natural Reserve, Peru, assessed using passive acoustic monitoring: Tropical Conservation Science, v. 9, p. 832–851, doi:10.1177/194008291600900216.

Apley, D.W., and Zhu, J., 2020, Visualizing the effects of predictor variables in black box supervised learning models: Journal of the Royal Statistical Society Series B, v. 82, p. 1059–1086.

Arbelaitz, O., Gurrutxaga, I., Muguerza, J., Pérez, J.M., and Perona, I., 2013, An extensive comparative study of cluster validity indices: Pattern Recognition, v. 46, p. 243–256, doi:10.1016/j.patcog.2012.07.021.

Aria, M., and Cuccurullo, C., 2017, bibliometrix: An R-tool for comprehensive science mapping analysis: Journal of Informetrics, v. 11, p. 959–975, doi:10.1016/j.joi.2017.08.007.

Asner, G.P., Llactayo, W., Tupayachi, R., and Luna, E.R., 2013, Elevated rates of gold mining in the Amazon revealed through high-resolution monitoring: Proceedings of the National Academy of Sciences of the United States of America, v. 110, p. 18454–18459, doi:10.1073/pnas.1318271110.

Asner, G.P., and Tupayachi, R., 2017, Accelerated losses of protected forests from gold mining in the Peruvian Amazon: Environmental Research Letters, v. 12.

Ator, S.W., García, A.M., Schwarz, G.E., Blomquist, J.D., and Sekellick, A.J., 2019, Toward explaining nitrogen and phosphorus trends in Chesapeake Bay tributaries, 1992–2012: JAWRA Journal of the American Water Resources Association, v. 55, p. 1149–1168, doi:10.1111/1752-1688.12756.

Baban, S.M.J., 1993, Detecting water quality parameters in the norfolk broads, U.K., using landsat imagery: International Journal of Remote Sensing, v. 14, p. 1247–1267, doi:10.1080/01431169308953955.

Ballard, T.C., Sinha, E., and Michalak, A.M., 2019, Long-term changes in precipitation and temperature have already impacted nitrogen loading: Environmental Science & Technology, v. 53, p. 5080–5090, doi:10.1021/acs.est.8b06898.

Barysheva, L., 1987, On the issue of intercorrespondence of color scales used in limnology: Remote Monitoring of Large Lakes, p. 60–65.

Bayley, S.E., Creed, I.F., Sass, G.Z., and Wong, A.S., 2007, Frequent regime shifts in trophic states in shallow lakes on the Boreal Plain: Alternative “unstable” states? Limnology and Oceanography, v. 52, p. 2002–2012, doi:10.4319/lo.2007.52.5.2002.

Biber, K., Khan, S.D., and Shah, M.T., 2015, The source and fate of sediment and mercury in Hunza River basin, Northern Areas, Pakistan: Hydrological Processes, v. 29, p. 579–587, doi:10.1002/hyp.10175.

Bilotta, G.S., and Brazier, R.E., 2008, Understanding the influence of suspended solids on water quality and aquatic biota: Water Research, v. 42, p. 2849–2861, doi:10.1016/j.watres.2008.03.018.

Binding, C.E., Greenberg, T.A., Watson, S.B., Rastin, S., and Gould, J., 2015, Long term water clarity changes in North America’s Great Lakes from multi-sensor satellite observations: Limnology and Oceanography, v. 60, p. 1976–1995, doi:10.1002/lno.10146.

Binding, C.E., Jerome, J.H., Bukata, R.P., and Booty, W.G., 2007, Trends in water clarity of the lower Great Lakes from remotely sensed aquatic color: Journal of Great Lakes Research, v. 33, p. 828–841, doi:10.3394/0380-1330(2007)33[828:TIWCOT]2.0.CO;2.

Bioucas-dias, J.M., Plaza, A., Camps-valls, G., Scheunders, P., Nasrabadi, N.M., and Chanussot, J., 2013, Hyperspectral Remote Sensing Data Analysis and Future Challenges: IEEE Geoscience and Remote Sensing Magazine, p. 6–36, doi:10.1109/MGRS.2013.2244672.

Bornmann, L., and Mutz, R., 2015, Growth rates of modern science: A bibliometric analysis based on the number of publications and cited references: Journal of the Association for Information Science and Technology, v. 66, p. 2215–2222, doi:10.1002/asi.23329.

Bose-O’Reilly, S., Schierl, R., Nowak, D., Siebert, U., William, J.F., Owi, F.T., and Ir, Y.I., 2016, A preliminary study on health effects in villagers exposed to mercury in a small-scale artisanal gold mining area in Indonesia: Environmental Research, v. 149, p. 274–281, doi:10.1016/j.envres.2016.04.007.

Box, E.O., Holben, B.N., and Kalb, V., 1989, Accuracy of the AVHRR vegetation index as a predictor of biomass, primary productivity and net CO2 flux: Vegetation, v. 80, p. 71–89, doi:10.1007/BF00048034.

Brando, V.E. et al., 2015, High-resolution satellite turbidity and sea surface temperature observations of river plume interactions during a significant flood event: Ocean Science, v. 11, p. 909–920, doi:10.5194/os-11-909-2015.

Brando, V.E., and Dekker, A.G., 2003, Satellite hyperspectral remote sensing for estimating estuarine and coastal water quality: IEEE Transactions on Geoscience and Remote Sensing, v. 41, p. 1378–1387, doi:10.1109/TGRS.2003.812907.

Bresciani, M., Bolpagni, R., Laini, A., Matta, E., Bartoli, M., and Giardino, C., 2013, Multitemporal analysis of algal blooms with MERIS images in a deep meromictic lake: European Journal of Remote Sensing, v. 46, p. 445–458, doi:10.5721/EuJRS20134626.

Bresciani, M., Stroppiana, D., Odermatt, D., Morabito, G., and Giardino, C., 2011, Assessing remotely sensed chlorophyll-a for the implementation of the Water Framework Directive in European perialpine lakes: Science of the Total Environment, v. 409, p. 3083–3091, doi:10.1016/j.scitotenv.2011.05.001.

Bresciani, M., Vascellari, M., Giardino, C., and Matta, E., 2012, Remote sensing supports the definition of the water quality status of Lake Omodeo (Italy): European Journal of Remote Sensing, v. 45, p. 349–360, doi:10.5721/EuJRS20124530.

Brezonik, P., Menken, K.D., and Bauer, M., 2005, Landsat-based remote sensing of lake water quality characteristics, including chlorophyll and colored dissolved organic matter (CDOM): Lake and Reservoir Management, v. 21, p. 373–382, doi:10.1080/07438140509354442.

Bricaud, A., Morel, A., and Prieur, L., 1981, Absorption by dissolved organic matter of the sea (yellow substance) in the UV and visible domains1: Limnology and Oceanography, v. 26, p. 43–53, doi:10.4319/lo.1981.26.1.0043.

Brivio, P.A., Giardino, C., and Zilioli, E., 2001, Validation of satellite data for quality assurance in lake monitoring applications.: Science of The Total Environment, v. 268, p. 3–18, doi:10.1016/S0048-9697(00)00693-8.

Brunner, M.I., Melsen, L.A., Newman, A.J., Wood, A.W., and Clark, M.P., 2020, Future streamflow regime changes in the United States: assessment using functional classification: Hydrology and Earth System Sciences, v. 24, p. 3951–3966, doi:https://doi.org/10.5194/hess-24-3951-2020.

Bruno, D.E., Ruban, D.A., Tiess, G., Pirrone, N., Perrotta, P., Mikhailenko, A. V., Ermolaev, V.A., and Yashalova, N.N., 2020, Artisanal and small-scale gold mining, meandering tropical rivers, and geological heritage: Evidence from Brazil and Indonesia: Science of the Total Environment, v. 715, p. 136907, doi:10.1016/j.scitotenv.2020.136907.

Buiteveld, H., Hakvoort, J.H.M., and Donze, M., 1994, Optical properties of pure water, *in* Jaffe, J.S. ed., Proceedings of SPIE 2258, p. 174–183, doi:10.1117/12.190060.

Bukata, R.P., 2013, Retrospection and introspection on remote sensing of inland water quality : " Like Déjà Vu All Over Again ": Journal of Great Lakes Research, v. 39, p. 2–5, doi:10.1016/j.jglr.2013.04.001.

Bukata, R.P., Bruton, J.E., Jerome, J.H., Jain, S.C., and Zwick, H.H., 1981, Optical water quality model of Lake Ontario 2: Determination of chlorophyll a and suspended mineral concentrations of natural waters from submersible and low altitude optical sensors: Applied Optics, v. 20, p. 1704, doi:10.1364/ao.20.001704.

Bukata, R.P., Jerome, J.H., and Bruton, J.E., 1988, Particulate concentrations in Lake St. Clair as recorded by a shipborne multispectral optical monitoring system: Remote Sensing of Environment, v. 25, p. 201–229, doi:10.1016/0034-4257(88)90101-0.

Bukata, R.P., Jerome, J.H., Kondratyev, K.Ya., Pozdnyakov, D.V., and Kotykhov, A.A., 1997, Modelling the radiometric color of inland waters: Implications to a) remote sensing and b) limnological color scales: Journal of Great Lakes Research, v. 23, p. 254–269, doi:10.1016/S0380-1330(97)70910-9.

Byrnes, D.K., Meter, K.J.V., and Basu, N.B., 2020, Long-term shifts in U.S. nitrogen sources and sinks revealed by the new TREND-Nitrogen data set (1930–2017): Global Biogeochemical Cycles, v. 34, p. e2020GB006626, doi:10.1029/2020GB006626.

Camps-Valls, G., 2009, Machine learning in remote sensing data processing, *in* 2009 IEEE International Workshop on Machine Learning for Signal Processing, IEEE, p. 1–6, doi:10.1109/MLSP.2009.5306233.

Cañas, C.M., and Waylen, P.R., 2012, Modelling production of migratory catfish larvae (Pimelodidae) on the basis of regional hydro- Climatology features of the Madre de Dios Basin in southeastern Peru: Hydrological Processes, v. 26, p. 996–1007, doi:10.1002/hyp.8192.

Canfield, D.E., Bachmann, R.W., Stephens, D.B., Hoyer, M.V., Bacon, L., Williams, S., and Scott, M., 2016, Monitoring by citizen scientists demonstrates water clarity of Maine (USA) lakes is stable, not declining, due to cultural eutrophication: Inland Waters, v. 6, p. 11–27, doi:10.5268/IW-6.1.864.

Cao, Z., Ma, R., Duan, H., Pahlevan, N., Melack, J., Shen, M., and Xue, K., 2020, A machine learning approach to estimate chlorophyll-a from Landsat-8 measurements in inland lakes: Remote Sensing of Environment, v. 248, p. 111974, doi:10.1016/j.rse.2020.111974.

Cardo, M.A., and Vargas, P.M., 2017, Proyecto: Plan nacional de accion sobre mercurio en el sector de la mineria de oro artesanal y de pequena escala en el Peru: Artisanal Gold Council

Carlson, R.E., 1977, A trophic state index for lakes: Limnology and Oceanography, v. 22, p. 361–369, doi:10.4319/lo.1977.22.2.0361.

Carpenter, S.R., Arani, B.M.S., Hanson, P.C., Scheffer, M., Stanley, E.H., and Nes, E.V., 2020, Stochastic dynamics of Cyanobacteria in long-term high-frequency observations of a eutrophic lake: Limnology and Oceanography Letters, v. 5, p. 331–336, doi:10.1002/lol2.10152.

Carpenter, D.J., and Carpenter, S.M., 1983, Modeling inland water quality using Landsat data: Remote Sensing of Environment, v. 13, p. 345–352, doi:10.1016/0034-4257(83)90035-4.

Carvalho, L. et al., 2013, Strength and uncertainty of phytoplankton metrics for assessing eutrophication impacts in lakes: Hydrobiologia, v. 704, p. 127–140, doi:10.1007/s10750-012-1344-1.

CEOS, 2018, Feasibility Study for an Aquatic Ecosystem Earth Observing System: Commonwealth Scientific and Industrial research Organization (CSIRO): Canberra, Australia.

Chang, N.-B., and Vannah, B., 2012, Monitoring the total organic carbon concentrations in a lake with the integrated data fusion and machine-learning (IDFM) technique: SPIE Optical Engineering + Applications, v. 8513, doi:10.1117/12.927632.

Chang, N.-B., Vannah, B.W., Yang, Y.J., and Elovitz, M., 2014, Integrated data fusion and mining techniques for monitoring total organic carbon concentrations in a lake: International Journal of Remote Sensing, v. 35, p. 1064–1093, doi:10.1080/01431161.2013.875632.

Choe, E., van der Meer, F., van Ruitenbeek, F., van der Werff, H., de Smeth, B., and Kim, K.W., 2008, Mapping of heavy metal pollution in stream sediments using combined geochemistry, field spectroscopy, and hyperspectral remote sensing: A case study of the Rodalquilar mining area, SE Spain: Remote Sensing of Environment, v. 112, p. 3222–3233, doi:10.1016/j.rse.2008.03.017.

Cialdi, A., and Secchi, P.A., 1865, Sur la transparence de la mer: Comptes rendus hebdomadaire de sceances de l'Academie des Sciences, v. 61, p. 100–104.

Cole, J.J. et al., 2007, Plumbing the global carbon cycle: Integrating inland waters into the terrestrial carbon budget: Ecosystems, v. 10, p. 171–184, doi:10.1007/s10021-006-9013-8.

Collins, S.M. et al., 2019, Winter precipitation and summer temperature predict lake water quality at macroscales: Water Resources Research, v. 55, p. 2708–2721, doi:10.1029/2018WR023088.

Concha, J.A., and Schott, J.R., 2016, Retrieval of color producing agents in Case 2 waters using Landsat 8: Remote Sensing of Environment, v. 185, p. 95–107, doi:10.1016/j.rse.2016.03.018.

Cooley, S.W., Smith, L.C., Stepan, L., and Mascaro, J., 2017, Tracking dynamic northern surface water changes with high-frequency planet CubeSat imagery: Remote Sensing, v. 9, p. 1–21, doi:10.3390/rs9121306.

Cui, L., Qiu, Y., Fei, T., Liu, Y., and Wu, G., 2013, Using remotely sensed suspended sediment concentration variation to improve management of Poyang Lake, China: Lake and Reservoir Management, v. 29, p. 47–60, doi:10.1080/10402381.2013.768733.

Cui, L., Wu, G., and Liu, Y., 2009, Monitoring the impact of backflow and dredging on water clarity using MODIS images of Poyang Lake, China: Hydrological Processes, v. 23, p. 342–350, doi:10.1002/hyp.7163.

Curtarelli, M.P., Ogashawara, I., Alcântara, E.H., and Stech, J.L., 2015, Coupling remote sensing bio-optical and three-dimensional hydrodynamic modeling to study the phytoplankton dynamics in a tropical hydroelectric reservoir: Remote Sensing of Environment, v. 157, p. 185–198, doi:10.1016/j.rse.2014.06.013.

Dall'Olmo, G., and Gitelson, A.A., 2006, Effect of bio-optical parameter variability and uncertainties in reflectance measurements on the remote estimation of chlorophyll-a concentration in turbid productive waters: modeling results: Applied Optics, v. 45, p. 3577, doi:10.1364/AO.45.003577.

Davies, D.L., and Bouldin, D.W., 1979, A cluster separation measure: IEEE Transactions on Pattern Analysis and Machine Intelligence, v. PAMI-1, p. 224–227, doi:10.1109/TPAMI.1979.4766909.

Dekker, A.G., and Peters, S.W.M., 1993, The use of the thematic mapper for the analysis of eutrophic lakes: A case study in the Netherlands: International Journal of Remote Sensing, v. 14, p. 799–821, doi:10.1080/01431169308904379.

Dekker, A.G., and Seyhan, E., 1988, The remote sensing loosdrecht lakes project: International Journal of Remote Sensing, v. 9, p. 1761–1773, doi:10.1080/01431168808954976.

Dekker, A.G., Seyhan, E., and Malthus, T.J., 1991, Quantitative Modeling of Inland Water Quality for High-Resolution MSS Systems: IEEE Transactions on Geoscience and Remote Sensing, v. 29, p. 89–95, doi:10.1109/36.103296.

Dekker, A.G., Vos, R.J., and Peters, S.W.M., 2002, Analytical algorithms for lake water TSM estimation for retrospective analyses of TM and SPOT sensor data: International Journal of Remote Sensing, v. 23, p. 15–35, doi:10.1080/01431160010006917.

Dekker, A.G., Vos, R.J., and Peters, S.W.M., 2001, Comparison of remote sensing data, model results and in situ data for total suspended matter (TSM) in the southern Frisian lakes: Science of the Total Environment, v. 268, p. 197–214, doi:10.1016/S0048-9697(00)00679-3.

Dethier, E.N., Renshaw, C.E., and Magilligan, F.J., 2020, Toward improved accuracy of remote sensing approaches for quantifying suspended sediment: Implications for suspended-sediment monitoring: Journal of Geophysical Research: Earth Surface, v. 125, p. e2019JF005033, doi:10.1029/2019JF005033.

Dethier, E.N., Sartain, S.L., and Lutz, D.A., 2019, Heightened levels and seasonal inversion of riverine suspended sediment in a tropical biodiversity hot spot due to artisanal gold mining: Proceedings of the National Academy of Sciences of the United States of America, v. 116, p. 23936–23941, doi:10.1073/pnas.1907842116.

Devred, E., Turpie, K.R., Moses, W., Klemas, V. V., Moisan, T., Babin, M., Toro-Farmer, G., Forget, M.H., and Jo, Y.H., 2013, Future retrievals of water column bio-optical properties using the hyperspectral infrared imager (hyspiri): Remote Sensing, v. 5, p. 6812–6837, doi:10.3390/rs5126812.

Dierssen, H.M., Kudela, R.M., and Ryan, J.P., 2006, Red and Black Tides : Quantitative Analysis of Water-Leaving Radiance and Perceived Color for Phytoplankton , Colored Dissolved Organic Matter , and Suspended Sediments Author (s): Heidi M . Dierssen , Raphael M . Kudela , John P . Ryan and Richard C .: Limnology and Oceanography, v. 51, p. 2646–2659.

Diringer, S.E., Berky, A.J., Marani, M., Ortiz, E.J., Karatum, O., Plata, D.L., Pan, W.K., and Hsu-Kim, H., 2020, Deforestation due to artisanal and small-scale gold mining exacerbates soil and mercury mobilization in Madre de Dios, Peru: Environmental Science and Technology, v. 54, p. 286–296, doi:10.1021/acs.est.9b06620.

Diringer, S., Berky, A., Pan, W.K.Y., and Hsu-kim, H., 2015, River transport of mercury from artisanal and small-scale gold mining and risks for dietary mercury exposure in Madre de Dios, Peru: Environmental Science Processes & Impacts, p. 478–487, doi:10.1039/c4em00567h.

Downing, J.A., 2014, Limnology and oceanography: Two estranged twins reuniting by global change: Inland Waters, v. 4, p. 215–232, doi:10.5268/IW-4.2.753.

Downing, J.A. et al., 2006, The global abundance and size distribution of lakes, ponds, and impoundments: Limnology and Oceanography, v. 51, p. 2388–2397, doi:10.4319/lo.2006.51.5.2388.

Doxaran, D., Froidefond, J.M., and Castaing, P., 2002a, A reflectance band ratio used to estimate suspended matter concentrations in sediment-dominated coastal waters A re ectance band ratio used to estimate suspended matter concentrations in sediment-dominated coastal w: Int. J. Remote Sensing, v. 23, p. 5079–5085, doi:10.1080/0143116021000009912.

Doxaran, D., Froidefond, J.M., Lavender, S., and Castaing, P., 2002b, Spectral signature of highly turbid waters: Application with SPOT data to quantify suspended particulate matter concentrations: Remote Sensing of Environment, v. 81, p. 149–161, doi:10.1016/S0034-4257(01)00341-8.

Driscoll, C.T., Mason, R.P., Chan, H.M., Jacob, D.J., and Pirrone, N., 2013, Mercury as a global pollutant: Sources, pathways, and effects: Environmental Science & Technology, v. 47, p. 4967–4983.

Duan, H., Tao, M., Loiselle, S.A., Zhao, W., Cao, Z., Ma, R., and Tang, X., 2017, MODIS observations of cyanobacterial risks in a eutrophic lake: Implications for long-term safety evaluation in drinking-water source: Water Research, v. 122, p. 455–470, doi:10.1016/j.watres.2017.06.022.

Duan, H., Zhang, Y., Zhang, B., Song, K., and Wang, Z., 2007, Assessment of chlorophyll-a concentration and trophic state for lake chagan using landsat TM and field spectral data: Environmental Monitoring and Assessment, v. 129, p. 295–308, doi:10.1007/s10661-006-9362-y.

Duane Nellis, M., Harrington, J. a., and Wu, J., 1998, Remote sensing of temporal and spatial variations in pool size, suspended sediment, turbidity, and Secchi depth in Tuttle Creek Reservoir, Kansas: 1993: Geomorphology, v. 21, p. 281–293, doi:10.1016/S0169-555X(97)00067-6.

Dunn, O.J., 1961, Multiple comparisons among means: Journal of the American Statistical Association, v. 56, p. 52–64, doi:10.2307/2282330.

Dvornikov, Y. et al., 2018, Terrestrial CDOM in lakes of Yamal Peninsula: Connection to lake and lake catchment properties: Remote Sensing, v. 10, p. 1–21, doi:10.3390/rs10020167.

Dwyer, J.L., Roy, D.P., Sauer, B., Jenkerson, C.B., Zhang, H.K., and Lymburner, L., 2018, Analysis ready data: Enabling analysis of the landsat archive: Remote Sensing, v. 10, p. 1–19, doi:10.3390/rs10091363.

Eagles-Smith, C.A., Silbergeld, E.K., Basu, N., Bustamante, P., Diaz-Barriga, F., Hopkins, W.A., Kidd, K.A., and Nyland, J.F., 2018, Modulators of mercury risk to wildlife and humans in the context of rapid global change: Ambio, v. 47, p. 170–197, doi:10.1007/s13280-017-1011-x.

Espejo, J.C., Messinger, M., Rom, F., Ascorra, C., Fernandez, L.E., and Silman, M., 2018, Deforestation and forest degradation due to gold mining in the Peruvian Amazon : A 34-year perspective: Remote Sensing, v. 10, p. 1–17, doi:10.3390/rs10121903.

Falcini, F. et al., 2012, Linking the historic 2011 Mississippi River flood to coastal wetland sedimentation: Nature Geoscience, v. 5, p. 803–807, doi:10.1038/ngeo1615.

Fan, J., Wang, X., Wu, L., Zhou, H., Zhang, F., Yu, X., Lu, X., and Xiang, Y., 2018, Comparison of Support Vector Machine and Extreme Gradient Boosting for predicting daily global solar radiation using temperature and precipitation in humid subtropical climates: A case study in China: Energy Conversion and Management, v. 164, p. 102–111, doi:10.1016/j.enconman.2018.02.087.

Fang, L., Chen, S., Li, H., and Gu, C., 2008, Monitoring water constituents and salinity variations of saltwater using EO-1 Hyperion satellite imagery in the Pearl River Estuary, China, *in* IGARSS 2008 - 2008 IEEE International Geoscience and Remote Sensing Symposium, IEEE, v. 1, p. I-438- I–441, doi:10.1109/IGARSS.2008.4778889.

Feldman, G. et al., 1989, Ocean color: Availability of the global data set: Eos, Transactions American Geophysical Union, v. 70, p. 634, doi:10.1029/89EO00184.

Feng, L., Hu, C., Han, X., Chen, X., and Qi, L., 2015, Long-term distribution patterns of chlorophyll-a concentration in China's largest freshwater lake: MERIS full-resolution observations with a practical approach: Remote Sensing, v. 7, p. 275–299, doi:10.3390/rs70100275.

Ferring, D., and Hausermann, H., 2019, The political ecology of landscape change, malaria, and cumulative vulnerability in central Ghana's gold mining country: Annals of the American Association of Geographers, v. 109, p. 1074–1091, doi:10.1080/24694452.2018.1535885..

Fichot, C.G., Downing, B.D., Bergamaschi, B.A., Windham-Myers, L., Marvin-Dipasquale, M., Thompson, D.R., and Gierach, M.M., 2016, High-Resolution Remote Sensing of Water Quality in the San Francisco Bay-Delta Estuary: Environmental Science and Technology, v. 50, p. 573–583, doi:10.1021/acs.est.5b03518.

Filazzola, A. et al., 2020, A database of chlorophyll and water chemistry in freshwater lakes: Scientific Data, v. 7, p. 310, doi:10.1038/s41597-020-00648-2.

Finger, F., Knox, A., Bertuzzo, E., Mari, L., Bompangue, D., Gatto, M., Rodriguez-Iturbe, I., and Rinaldo, A., 2014, Cholera in the Lake Kivu region (DRC): Integrating remote sensing and spatially explicit epidemiological modeling: Water Resources Research, v. 50, p. 5624–5637, doi:10.1002/2014WR015521.

Fleck, J.A., Marvin-DiPasquale, M., Eagles-Smith, C.A., Ackerman, J.T., Lutz, M.A., Tate, M., Alpers, C.N., Hall, B.D., Krabbenhoft, D.P., and Eckley, C.S., 2016, Mercury and methylmercury in aquatic sediment across western North America: Science of the Total Environment, v. 568, p. 727–738, doi:10.1016/j.scitotenv.2016.03.044.

Fölster, J., Johnson, R.K., Futter, M.N., and Wilander, A., 2014, The Swedish monitoring of surface waters: 50 years of adaptive monitoring: AMBIO, v. 43, p. 3–18, doi:10.1007/s13280-014-0558-z.

Fox, J., 2009, Aspects of the Social Organization and Trajectory of the R Project: The R Journal, v. 1.

Fraterrigo, J.M., and Downing, J.A., 2008, The influence of land use on lake nutrients varies with watershed transport capacity: Ecosystems, v. 11, p. 1021–1034, doi:10.1007/s10021-008-9176-6.

Friedman, J., Hastie, T., and Tibshirani, R., 2010, Regularization Paths for Generalized Linear Models via Coordinate Descent: Journal of statistical software, v. 33, p. 1–22.

G. Coble, P., 2007, Marine Optical Biogeochemistry: The Chemistry of Ocean Color: Chemical Reviews, v. 107, p. 402–418, doi:10.1021/cr050350+.

Garaba, S.P., Badewien, T.H., Braun, A., Schulz, A.C., and Zielinksi, O., 2014, Using ocean colour remote sensing products to estimate turbidity at the Wadden sea time series station Spiekeroog: Journal of the European Optical Society, v. 9, doi:10.2971/jeos.2014.14020.

Garaba, S.P., and Zielinski, O., 2015, An assessment of water quality monitoring tools in an estuarine system: Remote Sensing Applications: Society and Environment, v. 2, p. 1–10, doi:10.1016/j.rsase.2015.09.001.

García-Sánchez, A., Contreras, F., Adams, M., and Santos, F., 2006, Atmospheric mercury emissions from polluted gold mining areas (Venezuela): Environmental Geochemistry and Health, v. 28, p. 529–540, doi:10.1007/s10653-006-9049-x.

Gardner, J.R., Yang, X., Topp, S.N., Ross, M.R.V., Altenau, E.H., and Pavelsky, T.M., 2021, The Color of Rivers: Geophysical Research Letters, v. 48, p. e2020GL088946, doi:https://doi.org/10.1029/2020GL088946.

Gardner, J., Yang, X., Topp, S., Ross, M., and Pavelsky, T., 2020, River Surface Reflectance (riverSR) Database:, doi:10.5281/zenodo.3838387.

Georganos, S., Grippa, T., Vanhuysse, S., Lennert, M., Shimoni, M., and Wolff, E., 2018, Very high resolution object-based land use-land cover urban classification using extreme gradient boosting: IEEE Geoscience and Remote Sensing Letters, v. 15, p. 607–611, doi:10.1109/LGRS.2018.2803259.

Gerson, J.R., Driscoll, C.T., Hsu-kim, H., and Bernhardt, E.S., 2018, Senegalese artisanal gold mining leads to elevated total mercury and methylmercury concentrations in soils, sediments, and rivers: Elementa: Science of the Anthropocene, v. 6, doi:https://doi.org/10.1525/elementa.274.

Gerten, D., and Adrian, R., 2002, Effects of climate warming, North Atlantic Oscillation, and El Niño-Southern Oscillation on thermal conditions and plankton dynamics in Northern Hemispheric lakes: The Scientific World JOURNAL, v. 2, p. 586–606, doi:10.1100/tsw.2002.141.

Gholizadeh, M., Melesse, A., and Reddi, L., 2016, A comprehensive review on water quality parameters estimation using remote sensing techniques: Sensors, v. 16, p. 1298, doi:10.3390/s16081298.

Giardino, C. et al., 2019a, Imaging Spectrometry of Inland and Coastal Waters : State of the Art , Achievements and Perspectives: Surveys in Geophysics, v. 40, p. 401–429, doi:10.1007/s10712-018-9476-0.

Giardino, C., Kõks, K.-L., Bolpagni, R., Luciani, G., Candiani, G., Lehmann, M.K., Woerd, H.J.V. der, and Bresciani, M., 2019b, The color of water from space: A case study for Italian lakes from Sentinel-2: Geospatial Analyses of Earth Observation (EO) data, doi:10.5772/intechopen.86596.

Gitelson, A., Garbuzov, G., Szilagyi, F., Mittenzwey, K.H., Karnieli, A., and Kaiser, A., 1993, Quantitative remote sensing methods for real-time monitoring of inland waters quality: International Journal of Remote Sensing, v. 14, p. 1269–1295, doi:10.1080/01431169308953956.

Gitelson, A., Mayo, M., Yacobi, Y.Z., Parparov, A., and Berman, T., 1994, The use of high-spectral-resolution radiometer data for detection of low chlorophyll concentrations in Lake Kinneret: Journal of Plankton Research, v. 16, p. 993–1002, doi:10.1093/plankt/16.8.993.

Gonzalez, D.J.X., 2015, Mercury exposure and risk among women of childbearing age in Madre de Dios, Peru: Tropical Resources Bulletin, v. 34, p. 16–24.

Gordon, H.R., Brown, O.B., Evans, R.H., Brown, J.W., Smith, R.C., Baker, K.S., and Clark, D.K., 1988, A semianalytic radiance model of ocean color: Journal of Geophysical Research, v. 93, p. 10909, doi:10.1029/JD093iD09p10909.

Gordon, H.R., Brown, O.B., and Jacobs, M.M., 1975, Computed Relationships Between the Inherent and Apparent Optical Properties of a Flat Homogeneous Ocean: Applied Optics, v. 14, p. 417, doi:10.1364/AO.14.000417.

Gordon, H.R., and Wang, M., 1994, Retrieval of water-leaving radiance and aerosol optical thickness over the oceans with SeaWiFS: a preliminary algorithm: Applied Optics, v. 33, p. 443, doi:10.1364/AO.33.000443.

Gorelick, N., Hancher, M., Dixon, M., Ilyushchenko, S., Thau, D., and Moore, R., 2017, Google Earth Engine: Planetary-scale geospatial analysis for everyone: Remote Sensing of Environment, v. 202, p. 18–27, doi:10.1016/j.rse.2017.06.031.

Govender, M., Chetty, K., and Bulcock, H., 2007, A review of hyperspectral remote sensing and its application in vegetation and water resource studies: Water SA, v. 33, p. 145–151, doi:10.4314/wsa.v33i2.49049.

Gower, J.F.R., Brown, L., and Borstad, G.A., 2004, Observation of chlorophyll fluorescence in west coast waters of canada using the MODIS satellite sensor: Canadian Journal of Remote Sensing, v. 30, p. 17–25, doi:10.5589/m03-048.

Gower, J.F.R., Doerffer, R., and Borstad, G.A., 1999, Interpretation of the 685nm peak in water-leaving radiance spectra in terms of fluorescence, absorption and scattering, and its observation by MERIS: International Journal of Remote Sensing, v. 20, p. 1771–1786, doi:10.1080/014311699212470.

Gower, J., King, S., Borstad, G., and Brown, L., 2005, Detection of intense plankton blooms using the 709 nm band of the MERIS imaging spectrometer : International Journal of Remote Sensing , v. 26, p. 2005–2012, doi:10.1080/01431160500075857.

Griffin, C.G., Finlay, J.C., Brezonik, P.L., Olmanson, L., and Hozalski, R.M., 2018a, Limitations on using CDOM as a proxy for DOC in temperate lakes: Water Research, v. 144, p. 719–727, doi:10.1016/j.watres.2018.08.007.

Griffin, C.G., Frey, K.E., Rogan, J., and Holmes, R.M., 2011, Spatial and interannual variability of dissolved organic matter in the Kolyma River, East Siberia, observed using satellite imagery: Journal of Geophysical Research: Biogeosciences, v. 116, p. 1–12, doi:10.1029/2010JG001634.

Griffin, C.G., McClelland, J.W., Frey, K.E., Fiske, G., and Holmes, R.M., 2018b, Quantifying CDOM and DOC in major Arctic rivers during ice-free conditions using Landsat TM and ETM+ data: Remote Sensing of Environment, v. 209, p. 395–409, doi:10.1016/j.rse.2018.02.060.

Gunn, J.M., Snucins, E.D.E.D., Yan, N.D., and Arts, M.T., 2001, Use of water clarity to monitor the effects of climate change and other stressors on oligotrophic lakes: Environmental Monitoring and Assessment, v. 67, p. 69–88, doi:10.1023/A:1006435721636.

Gutleb, A.C., Schenck, C., and Stalb, E., 1997, Giant otter (Pteronura brasiliensis) at risk? Total mercury and methylmercury levels in fish and otter scats, Peru: Ambio, v. 26, p. 511–514.

Ha, E., Basu, N., Bose-O'Reilly, S., Dorea, J.G., McSorley, E., Sakamoto, M., and Chan, H.M., 2017, Current progress on understanding the impact of mercury on human health: Environmental Research, v. 152, p. 419–433, doi:10.1016/j.envres.2016.06.042.

Hansen, M.C. et al., 2013, High-resolution global maps of 21st-century forest cover change: Science, v. 342, p. 850–853, doi:10.1126/science.1244693.

Hastie, T.T., 2009, The Elements of Statistical Learning: Math. Intell., v. 27, p. 83–85, doi:10.1007/b94608.

He, W., Chen, S., Liu, X., and Chen, J., 2008, Water quality monitoring in a slightly-polluted inland water body through remote sensing - Case study of the Guanting Reservoir in Beijing, China: Frontiers of Environmental Science and Engineering in China, v. 2, p. 163–171, doi:10.1007/s11783-008-0027-7.

Heathcote, A.J., and Downing, J.A., 2012, Impacts of eutrophication on carbon burial in freshwater lakes in an intensively agricultural landscape: Ecosystems, v. 15, p. 60–70, doi:10.1007/s10021-011-9488-9.

Hedger, R., Nils, O., Malthus, T., and Atkinson, P., 2002, Coupling remote sensing with computational fluid dynamics modelling to estimate lake chlorophyll-a concentration: Remote Sensing of Environment, v. 79, p. 116–122, doi:10.1016/S0034-4257(01)00244-9.

Heege, T., Kiselev, V., Wettle, M., and Hung, N.N., 2014, Operational multi-sensor monitoring of turbidity for the entire Mekong Delta: International Journal of Remote Sensing, v. 35, p. 2910–2926, doi:10.1080/01431161.2014.890300.

Heiskanen, J.J. et al., 2015, Effects of water clarity on lake stratification and lake-atmosphere heat exchange: Journal of Geophysical Research, v. 120, p. 7412–7428, doi:10.1002/2014JD022938.

Hellweger, F.L., Miller, W., and Oshodi, K.S., 2007, Mapping turbidity in the Charles River, Boston using a high-resolution satellite: Environmental Monitoring and Assessment, v. 132, p. 311–320, doi:10.1007/s10661-006-9535-8.

Hestir, E.L., Brando, V.E., Bresciani, M., Giardino, C., Matta, E., Villa, P., and Dekker, A.G., 2015, Measuring freshwater aquatic ecosystems: The need for a hyperspectral global mapping satellite mission: Remote Sensing of Environment, v. 167, p. 181–195, doi:10.1016/j.rse.2015.05.023.

Hicks, B.J., Stichbury, G.A., Brabyn, L.K., Allan, M.G., and Ashraf, S., 2013, Hindcasting water clarity from Landsat satellite images of unmonitored shallow lakes in the Waikato region, New Zealand: Environmental Monitoring and Assessment, v. 185, p. 7245–7261, doi:10.1007/s10661-013-3098-2.

Hill, R.A., Weber, M.H., Debbout, R.M., Leibowitz, S.G., and Olsen, A.R., 2018, The Lake-Catchment (LakeCat) Dataset: characterizing landscape features for lake basins within the conterminous USA: Freshwater Science, v. 37, p. 208–221, doi:10.1086/697966.

Hintelmann, H., and Evans, R.D., 1997, Application of stable isotopes in environmental tracer studies - Measurement of monomethylmercury (CH3Hg+) by isotope dilution ICP-MS and detection of species transformation: Fresenius' Journal of Analytical Chemistry, v. 358, p. 378–385, doi:10.1007/s002160050433.

Ho, J.C., Michalak, A.M., and Pahlevan, N., 2019, Widespread global increase in intense lake phytoplankton blooms since the 1980s: Nature, v. 574, p. 667–670, doi:10.1038/s41586-019-1648-7.

Hollander, M., and Wolfe, D.A., 1973, *in* Nonparametric Statistical Methods, 3rd Edition, New York, John Wiley & Sons, p. 115–120, https://www.wiley.com/en-us/Nonparametric+Statistical+Methods%2C+3rd+Edition-p-9780470387375 (accessed September 2020).

Hou, X., Feng, L., Duan, H., Chen, X., Sun, D., and Shi, K., 2017, Fifteen-year monitoring of the turbidity dynamics in large lakes and reservoirs in the middle and lower basin of the Yangtze River, China: Remote Sensing of Environment, v. 190, p. 107–121, doi:10.1016/j.rse.2016.12.006.

Houser, J.N., 2006, Water color affects the stratification, surface temperature, heat content, and mean epilimnetic irradiance of small lakes: Canadian Journal of Fisheries and Aquatic Sciences, v. 63, p. 2447–2455, doi:10.1139/f06-131.

Hu, C., 2009, A novel ocean color index to detect floating algae in the global oceans: Remote Sensing of Environment, v. 113, p. 2118–2129, doi:10.1016/j.rse.2009.05.012.

Huang, C., Guo, Y., Yang, H., Li, Y., Zou, J., Zhang, M., Lyu, H., Zhu, A., and Huang, T., 2015, Using Remote Sensing to Track Variation in Phosphorus and Its Interaction with Chlorophyll-a and Suspended Sediment: IEEE Journal of Selected Topics in Applied Earth Observations and Remote Sensing, v. 8, p. 4171–4180, doi:10.1109/JSTARS.2015.2438293.

Huang, C., Li, Y., Yang, H., Sun, D., Yu, Z., Zhang, Z., Chen, X., and Xu, L., 2014, Detection of algal bloom and factors influencing its formation in Taihu Lake from 2000 to 2011 by MODIS: Environmental Earth Sciences, v. 71, p. 3705–3714, doi:10.1007/s12665-013-2764-6.

Hughes, R.M., and Peck, D.V., 2008, Acquiring data for large aquatic resource surveys: the art of compromise among science, logistics, and reality: Journal of the North American Benthological Society, v. 27, p. 837–859, doi:10.1899/08-028.1.

Huisman, J., Codd, G.A., Paerl, H.W., Ibelings, B.W., Verspagen, J.M.H., and Visser, P.M., 2018, Cyanobacterial blooms: Nature Reviews Microbiology, v. 16, p. 471–483, doi:10.1038/s41579-018-0040-1.

Hunter, P.D., Tyler, A.N., Willby, N.J., and Gilvear, D.J., 2008, The spatial dynamics of vertical migration by Microcystis aeruginosa in a eutrophic shallow lake: A case study using high spatial resolution time-series airborne remote sensing: Limnology and Oceanography, v. 53, p. 2391–2406, doi:10.4319/lo.2008.53.6.2391.

Hutchinson, E., 1973, Marginalia: Eutrophication: The scientific background of a contemporary practical problem on JSTOR: Sigma Xi, The Scientific Research Society, v. 61, p. 269–279.

Imen, S., Chang, N. Bin, and Yang, Y.J., 2015, Developing the remote sensing-based early warning system for monitoring TSS concentrations in Lake Mead: Journal of Environmental Management, v. 160, p. 73–89, doi:10.1016/j.jenvman.2015.06.003.

Imura, N., Sukegawa, E., Pan, S.-K., Nagao, K., Kim, J.-Y., Kwan, T., and Ukita, T., 1971, Chemical methylation of inorganic mercury with methylcobalamin, a vitamin B12 analog: Science, v. 172, p. 1248–1249.

IOCCG, 2018, Earth Observations in Support of Global Water Quality Monitoring: Greb, S., Dekker, A., Binding, C., Eds.; IOCCG Report Series, No. 17; International Ocean Colour Coordinating Group: Dartmouth, NS, Canada

IOCCG, 2008, Why Ocean Colour ? The Societal Benefits of Ocean-Colour Radiometry: Platt, T., Hoepffner, N., Stuart, V., Brown, C., Eds.; Reports of the International Ocean-Colour Coordinating Group: Dartmouth, NS, Canada,

Izagirre, O., Serra, A., Guasch, H., and Elosegi, A., 2009, Effects of sediment deposition on periphytic biomass, photosynthetic activity and algal community structure: Science of the Total Environment, v. 407, p. 5694–5700, doi:10.1016/j.scitotenv.2009.06.049.

Jain, A.K., and Moreau, J.V., 1987, Bootstrap technique in cluster analysis: Pattern Recognition, v. 20, p. 547–568, doi:10.1016/0031-3203(87)90081-1.

Jensen, D., Simard, M., Cavanaugh, K., Sheng, Y., Fichot, C.G., Pavelsky, T., and Twilley, R., 2019, Improving the Transferability of Suspended Solid Estimation in Wetland and Deltaic Waters with an Empirical Hyperspectral Approach: Remote Sensing, v. 11, p. 1629, doi:10.3390/rs11131629.

Jeppesen, E. et al., 2005, Lake responses to reduced nutrient loading - An analysis of contemporary long-term data from 35 case studies: Freshwater Biology, v. 50, p. 1747–1771, doi:10.1111/j.1365-2427.2005.01415.x.

Jones, J.W., 2015, Efficient wetland surface water detection and monitoring via Landsat: Comparison with in situ data from the Everglades Depth Estimation Network: Remote Sensing, v. 7, p. 12503–12538, doi:10.3390/rs70912503.

Jones, J.W., 2019, Improved automated detection of subpixel-scale inundation—revised dynamic surface water extent (DSWE) partial surface water tests: Remote Sensing, v. 11, p. 374, doi:10.3390/rs11040374.

Julian, J.P., Doyle, M.W., and Stanley, E.H., 2008, Empirical modeling of light availability in rivers: Journal of Geophysical Research: Biogeosciences, v. 113, p. 1–16, doi:10.1029/2007JG000601.

Just, A., De Carli, M., Shtein, A., Dorman, M., Lyapustin, A., and Kloog, I., 2018, Correcting measurement error in satellite aerosol optical depth with machine learning for modeling PM2.5 in the Northeastern USA: Remote Sensing, v. 10, p. 803, doi:10.3390/rs10050803.

Kallio, K., Koponen, S., Ylöstalo, P., Kervinen, M., Pyhälahti, T., and Attila, J., 2015, Validation of MERIS spectral inversion processors using reflectance, IOP and water quality measurements in boreal lakes: Remote Sensing of Environment, v. 157, p. 147–157, doi:10.1016/j.rse.2014.06.016.

Kefford, B.J., Zalizniak, L., Dunlop, J.E., Nugegoda, D., and Choy, S.C., 2010, How are macroinvertebrates of slow flowing lotic systems directly affected by suspended and deposited sediments? Environmental Pollution, v. 158, p. 543–550, doi:10.1016/j.envpol.2009.08.008.

Keiser, D.A., Kling, C.L., and Shapiro, J.S., 2019, The low but uncertain measured benefits of US water quality policy: Proceedings of the National Academy of Sciences, v. 116, p. 5262–5269, doi:10.1073/pnas.1802870115.

Keiser, D.A., and Shapiro, J.S., 2019, Consequences of the Clean Water Act and the demand for water quality: The Quarterly Journal of Economics, v. 134, p. 349–396, doi:10.1093/qje/qjy019.

Kendall, M.G., 1948, Rank correlation methods: Oxford, England, Griffin, Rank correlation methods.

Keogh, E., and Kasetty, S., 2003, On the need for time series data mining benchmarks: a survey and empirical demonstration: Data Mining and knowledge discovery, v. 7, p. 349–371.

Kim, M., and Ramakrishna, R.S., 2005, New indices for cluster validity assessment: Pattern Recognition Letters, v. 26, p. 2353–2363, doi:10.1016/j.patrec.2005.04.007.

Kirk, J.T.O., and Tyler, P.A., 1986, The spectral absorption and scattering properties of dissolved and particulate components in relation to the underwater light field of some tropical Australian fresh waters: Freshwater Biology, v. 16, p. 573–583, doi:10.1111/j.1365-2427.1986.tb01001.x.

Kiselev, V., Bulgarelli, B., and Heege, T., 2015, Sensor independent adjacency correction algorithm for coastal and inland water systems: Remote Sensing of Environment, v. 157, p. 85–95, doi:10.1016/j.rse.2014.07.025.

Kishino, M., Booth, C.R., and Okami, N., 1984, Underwater radiant energy absorbed by phytoplankton, detritus, dissolved organic matter, and pure water: Limnology and Oceanography, v. 29, p. 340–349, doi:10.4319/lo.1984.29.2.0340.

Kloiber, S.M., Brezonik, P.L., and Bauer, M.E., 2002, Application of Landsat imagery to regional-scale assessments of lake clarity: Water Research, v. 36, p. 4330–4340, doi:10.1016/S0043-1354(02)00146-X.

Knaeps, E., Ruddick, K.G., Doxaran, D., Dogliotti, A.I., Nechad, B., Raymaekers, D., and Sterckx, S., 2015, A SWIR based algorithm to retrieve total suspended matter in extremely turbid waters: Remote Sensing of Environment, v. 168, p. 66–79, doi:10.1016/j.rse.2015.06.022.

Kneubühler, M., and Damm-Reiser, A., 2018, Recent progress and developments in imaging spectroscopy: Remote Sensing, v. 10, p. 1–4, doi:10.3390/rs10091497.

Knoll, L.B., Williamson, C.E., Pilla, R.M., Leach, T.H., Brentrup, J.A., and Fisher, T.J., 2018, Browning-related oxygen depletion in an oligotrophic lake: Inland Waters, v. 8, p. 255–263, doi:10.1080/20442041.2018.1452355.

Kudela, R.M., Palacios, S.L., Austerberry, D.C., Accorsi, E.K., Guild, L.S., and Torres-Perez, J., 2015, Application of hyperspectral remote sensing to cyanobacterial blooms in inland waters: Remote Sensing of Environment, v. 167, p. 196–205, doi:10.1016/j.rse.2015.01.025.

Kuhn, C. et al., 2019, Performance of Landsat-8 and Sentinel-2 surface reflectance products for river remote sensing retrievals of chlorophyll-a and turbidity: Remote Sensing of Environment, v. 224, p. 104–118, doi:10.1016/j.rse.2019.01.023.

Kuhn, C.D., Bogard, M., Johnston, S.E., John, A., Vermote, E.F., Spencer, R., Dornblaser, M., Wickland, K.P., Striegl, R.G., and Butman, D., 2020, Satellite and airborne remote sensing of gross primary productivity in boreal Alaskan lakes: Environmental Research Letters, doi:10.1088/1748-9326/aba46f.

Kutser, T., 2009, Passive optical remote sensing of cyanobacteria and other intense phytoplankton blooms in coastal and inland waters: International Journal of Remote Sensing, v. 30, p. 4401–4425, doi:10.1080/01431160802562305.

Kutser, T., Alikas, K., Kothawala, D.N., and Köhler, S.J., 2015a, Impact of iron associated to organic matter on remote sensing estimates of lake carbon content: Remote Sensing of Environment, v. 156, p. 109–116, doi:10.1016/j.rse.2014.10.002.

Kutser, T., and Arst, H., 1994, Remote sensing reflectance model of optically active components of turbid waters, *in* Proc. SPIE 2319, Oceanic Remote Sensing and Sea Ice Monitoring, v. 2319, p. 85–91, doi:10.1117/12.197269.

Kutser, T., Paavel, B., Verpoorter, C., Ligi, M., Soomets, T., Toming, K., and Casal, G., 2016, Remote sensing of black lakes and using 810 nm reflectance peak for retrieving water quality parameters of optically complex waters: Remote Sensing, v. 8, doi:10.3390/rs8060497.

Kutser, T., Pierson, D.C., Tranvik, L., Reinart, A., Sobek, S., and Kallio, K., 2005, Using Satellite Remote Sensing to Estimate the Colored Dissolved Organic Matter Absorption Coefficient in Lakes: Ecosystems, v. 8, p. 709–720, doi:10.1007/s10021-003-0148-6.

Kutser, T., Tranvik, L., and Pierson, D.C., 2009a, Variations in colored dissolved organic matter between boreal lakes studied by satellite remote sensing: Journal of Applied Remote Sensing, v. 3, p. 033538, doi:10.1117/1.3184437.

Kutser, T., Vahtmäe, E., and Praks, J., 2009b, A sun glint correction method for hyperspectral imagery containing areas with non-negligible water leaving NIR signal: Remote Sensing of Environment, v. 113, p. 2267–2274, doi:10.1016/j.rse.2009.06.016.

Kutser, T., Verpoorter, C., Paavel, B., and Tranvik, L.J., 2015b, Estimating lake carbon fractions from remote sensing data: Remote Sensing of Environment, v. 157, p. 138–146, doi:10.1016/j.rse.2014.05.020.

Lary, D.J., Alavi, A.H., Gandomi, A.H., and Walker, A.L., 2016, Machine learning in geosciences and remote sensing: Geoscience Frontiers, v. 7, p. 3–10, doi:10.1016/j.gsf.2015.07.003.

Le, C., Li, Y., Zha, Y., Wang, Q., Zhang, H., and Yin, B., 2011, Remote sensing of phycocyanin pigment in highly turbid inland waters in Lake Taihu, China: International Journal of Remote Sensing, v. 32, p. 8253–8269, doi:10.1080/01431161.2010.533210.

Lee, B.Z. et al., 2018, Global Water Clarity : Continuing a Century-Long Monitoring: Eos, v. 99, p. 1–10, doi:10.1029/2018EO097251.

Lee, Z., Shang, S., Qi, L., Yan, J., and Lin, G., 2016, A semi-analytical scheme to estimate Secchi-disk depth from Landsat-8 measurements: Remote Sensing of Environment, v. 177, p. 101–106, doi:10.1016/j.rse.2016.02.033.

Leech, D.M., Pollard, A.I., Labou, S.G., and Hampton, S.E., 2018, Fewer blue lakes and more murky lakes across the continental U.S.: Implications for planktonic food webs: Limnology and Oceanography, p. 1–20, doi:10.1002/LNO.10967.

Li, M., Ma, L., Blaschke, T., Cheng, L., and Tiede, D., 2016, A systematic comparison of different object-based classification techniques using high spatial resolution imagery in agricultural environments: International Journal of Applied Earth Observation and Geoinformation, v. 49, p. 87–98, doi:10.1016/j.jag.2016.01.011.

Liao, T.W., 2005, Clustering of time series data-a survey: Pattern Recognition, v. 38, p. 1857–1874, doi:10.1016/j.patcog.2005.01.025.

Lillesand, T.M., Johnson, W.L., and Deuell, R.L., 1983, Use of landsat data to predict the trophic state of Minnesota lakes: Photogrammetric Engineering and Remote Sensing, v. 49, p. 219–229.

Lin, S., Novitski, L.N., Qi, J., and Stevenson, R.J., 2018, Landsat TM/ETM+ and machine-learning algorithms for limnological studies and algal bloom management of inland lakes: Journal of Applied Remote Sensing, v. 12, p. 1–17, doi:10.1117/1.JRS.12.026003.

Liu, Y.S., Islam, M.A., and Gao, J., 2003, Quantification of shallow water quality parameters by means of remote sensing : Progress in Physical Geography, v. 27, p. 24–43, doi:Doi 10.1191/0309133303pp357ra.

Lobo, F., Costa, M., Novo, E., and Telmer, K., 2016, Distribution of artisanal and small-scale gold mining in the Tapajós River Basin (Brazilian Amazon) over the past 40 years and relationship with water siltation: Remote Sensing, v. 8, p. 579, doi:10.3390/rs8070579.

Long, C.M., and Pavelsky, T.M., 2013, Remote sensing of suspended sediment concentration and hydrologic connectivity in a complex wetland environment: Remote Sensing of Environment, v. 129, p. 197–209, doi:10.1016/j.rse.2012.10.019.

Lottig, N.R., Tan, P.N., Tylerwagner, T., Cheruveli, K.S., Soranno, P.A., Stanley, E.H., Scott, C.E., Stow, C.A., and Yuan, S., 2017, Macroscale patterns of synchrony identify complex relationships among spatial and temporal ecosystem drivers: Ecosphere, v. 8, doi:10.1002/ecs2.2024.

Lunetta, R.S., Schaeffer, B.A., Stumpf, R.P., Keith, D., Jacobs, S.A., and Murphy, M.S., 2015, Evaluation of cyanobacteria cell count detection derived from MERIS imagery across the eastern USA: Remote Sensing of Environment, v. 157, p. 24–34, doi:10.1016/j.rse.2014.06.008.

Lymburner, L., Botha, E., Hestir, E., Anstee, J., Sagar, S., Dekker, A., and Malthus, T., 2016, Landsat 8: Providing continuity and increased precision for measuring multi-decadal time series of total suspended matter: Remote Sensing of Environment, v. 185, p. 108–118, doi:10.1016/j.rse.2016.04.011.

Ma, T. et al., 2020, China’s improving inland surface water quality since 2003: Science Advances, v. 6, p. eaau3798, doi:10.1126/sciadv.aau3798.

Maberly, S.C. et al., 2020, Global lake thermal regions shift under climate change: Nature Communications, v. 11, p. 1232, doi:10.1038/s41467-020-15108-z.

Malthus, T.J., Hestir, E.L., Dekker, A.G., and Brando, V.E., 2012, The case for a global inland water quality product: IEEE IGARSS, p. 5234–5237, doi:10.1109/IGARSS.2012.6352429.

Markham, K.E., and Sangermano, F., 2018, Evaluating wildlife vulnerability to mercury pollution from artisanal and small-scale gold mining in Madre de Dios, Peru: Tropical Conservation Science, v. 11, doi:10.1177/1940082918794320.

Marshall, C.T., and Peters, R.H., 1989, General patterns in the seasonal development of chlorophyll a for temperate lakes: Limnology and Oceanography, v. 34, p. 856–867, doi:10.4319/lo.1989.34.5.0856.

Martin, J., Eugenio, F., Marcello, J., and Medina, A., 2016, Automatic sun glint removal of multispectral high-resolution WorldView-2 imagery for retrieving coastal shallow water parameters: Remote Sensing, v. 8, p. 1–16, doi:10.3390/rs8010037.

Martinuzzi, S., Januchowski-Hartley, S.R., Pracheil, B.M., McIntyre, P.B., Plantinga, A.J., Lewis, D.J., and Radeloff, V.C., 2014, Threats and opportunities for freshwater conservation under future land use change scenarios in the United States: Global Change Biology, v. 20, p. 113–124, doi:10.1111/gcb.12383.

Masek, J.G., Vermote, E.F., Saleous, N.E., Wolfe, R., Hall, F.G., Huemmrich, K.F., Feng Gao, Kutler, J., and Teng-Kui Lim, 2006, A Landsat surface reflectance dataset for North America, 1990-2000: IEEE Geoscience and Remote Sensing Letters, v. 3, p. 68–72, doi:10.1109/LGRS.2005.857030.

Matsuzaki, S.-I.S., Lathrop, R.C., Carpenter, S.R., Walsh, J.R., Zanden, M.J.V., Gahler, M.R., and Stanley, E.H., 2020, Climate and food web effects on the spring clear-water phase in two north-temperate eutrophic lakes: Limnology and Oceanography, v. n/a, doi:10.1002/lno.11584.

Matthews, M.W., 2011, A current review of empirical procedures of remote sensing in Inland and near-coastal transitional waters: International Journal of Remote Sensing, v. 32, p. 6855–6899, doi:10.1080/01431161.2010.512947.

Matthews, E., 1983, Global Vegetation and Land Use: New High-Resolution Data Bases for Climate Studies: Journal of Climate and Applied Meteorology, v. 22, p. 474–487, doi:10.1175/1520-0450(1983)022<0474:GVALUN>2.0.CO;2.

Matthews, M.W., Bernard, S., and Robertson, L., 2012, An algorithm for detecting trophic status (chlorophyll-a), cyanobacterial-dominance, surface scums and floating vegetation in inland and coastal waters: Remote Sensing of Environment, v. 124, p. 637–652, doi:10.1016/j.rse.2012.05.032.

Matthews, M.W., Bernard, S., and Winter, K., 2010, Remote sensing of cyanobacteria-dominant algal blooms and water quality parameters in Zeekoevlei, a small hypertrophic lake, using MERIS: Remote Sensing of Environment, v. 114, p. 2070–2087, doi:10.1016/j.rse.2010.04.013.

Maurice-Bourgoin, L., Quemerais, B., Moreira-Turcq, P., and Seyler, P., 2003, Transport, distribution and speciation of mercury in the Amazon River at the confluence of black and white waters of the Negro and Solimões Rivers: Hydrological Processes, v. 17, p. 1405–1417, doi:10.1002/hyp.1292.

Mazumder, A., and Taylor, W.D., 1994, Thermal Structure of Lakes Varying in Size and Water Clarity: Limnology and Oceanography, v. 39, p. 968–976.

McCabe, M.F. et al., 2017, The future of Earth observation in hydrology: Hydrology and Earth System Sciences, v. 21, p. 1–56, doi:10.5194/hess-21-3879-2017.

McCormick, P. V., and Cairns, J., 1994, Algae as indicators of environmental change: Journal of Applied Phycology, v. 6, p. 509–526, doi:10.1007/BF02182405.

McCullough, I.M., Loftin, C.S., and Sader, S.A., 2012, Combining lake and watershed characteristics with Landsat TM data for remote estimation of regional lake clarity: Remote Sensing of Environment, v. 123, p. 109–115, doi:10.1016/j.rse.2012.03.006.

McCullough, I.M., Loftin, C.S., and Sader, S.A., 2013, Landsat imagery reveals declining clarity of Maine's lakes during 1995–2010: Freshwater Science, v. 32, p. 741–752, doi:10.1899/12-070.1.

McDonald, C.P., Stets, E.G., Striegl, R.G., and Butman, D., 2013, Inorganic carbon loading as a primary driver of dissolved carbon dioxide concentrations in the lakes and reservoirs of the contiguous United States: Global Biogeochemical Cycles, v. 27, p. 285–295, doi:10.1002/gbc.20032.

McKay, L., Bondelid, T., Dewald, T., Johnston, J., Moore, R., and Rea, A., 2019, NHDPlus Version 2: User Guide: US EPA.

Medina-Cobo, M., Domínguez, J.A., Quesada, A., and de Hoyos, C., 2014, Estimation of cyanobacteria biovolume in water reservoirs by MERIS sensor: Water Research, v. 63, p. 10–20, doi:10.1016/j.watres.2014.06.001.

Megard, R.O., Settles, J.C., Boyer, H.A., and Combs, W.S., 1980, Light, Secchi Disks, and Trophic States: Limnology and Oceanography, v. 25, p. 373–377.

Mendonça, R., Müller, R.A., Clow, D., Verpoorter, C., Raymond, P., Tranvik, L.J., and Sobek, S., 2017, Organic carbon burial in global lakes and reservoirs: Nature Communications, v. 8, p. 1–6, doi:10.1038/s41467-017-01789-6.

Mertes, L.A.K., Smith, M.O., and Adams, J.B., 1993, Estimating suspended sediment concentrations in surface waters of the Amazon River wetlands from Landsat images: Remote Sensing of Environment, v. 43, p. 281–301, doi:10.1016/0034-4257(93)90071-5.

Messager, M.L., Lehner, B., Grill, G., Nedeva, I., and Schmitt, O., 2016, Estimating the volume and age of water stored in global lakes using a geo-statistical approach: Nature Communications, v. 7, p. 1–11, doi:10.1038/ncomms13603.

Meyer, M.F., Labou, S.G., Cramer, A.N., Brousil, M.R., and Luff, B.T., 2020, The global lake area, climate, and population dataset: Scientific Data, v. 7, p. 174, doi:10.1038/s41597-020-0517-4.

Meyer, H., Reudenbach, C., Hengl, T., Katurji, M., and Nauss, T., 2018, Improving performance of spatio-temporal machine learning models using forward feature selection and target-oriented validation: Environmental Modelling and Software, v. 101, p. 1–9, doi:10.1016/j.envsoft.2017.12.001.

Meyer, H., Reudenbach, C., Wöllauer, S., and Nauss, T., 2019, Importance of spatial predictor variable selection in machine learning applications – Moving from data reproduction to spatial prediction:, http://arxiv.org/abs/1908.07805.

Miller, R.L., and McKee, B.A., 2004, Using MODIS Terra 250 m imagery to map concentrations of total suspended matter in coastal waters: Remote Sensing of Environment, v. 93, p. 259–266, doi:10.1016/j.rse.2004.07.012.

Mishra, S., and Mishra, D.R., 2012, Normalized difference chlorophyll index: A novel model for remote estimation of chlorophyll-a concentration in turbid productive waters: Remote Sensing of Environment, v. 117, p. 394–406, doi:10.1016/j.rse.2011.10.016.

Mobley, C., 1994, Chapter 3: Optical Properties of Water, *in* Light and Water: Radiative Transfer in Natural Waters, Academic Press, p. 60–144.

Mobley, C.D., and Sundman, L.K., 2008, HydroLight 5 EcoLight 5 Technical documentation: Sequoia Scientific, Inc.

Mol, J.H., and Ouboter, P.E., 2004, Downstream effects of erosion from small-scale gold mining on the instream habitat and fish community of a small neotropical rainforest stream: Conservation Biology, v. 18, p. 201–214, doi:10.1111/j.1523-1739.2004.00080.x.

Molnar, C., 2020, Interpretable Machine Learning: A Guide for Making Black Box Models Explainable: Leanpub.

Monteith, D.T. et al., 2007, Dissolved organic carbon trends resulting from changes in atmospheric deposition chemistry: Nature, v. 450, p. 537–540, doi:10.1038/nature06316.

Morel, A., 2001, Bio-Optical Models *in* Encyclopedia of Ocean Sciences, volume 1, pp 317–326.

Morel, A.Y., and Gordon, H.R., 1980, Report of the working group on water color: Boundary-Layer Meteorology, v. 18, p. 343–355, doi:10.1007/BF00122030.

Morel Prieur, L., A., 1977, Analysis of variations in ocean color: Limnology and Oceangraphy., v. 22, p. 709–725, doi:10.4319/lo.1977.22.4.0709.

Moreno-Brush, M., Rydberg, J., Gamboa, N., Storch, I., and Biester, H., 2016, Is mercury from small-scale gold mining prevalent in the southeastern Peruvian Amazon? Environmental Pollution, v. 218, p. 150–159, doi:10.1016/j.envpol.2016.08.038.

Mueen, A., and Keogh, E., 2016, Extracting optimal performance from dynamic time warping, *in* Proceedings of the 22nd ACM SIGKDD International Conference on Knowledge Discovery and Data Mining, p. 2129–2130.

Müller, B., Bryant, L.D., Matzinger, A., and Wüest, A., 2012, Hypolimnetic oxygen depletion in eutrophic lakes: Environmental Science & Technology, v. 46, p. 9964–9971, doi:10.1021/es301422r.

Munson, K.M., Babi, D., and Lamborg, C.H., 2014, Determination of monomethylmercury from seawater with ascorbic acid-assisted direct ethylation: Limnology and Oceanography: Methods, v. 12, p. 1–9, doi:10.4319/lom.2014.12.1.

Nadaraya, E.A., 1964, On estimating regression: Theory of Probability & Its Applications, v. 9, p. 141–142, doi:10.1137/1109020.

Nasrabadi, T., Ruegner, H., Sirdari, Z.Z., Schwientek, M., and Grathwohl, P., 2016, Using total suspended solids (TSS) and turbidity as proxies for evaluation of metal transport in river water: Applied Geochemistry, v. 68, p. 1–9, doi:10.1016/j.apgeochem.2016.03.003.

National Academies of Sciences, E. and M., 2018, Thriving on Our Changing Planet: Washington, D.C., National Academies Press, doi:10.17226/24938.

Nelson, S.A.C., Soranno, P.A., Cheruvelil, K.S., Batzli, S.A., and Skole, D.L., 2003, Regional Assessment of lake water clarity using satellite remote sensing: Journal of Limnology, v. 62, p. 27–32, doi:10.4081/jlimnol.2003.s1.27.

Ng, S.M.Y., Antenucci, J.P., Hipsey, M.R., Tibor, G., and Zohary, T., 2011, Physical controls on the spatial evolution of a dinoflagellate bloom in a large lake: Limnology and Oceanography, v. 56, p. 2265–2281, doi:10.4319/lo.2011.56.6.2265.

Novo, E.M., Hansom, J.D., and Curran, P.J., 1989, The effect of sediment type on the relationship between reflectance and suspended sediment concentration: International Journal of Remote Sensing, v. 10, p. 1283–1289, doi:10.1080/01431168908903967.

Novoa, S., Doxaran, D., Ody, A., Vanhellemont, Q., Lafon, V., Lubac, B., and Gernez, P., 2017, Atmospheric corrections and multi-conditional algorithm for multi-sensor remote sensing of

suspended particulate matter in low-to-high turbidity levels coastal waters: Remote Sensing, v. 9, doi:10.3390/rs9010061.

Obrador, B., Staehr, P.A., and Christensen, J.P.C., 2014, Vertical patterns of metabolism in three contrasting stratified lakes: Limnology and Oceanography, v. 59, p. 1228–1240, doi:10.4319/lo.2014.59.4.1228.

Odermatt, D., Gitelson, A., Brando, V.E., and Schaepman, M., 2012, Review of constituent retrieval in optically deep and complex waters from satellite imagery: Remote Sensing of Environment, v. 118, p. 116–126, doi:10.1016/j.rse.2011.11.013.

Okullo, W., Hamre, B., Frette, O., Stamnes, J.J., Sorensen, K., Ssenyonga, T., Hokedal, J., Stamnes, K., and Steigen, A., 2011, Validation of MERIS water quality products in Murchison Bay, Lake Victoria - Preliminary results: International Journal of Remote Sensing, v. 32, p. 5541–5563, doi:10.1080/01431161.2010.506895.

Olden, J.D., Lawler, J.J., and Poff, N.L., 2008, Machine Learning Methods Without Tears: A Primer for Ecologists: The Quarterly Review of Biology, v. 83, p. 171–193, doi:10.1086/587826.

Oleksy, I.A., Baron, J.S., Leavitt, P.R., and Spaulding, S.A., 2020a, Nutrients and warming interact to force mountain lakes into unprecedented ecological states: Proceedings of the Royal Society B: Biological Sciences, v. 287, p. 20200304, doi:10.1098/rspb.2020.0304.

Oleksy, I.A., Beck, W.S., Lammers, R.W., Steger, C.E., Wilson, C., Christianson, K., Vincent, K., Johnson, G., Johnson, P.T.J., and Baron, J.S., 2020b, The role of warm, dry summers and variation in snowpack on phytoplankton dynamics in mountain lakes: Ecology, doi:10.1002/ecy.3132.

Oliver, S.K., Collins, S.M., Soranno, P.A., Wagner, T., Stanley, E.H., Jones, J.R., Stow, C.A., and Lottig, N.R., 2017, Unexpected stasis in a changing world: Lake nutrient and chlorophyll trends since 1990: Global Change Biology, v. 23, p. 5455–5467, doi:10.1111/gcb.13810.

Olmanson, L.G., Bauer, M.E., and Brezonik, P.L., 2008a, A 20-year Landsat water clarity census of Minnesota's 10,000 lakes: Remote Sensing of Environment, v. 112, p. 4086–4097, doi:10.1016/j.rse.2007.12.013.

Olmanson, L.G., Brezonik, P.L., and Bauer, M.E., 2011, Evaluation of medium to low resolution satellite imagery for regional lake water quality assessments: Water Resources Research, v. 47, p. 1–14, doi:10.1029/2011WR011005.

Olmanson, L.G., Brezonik, P.L., and Bauer, M.E., 2014, Geospatial and temporal analysis of a 20-year record of Landsat-based water clarity in Minnesota's 10,000 lakes: Journal of the American Water Resources Association, v. 50, p. 748–761, doi:10.1111/jawr.12138.

Olmanson, L.G., Brezonik, P.L., Finlay, J.C., and Bauer, M.E., 2016, Comparison of Landsat 8 and Landsat 7 for regional measurements of CDOM and water clarity in lakes: Remote Sensing of Environment, v. 185, p. 119–128, doi:10.1016/j.rse.2016.01.007.

Olmanson, L.G., Page, B.P., Finlay, J.C., Brezonik, P.L., Bauer, M.E., Griffin, C.G., and Hozalski, R.M., 2020, Regional measurements and spatial/temporal analysis of CDOM in 10,000+ optically variable Minnesota lakes using Landsat 8 imagery: Science of The Total Environment, v. 724, p. 138141, doi:10.1016/j.scitotenv.2020.138141.

O'Neil, J.M., Davis, T.W., Burford, M.A., and Gobler, C.J., 2012, The rise of harmful cyanobacteria blooms: The potential roles of eutrophication and climate change: Harmful Algae, v. 14, p. 313–334, doi:10.1016/j.hal.2011.10.027.

O'Reilly, C.M. et al., 2015, Rapid and highly variable warming of lake surface waters around the globe: Geophysical Research Letters, v. 42, p. 10,773-10,781, doi:10.1002/2015GL066235.

Ouillon, S., Douillet, P., and Andréfouët, S., 2004, Coupling satellite data with in situ measurements and numerical modeling to study fine suspended-sediment transport: A study for the lagoon of New Caledonia: Coral Reefs, v. 23, p. 109–122, doi:10.1007/s00338-003-0352-z.

Overeem, I., Hudson, B.D., Syvitski, J.P.M., Mikkelsen, A.B., Hasholt, B., van den Broeke, M.R., Noël, B.P.Y., and Morlighem, M., 2017, Substantial export of suspended sediment to the global oceans from glacial erosion in Greenland: Nature Geoscience, p. ngeo3046, doi:10.1038/ngeo3046.

Oyama, Y., Matsushita, B., and Fukushima, T., 2015, Distinguishing surface cyanobacterial blooms and aquatic macrophytes using Landsat/TM and ETM+ shortwave infrared bands: Remote Sensing of Environment, v. 157, p. 35–47, doi:10.1016/j.rse.2014.04.031.

Paerl, H.W.W., and Huisman, J., 2009, Climate change: A catalyst for global expansion of harmful cyanobacterial blooms: Environmental Microbiology Reports, v. 1, p. 27–37, doi:10.1111/j.1758-2229.2008.00004.x.

Page, B.P., Olmanson, L.G., and Mishra, D.R., 2019, A harmonized image processing workflow using Sentinel-2/MSI and Landsat-8/OLI for mapping water clarity in optically variable lake systems: Remote Sensing of Environment, v. 231, p. 111284, doi:10.1016/j.rse.2019.111284.

Pahlevan, N., Chittimalli, S.K., Balasubramanian, S. V., and Vellucci, V., 2019, Sentinel-2/Landsat-8 product consistency and implications for monitoring aquatic systems: Remote Sensing of Environment, v. 220, p. 19–29, doi:10.1016/j.rse.2018.10.027.

Pahlevan, N., Sarkar, S., Franz, B.A., Balasubramanian, S. V., and He, J., 2017, Sentinel-2 MultiSpectral Instrument (MSI) data processing for aquatic science applications: Demonstrations and validations: Remote Sensing of Environment, v. 201, p. 47–56, doi:10.1016/j.rse.2017.08.033.

Palacios, S.L., Kudela, R.M., Guild, L.S., Negrey, K.H., Torres-Perez, J., and Broughton, J., 2015, Remote sensing of phytoplankton functional types in the coastal ocean from the HyspIRI Preparatory Flight Campaign: Remote Sensing of Environment, v. 167, p. 269–280, doi:10.1016/j.rse.2015.05.014.

Palmer, S.C.J., Kutser, T., and Hunter, P.D., 2015a, Remote sensing of inland waters: Challenges, progress and future directions: Remote Sensing of Environment, v. 157, p. 1–8, doi:10.1016/j.rse.2014.09.021.

Palmer, S.C.J., Odermatt, D., Hunter, P.D., Brockmann, C., Présing, M., Balzter, H., and Tóth, V.R., 2015b, Satellite remote sensing of phytoplankton phenology in Lake Balaton using 10years of MERIS observations: Remote Sensing of Environment, v. 158, p. 441–452, doi:10.1016/j.rse.2014.11.021.

Paulsen, S.G., Hughes, R.M., and Larsen, D.P., 1998, Critical elements in describing and understanding our nation's aquatic resources: Journal of the American Water Resources Association, v. 34, p. 995–1005.

Pavelsky, T.M., and Smith, L.C., 2009, Remote sensing of suspended sediment concentration, flow velocity, and lake recharge in the Peace-Athabasca Delta, Canada: Water Resources Research, v. 45, p. 1–16, doi:10.1029/2008WR007424.

Pearson, K., 1896, Mathematical contributions to the theory of evolution. III. Regression, heredity, and panmixia: Philosophical Transactions of the Royal Society of London. Series A, containing papers of a mathematical or physical character, v. 187, p. 253–318.

Peck, D.V., Olsen, A.R., Weber, M.H., Paulsen, S.G., Peterson, C., and Holdsworth, S.M., 2013, Survey design and extent estimates for the National Lakes Assessment: Freshwater Science, v. 32, p. 1231–1245, doi:10.1899/11-075.1.

Peckham, S.D., Chipman, J.W., Lillesand, T.M., and Dodson, S.I., 2006, Alternate stable states and the shape of the lake trophic distribution: Hydrobiologia, v. 571, p. 401–407, doi:10.1007/s10750-006-0221-1.

Peckham, S.D., and Lillesand, T.M., 2006, Detection of spatial and temporal trends in Wisconsin lake water clarity using landsat-derived estimates of secchi depth: Lake and Reservoir Management, v. 22, p. 331–341, doi:10.1080/07438140609354367.

Pedregosa, F. et al., 2011, Scikit-learn: Machine Learning in Python: v. 12, p. 2825–2830, doi:10.1007/s13398-014-0173-7.2.

Pekel, J.F., Cottam, A., Gorelick, N., and Belward, A.S., 2016, High-resolution mapping of global surface water and its long-term changes: Nature, v. 540, p. 418–422, doi:10.1038/nature20584.

Pereira, L.S.F.F., Andes, L.C., Cox, A.L., and Ghulam, A., 2017, Measuring Suspended-Sediment Concentration and Turbidity in the Middle Mississippi and Lower Missouri Rivers using Landsat Data: JAWRA Journal of the American Water Resources Association, v. 63103, p. 1–11, doi:10.1111/1752-1688.12616.

Peterson, S.A., Urquhart, N.S., and Welch, E.B., 1999, Sample representativeness: A must for reliable regional lake condition estimates: Environmental Science and Technology, v. 33, p. 1559–1565, doi:10.1021/es980711l.

Philpot, W.D., 1987, Radiative transfer in stratified waters: a single-scattering approximation for irradiance: Applied Optics, v. 26, p. 4123, doi:10.1364/AO.26.004123.

Platt, T., and Sathyendranath, S., 1988, Oceanic Remote Primary Production: Estimation by Remote Sensing at Local and Regional Scales: Science, v. 241, p. 1613–1620.

Poikane, S. et al., 2011, Lake ecological assessment systems and intercalibration for the European Water Framework Directive: Aims, achievements and further challenges: Procedia Environmental Sciences, v. 9, p. 153–168, doi:10.1016/j.proenv.2011.11.024.

Politi, E., Cutler, M.E.J., and Rowan, J.S., 2015, Evaluating the spatial transferability and temporal repeatability of remote-sensing-based lake water quality retrieval algorithms at the European scale: a meta-analysis approach: International Journal of Remote Sensing, v. 36, p. 2995–3023, doi:10.1080/01431161.2015.1054962.

Pollard, A.I., Hampton, S.E., and Leech, D.M., 2018, The promise and potential of continental-scale limnology using the U.S. Environmental Protection Agency's National Lakes Assessment: Limnology and Oceanography Bulletin, v. 27, p. 36–41, doi:10.1002/lob.10238.

Potes, M., Costa, M.J., and Salgado, R., 2012, Satellite remote sensing of water turbidity in Alqueva reservoir and implications on lake modelling: Hydrology and Earth System Sciences, v. 16, p. 1623–1633, doi:10.5194/hess-16-1623-2012.

Qi, L., Hu, C., Duan, H., Barnes, B.B., and Ma, R., 2014, An EOF-based algorithm to estimate chlorophyll a concentrations in taihu lake from MODIS land-band measurements: Implications for near real-time applications and forecasting models: Remote Sensing, v. 6, p. 10694–10715, doi:10.3390/rs61110694.

Qin, B., Li, W., Zhu, G., Zhang, Y., Wu, T., and Gao, G., 2015, Cyanobacterial bloom management through integrated monitoring and forecasting in large shallow eutrophic Lake Taihu (China): Journal of Hazardous Materials, v. 287, p. 356–363, doi:10.1016/j.jhazmat.2015.01.047.

Randles, C.A. et al., 2017, The MERRA-2 aerosol reanalysis, 1980 onward. Part I: System description and data assimilation evaluation: Journal of Climate, v. 30, p. 6823–6850, doi:10.1175/JCLI-D-16-0609.1.

Raymond, P.A. et al., 2013, Global carbon dioxide emissions from inland waters: Nature, v. 503, p. 355.

Read, E.K., Carr, L., De Cicco, L., Dugan, H.A., Hanson, P.C., Hart, J.A., Kreft, J., Read, J.S., and Winslow, L.A., 2017, Water quality data for national-scale aquatic research: The Water Quality Portal: Water Resources Research, v. 53, p. 1735–1745, doi:10.1002/2016WR019993.

Ren, J. et al., 2018a, Remote observation of water clarity patterns in Three Gorges Reservoir and Dongting Lake of China and their probable linkage to the Three Gorges Dam based on Landsat 8 imagery: Science of the Total Environment, v. 625, p. 1554–1566, doi:10.1016/j.scitotenv.2018.01.036.

Ritchie, J.C., and Cooper, C.M., 1988, Comparison of measured suspended sediment concentrations with suspended sediment concentrations estimated from Landsat MSS data: International Journal of Remote Sensing, v. 9, p. 379–387, doi:10.1080/01431168808954861.

Ritchie, J.C., Cooper, C.M., and Schiebe, F.R., 1990, The relationship of MSS and TM digital data with suspended sediments, chlorophyll, and temperature in Moon Lake, Mississippi: Remote Sensing of Environment, v. 33, p. 137–148, doi:10.1016/0034-4257(90)90039-O.

Robert, E., Kergoat, L., Soumaguel, N., Merlet, S., Martinez, J.M., Diawara, M., and Grippa, M., 2017, Analysis of suspended particulate matter and its drivers in Sahelian Ponds and Lakes by remote sensing (landsat and MODIS): Gourma Region, Mali: Remote Sensing, v. 9, doi:10.3390/rs9121272.

Rocha, A.D., Groen, T.A., Skidmore, A.K., Darvishzadeh, R., and Willemen, L., 2017, The Naïve Overfitting Index Selection (NOIS): A new method to optimize model complexity for hyperspectral data: ISPRS Journal of Photogrammetry and Remote Sensing, v. 133, p. 61–74, doi:10.1016/j.isprsjprs.2017.09.012.

Rose, K.C., Greb, S.R., Diebel, M., and Turner, M.G., 2017a, Annual precipitation regulates spatial and temporal drivers of lake water clarity: Ecological Applications, v. 27, p. 632–643, doi:10.1002/eap.1471.

Ross, M.R.V., Topp, S.N., Appling, A.P., Yang, X., Kuhn, C., Butman, D., Simard, M., and Pavelsky, T.M., 2019, AquaSat: A data set to enable remote sensing of water quality for inland waters: Water Resources Research, v. 55, p. 10012–10025, doi:10.1029/2019WR024883.

Röttgers, R., McKee, D., and Utschig, C., 2014, Temperature and salinity correction coefficients for light absorption by water in the visible to infrared spectral region: Optics Express, v. 22, p. 25093, doi:10.1364/oe.22.025093.

Roulet, N., and Moore, T.R., 2006, Browning the waters: Nature, v. 444, p. 283–284, doi:10.1038/444283a.

Roy, D.P., Kovalskyy, V., Zhang, H.K., Vermote, E.F., Yan, L., Kumar, S.S., and Egorov, A., 2016, Characterization of Landsat-7 to Landsat-8 reflective wavelength and normalized difference vegetation index continuity: Remote Sensing of Environment, v. 185, p. 57–70, doi:10.1016/j.rse.2015.12.024.

Rügner, H., Schwientek, M., Beckingham, B., Kuch, B., and Grathwohl, P., 2013, Turbidity as a proxy for total suspended solids (TSS) and particle facilitated pollutant transport in catchments: Environmental Earth Sciences, v. 69, p. 373–380, doi:10.1007/s12665-013-2307-1.

Sanchez, J.F., Carnero, A.M., Rivera, E., Rosales, L.A., Christian Baldeviano, G., Asencios, J.L., Edgel, K.A., Vinetz, J.M., and Lescano, A.G., 2017, Unstable malaria transmission in the southern Peruvian Amazon and its association with gold mining, Madre de Dios, 2001-2012: American Journal of Tropical Medicine and Hygiene, v. 96, p. 304–311, doi:10.4269/ajtmh.16-0030.

Sandström, A., Philipson, P., Asp, A., Axenrot, T., Kinnerbäck, A., Ragnarsson-Stabo, H., and Holmgren, K., 2016, Assessing the potential of remote sensing-derived water quality data to explain variations in fish assemblages and to support fish status assessments in large lakes: Hydrobiologia, v. 780, p. 71–84, doi:10.1007/s10750-016-2784-9.

Sass, G.Z., Creed, I.F., Bayley, S.E., and Devito, K.J., 2008a, Interannual variability in trophic status of shallow lakes on the Boreal Plain: Is there a climate signal? Water Resources Research, v. 44, p. 1–11, doi:10.1029/2007WR006310.

Sass, G.Z., Creed, I.F., and Devito, K.J., 2008b, Spatial heterogeneity in trophic status of shallow lakes on the Boreal Plain: Influence of hydrologic setting: Water Resources Research, v. 44, doi:10.1029/2007WR006311.

Sathyendranath, S., 2000, Remote Sensing of Ocean Colour in Coastal, and Other Optically-Complex, Waters.:

Savoy, P., Appling, A.P., Heffernan, J.B., Stets, E.G., Read, J.S., Harvey, J.W., and Bernhardt, E.S., 2019, Metabolic rhythms in flowing waters: An approach for classifying river productivity regimes: Limnology and Oceanography, v. 64, p. 1835–1851, doi:10.1002/lno.11154.

Sawaya, K., Olmanson, L.G., Heinert, N., Brezonik, P., and Bauer, M., 2003, Extending satellite remote sensing to local scales: land and water resource monitoring using high-resolution imagery: Remote Sensing of Environment, v. 88, p. 144–156, doi:10.1016/j.rse.2003.04.0006.

Scarpace, F., Holmquist, K., and Fisher, L., 1979, Landsat analysis of lake quality: Photogrammetric Engineering and Remote Sensing, v. 45, p. 623–633.

Schaeffer, B.A., Iiames, J., Dwyer, J., Urquhart, E., Salls, W., Rover, J., and Seegers, B., 2018, An initial validation of Landsat 5 and 7 derived surface water temperature for U.S. lakes, reservoirs, and estuaries: International Journal of Remote Sensing, v. 00, p. 1–17, doi:10.1080/01431161.2018.1471545.

Scheffer, M., and van Nes, E.H., 2007, Shallow lakes theory revisited: various alternative regimes driven by climate, nutrients, depth and lake size: Hydrobiologia, v. 584, p. 455–466, doi:10.1007/s10750-007-0616-7.

Scheuhammer, A.M., Meyer, M.W., Sandheinrich, M.B., and Murray, M.W., 2007, Effects of environmental methylmercury on the health of wild birds, mammals, and fish: Ambio, v. 36, p. 12–18, doi:10.1579/0044-7447(2007)36[12:EOEMOT]2.0.CO;2.

Schiller, H., and Doerffer, R., 1999, Neural network for emulation of an inverse model operational derivation of Case II water properties from MERIS data: International Journal of Remote Sensing, v. 20, p. 1735–1746, doi:10.1080/014311699212443.

Schindler, D.W., 2010, Recent advances in the understanding and management of eutrophication: Limnology and Oceanography, v. 51, p. 356–363, doi:10.4319/lo.2006.51.1_part_2.0356.

Schroeder, T., Behnert, I., Schaale, M., Fischer, J., and Doerffer, R., 2007, Atmospheric correction algorithm for MERIS above case-2 waters: International Journal of Remote Sensing, v. 28, p. 1469–1486, doi:10.1080/01431160600962574.

Schwarz, A.M., and Hawes, I., 1997, Effects of changing water clarity on characean biomass and species composition in a large oligotrophic lake: Aquatic Botany, v. 56, p. 169–181, doi:10.1016/S0304-3770(96)01114-X.

Sen, P.K., 1968, Estimates of the regression coefficient based on Kendall's Tau: Journal of the American Statistical Association, v. 63, p. 1379–1389, doi:10.2307/2285891.

Seyhan, E., and Dekker, A., 1986, Application of Remote Sensing Techniques for Water Quality Monitoring: Hydrobiological Bulletin, v. 20, p. 41–50.

Shahzad, M.I., Meraj, M., Nazeer, M., Zia, I., Inam, A., Mehmood, K., and Zafar, H., 2018, Empirical estimation of suspended solids concentration in the Indus Delta Region using Landsat-7 ETM+ imagery: Journal of Environmental Management, v. 209, p. 254–261, doi:10.1016/J.JENVMAN.2017.12.070.

Sharma, S. et al., 2019, Widespread loss of lake ice around the Northern Hemisphere in a warming world: Nature Climate Change, v. 9, p. 227–231, doi:10.1038/s41558-018-0393-5.

Sheela, A.M., Letha, J., Joseph, S., Ramachandran, K.K., and Sanalkumar, S.P., 2011, Trophic state index of a lake system using IRS (P6-LISS III) satellite imagery: Environmental Monitoring and Assessment, v. 177, p. 575–592, doi:10.1007/s10661-010-1658-2.

Shen, M., Duan, H., Cao, Z., Xue, K., Loiselle, S., and Yesou, H., 2017, Determination of the downwelling diffuse attenuation coefficient of lakewater with the sentinel-3A OLCI: Remote Sensing, v. 9, doi:10.3390/rs9121246.

Shen, Z., Yu, X., Sheng, Y., Li, J., and Luo, J., 2015, A fast algorithm to estimate the deepest points of lakes for regional lake registration: PLOS ONE, v. 10, p. e0144700, doi:10.1371/journal.pone.0144700.

Shi, K., Li, Y., Li, L., and Lu, H., 2013, Absorption characteristics of optically complex inland waters: Implications for water optical classification: Journal of Geophysical Research: Biogeosciences, v. 118, p. 860–874, doi:10.1002/jgrg.20071.

Sobek, S., Tranvik, L.J., Prairie, Y.T., and Cole, J.J., 2007, Patterns and regulation of dissolved organic carbon: An analysis of 7,500 widely distributed lakes: v. 52, p. 1208–1219.

Sommer, U. et al., 2012, Beyond the Plankton Ecology Group (PEG) Model: Mechanisms Driving Plankton Succession: Annual Review of Ecology, Evolution, and Systematics, v. 43, p. 429–448.

Sommer, U., Gliwicz, Z.M., Lampert, W., and Duncan, A., 1986, The PEG-model of seasonal succession of planktonic events in fresh waters: Arch. Hydrobiol, v. 106, p. 433–471.

Song, K. et al., 2013, Remote estimation of chlorophyll-a in turbid inland waters: Three-band model versus GA-PLS model: Remote Sensing of Environment, v. 136, p. 342–357, doi:10.1016/j.rse.2013.05.017.

Song, K., 2011, Water quality monitoring using Landsat Themate Mapper data with empirical algorithms in Chagan Lake, China: Journal of Applied Remote Sensing, v. 5, p. 053506, doi:10.1117/1.3559497.

Sonnenburg, S. et al., 2007, The Need for Open Source Software in Machine Learning: Journal of Machine Learning Research, v. 8, p. 600–611, doi:citeulike-article-id:11849756.

Soranno, P.A. et al., 2014, Cross-scale interactions: Quantifying multi-scaled cause-effect relationships in macrosystems: Frontiers in Ecology and the Environment, v. 12, p. 65–73, doi:10.1890/120366.

Soranno, P.A. et al., 2017, LAGOS-NE: A multi-scaled geospatial and temporal database of lake ecological context and water quality for thousands of U.S. lakes: GigaScience, p. 1–22, doi:10.1093/gigascience/gix101.

Spyrakos, E. et al., 2020, Moving towards global satellite based products for monitoring of inland and coastal waters. Regional examples from Europe and South America, *in* 2020 IEEE Latin American GRSS ISPRS Remote Sensing Conference (LAGIRS), p. 363–368, doi:10.1109/LAGIRS48042.2020.9165653.

Spyrakos, E. et al., 2017, Optical types of inland and coastal waters: Limnology and Oceanography, doi:10.1002/lno.10674.

Srebotnjak, T., Carr, G., De Sherbinin, A., and Rickwood, C., 2012, A global Water Quality Index and hot-deck imputation of missing data: Ecological Indicators, v. 17, p. 108–119, doi:10.1016/j.ecolind.2011.04.023.

Stanley, E.H., Collins, S.M., Lottig, N.R., Oliver, S.K., Webster, K.E., Cheruvelil, K.S., and Soranno, P.A., 2019, Biases in lake water quality sampling and implications for macroscale research: Limnology and Oceanography, v. 64, p. 1572–1585, doi:10.1002/lno.11136.

Stets, E.G., Sprague, L.A., Oelsner, G.P., Johnson, H.M., Murphy, J.C., Ryberg, K., Vecchia, A.V., Zuellig, R.E., Falcone, J.A., and Riskin, M.L., 2020, Landscape drivers of dynamic change in water quality of U.S. rivers: Environmental Science & Technology, v. 54, p. 4336–4343, doi:10.1021/acs.est.9b05344.

Stumpf, R.P., and Pennock, J.R., 1989, Calibration of a general optical equation for remote sensing of suspended sediments in a moderately turbid estuary: Journal of Geophysical Research, v. 94, p. 14363, doi:10.1029/JC094iC10p14363.

Sun, D., Qiu, Z., Li, Y., Shi, K., and Gong, S., 2014, Detection of Total Phosphorus Concentrations of Turbid Inland Waters Using a Remote Sensing Method: Water, Air, & Soil Pollution, v. 225, p. 1953, doi:10.1007/s11270-014-1953-6.

Svirčev, Z., Simeunović, J., Subakov-Simić, G., Krstić, S., Pantelić, D., and Dulić, T., 2013, Cyanobacterial blooms and their toxicity in Vojvodina Lakes, Serbia: International Journal of Environmental Research, v. 7, p. 745–758.

Syvitski, J.P.M., 2005, Impact of Humans on the Flux of Terrestrial Sediment to the Global Coastal Ocean: Science, v. 308, p. 376–380, doi:10.1126/science.1109454.

Tarpley, J.D., Schneider, S.R., and Money, R.L., 1984, Global Vegetation Indices from the NOAA-7 Meteorological Satellite: Journal of Climate and Applied Meterology, v. 23, p. 491–494, doi:10.1175/1520-0450(1984)023<0491:GVIFTN>2.0.CO;2.

Telmer, K., Costa, M., Angélica, R.S., Araujo, E.S., and Maurice, Y., 2006, The source and fate of sediment and mercury in the Tapajos River, Para, Brazilian Amazon: Ground- and space-based evidence: Journal of Environmental Management, v. 81, p. 101–113, doi:10.1016/j.jenvman.2005.09.027.

Telmer, K.H., and Veiga, M.M., 2009, World emissions of mercury from artisanal and small scale gold mining, *in* Mason, R. and Pirrone, N. eds., Mercury fate and transport in the global atmosphere, Springer, p. 131–172.

Therneau, T., and Atkinson, B., 2019, rpart: Recursive Partitioning and Regression Trees.:

Thrane, J.-E., Hessen, D.O., and Andersen, T., 2014, The Absorption of Light in Lakes: Negative Impact of Dissolved Organic Carbon on Primary Productivity: Ecosystems, v. 17, p. 1040–1052, doi:10.1007/s10021-014-9776-2.

Todorova, S.G., Driscoll, C.T., Matthews, D.A., Effler, S.W., Hines, M.E., and Henry, E.A., 2009, Evidence for regulation of monomethyl mercury by nitrate in a seasonally stratified, eutrophic lake: Environmental Science and Technology, v. 43, p. 6572–6578, doi:10.1021/es900887b.

Toming, K., Kutser, T., Laas, A., Sepp, M., Paavel, B., and Nõges, T., 2016, First experiences in mapping lakewater quality parameters with sentinel-2 MSI imagery: Remote Sensing, v. 8, p. 1–14, doi:10.3390/rs8080640.

Topp, S.N., Pavelsky, T.M., Jensen, D., Simard, M., and Ross, M.R.V., 2020a, Research trends in the use of remote sensing for inland water quality science: moving towards multidisciplinary applications: Water, v. 12, p. 169, doi:10.3390/w12010169.

Topp, S.N., Pavelsky, T.M., Yang, X., Ross, M.R.V., and Gardner, J., 2020b, LimnoSat-US: A Remote Sensing Dataset for U.S. Lakes from 1984-2020: Zenodo, doi:10.5281/zenodo.4139695.

Torbick, N., Hession, S., Hagen, S., Wiangwang, N., Becker, B., and Qi, J., 2013, Mapping inland lake water quality across the Lower Peninsula of Michigan using Landsat TM imagery: International Journal of Remote Sensing, v. 34, p. 7607–7624, doi:10.1080/01431161.2013.822602.

Torbick, N., Hession, S., Stommel, E., and Caller, T., 2014, Mapping amyotrophic lateral sclerosis lake risk factors across northern New England: International Journal of Health Geographics, v. 13, doi:10.1186/1476-072X-13-1.

Tranvik, L.J. et al., 2009, Lakes and reservoirs as regulators of carbon cycling and climate: Limnology and Oceanography, v. 54, p. 2298–2314, doi:10.4319/lo.2009.54.6_part_2.2298.

Tucker, C.J., 1979, Red and photographic infrared linear combinations for monitoring vegetation: Remote Sensing of Environment, v. 8, p. 127–150, doi:10.1016/0034-4257(79)90013-0.

Tucker, C.J., Fung, I.Y., Keeling, C.D., and Gammon, R.H., 1986, Relationship between atmospheric CO2 variations and a satellite-derived vegetation index: Nature, v. 319, p. 195–199, doi:10.1038/319195a0.

Tyler, A.N., Hunter, P.D., Spyrakos, E., Groom, S., Constantinescu, A.M., and Kitchen, J., 2016, Developments in Earth observation for the assessment and monitoring of inland, transitional, coastal and shelf-sea waters: Science of the Total Environment, v. 572, p. 1307–1321, doi:10.1016/j.scitotenv.2016.01.020.

Tyler, A.N., Svab, E., Preston, T., Présing, M., and Kovács, W.A., 2006, Remote sensing of the water quality of shallow lakes: A mixture modelling approach to quantifying phytoplankton in water characterized by high-suspended sediment: International Journal of Remote Sensing, v. 27, p. 1521–1537, doi:10.1080/01431160500419311.

UNEP, 2018, Global mercury assessment: https://www.unenvironment.org/resources/publication/global-mercury-assessment-2018.

Van der Woerd, H.J., and Wernand, M.R., 2018, Hue-Angle Product for Low to Medium Spatial Resolution Optical Satellite Sensors: Remote Sensing, v. 10, p. 180, doi:10.3390/rs10020180.

Vanhellemont, Q., and Ruddick, K., 2018, Atmospheric correction of metre-scale optical satellite data for inland and coastal water applications: Remote Sensing of Environment, v. 216, p. 586–597, doi:10.1016/j.rse.2018.07.015.

del Vecchio, R., and Blough, N. V, 2006, Influence of Ultraviolet Radiation on the Chromophoric Dissolved Organic Matter in Natural Waters, *in* Ghetti, F., Checcucci, G., and Bornman, J.F. eds., Environmental UV Radiation: Impact on Ecosystems and Human Health and Predictive Models, Dordrecht, Springer Netherlands, p. 203–216.

Veiga, M.M., Maxson, P.A., and Hylander, L.D., 2006, Origin and consumption of mercury in small-scale gold mining: Journal of Cleaner Production, v. 14, p. 436–447, doi:10.1016/j.jclepro.2004.08.010.

Venables, W.N., and Ripley, B.D., 2002, Modern Applied Statistics with S: New York, Springer.

Verdin, J.P., 1985, Bureau of Reclamation Monitoring Water Quality Conditions in a Large Western Reservoir with Landsat Imagery: Photogrammetric Engineering and Remote Sensing, v. 51, p. 343–353.

Vermote, E., Justice, C., Claverie, M., and Franch, B., 2016, Preliminary analysis of the performance of the Landsat 8/OLI land surface reflectance product: Remote Sensing of Environment, v. 185, p. 46–56, doi:10.1016/j.rse.2016.04.008.

Verpoorter, C., Kutser, T., Seekell, D.A., and Tranvik, L.J., 2014, A global inventory of lakes based on high-resolution satellite imagery: Geophysical Research Letters, v. 41, p. 6396–6402, doi:10.1002/2014GL060641.

Volpe, V., Silvestri, S., and Marani, M., 2011, Remote sensing retrieval of suspended sediment concentration in shallow waters: Remote Sensing of Environment, v. 115, p. 44–54, doi:10.1016/j.rse.2010.07.013.

Walker, N.D., 1996, Satellite assessment of Mississippi River plume variability: Causes andpredictability: Remote Sensing of Environment, v. 58, p. 21–35, doi:10.1016/0034-4257(95)00259-6.

Wang, S. et al., 2020, Changes of water clarity in large lakes and reservoirs across China observed from long-term MODIS: Remote Sensing of Environment, v. 247, p. 111949, doi:10.1016/j.rse.2020.111949.

Wang, W., Lee, X., Xiao, W., Liu, S., Schultz, N., Wang, Y., Zhang, M., and Zhao, L., 2018, Global lake evaporation accelerated by changes in surface energy allocation in a warmer climate: Nature Geoscience, v. 11, p. 410–414, doi:10.1038/s41561-018-0114-8.

Wang, S., Li, J., Shen, Q., Zhang, B., Zhang, F., and Lu, Z., 2015, MODIS-Based radiometric color extraction and classification of inland water with the forel-ule scale: A case study of lake Taihu: IEEE Journal of Selected Topics in Applied Earth Observations and Remote Sensing, v. 8, p. 907–918, doi:10.1109/JSTARS.2014.2360564.

Wang, M., Nim, C.J., Son, S.H., and Shi, W., 2012, Characterization of turbidity in Florida's Lake Okeechobee and Caloosahatchee and St. Lucie Estuaries using MODIS-Aqua measurements: Water Research, v. 46, p. 5410–5422, doi:10.1016/j.watres.2012.07.024.

Wang, M., Son, S., Zhang, Y., and Shi, W., 2013, Remote sensing of water optical property for China's inland lake taihu using the SWIR atmospheric correction with 1640 and 2130 nm bands: IEEE Journal of Selected Topics in Applied Earth Observations and Remote Sensing, v. 6, p. 2505–2516, doi:10.1109/JSTARS.2013.2243820.

Wang, Y., Xia, H., Fu, J., and Sheng, G., 2004, Water quality change in reservoirs of Shenzhen, China: detection using LANDSAT/TM data: Science of The Total Environment, v. 328, p. 195–206, doi:10.1016/j.scitotenv.2004.02.020.

Wass, P.D., Marks, S.D., Finch, J.W., Leeks, G.J.L., and Ingram, J.K., 1997, Monitoring and preliminary interpretation of in-river turbidity and remote sensed imagery for suspended sediment transport studies in the Humber catchment: Science of The Total Environment, v. 194–195, p. 263–283, doi:10.1016/S0048-9697(96)05370-3.

Watanabe, F.S.Y., Alcântara, E., Rodrigues, T.W.P., Imai, N.N., Barbosa, C.C.F., and Rotta, L.H. da S., 2015, Estimation of chlorophyll-a concentration and the trophic state of the barra bonita hydroelectric reservoir using OLI/landsat-8 images: International Journal of Environmental Research and Public Health, v. 12, p. 10391–10417, doi:10.3390/ijerph120910391.

Watson, G.S., 1964, Smooth regression analysis: Sankhyā: The Indian Journal of Statistics, Series A (1961-2002), v. 26, p. 359–372.

Webster, K.E., Soranno, P.A., Cheruvelil, K.S., Bremigan, M.T., Downing, J.A., Vaux, P.D., Asplund, T.R., Bacon, L.C., and Connor, J., 2008, An empirical evaluation of the nutrient-color paradigm for lakes: Limnology and Oceanography, v. 53, p. 1137–1148, doi:10.4319/lo.2008.53.3.1137.

Wen, Z., Song, K., Shang, Y., Fang, C., Li, L., Lv, L., Lv, X., and Chen, L., 2017, Carbon dioxide emissions from lakes and reservoirs of China: A regional estimate based on the calculated pCO2: Atmospheric Environment, v. 170, p. 71–81, doi:10.1016/j.atmosenv.2017.09.032.

Wernand, M.R., 2010, On the history of the Secchi disc: Journal of the European Optical Society, v. 5, doi:10.2971/jeos.2010.10013s.

Willmott, C.J., 1981, On the validation of Models: Physical Geography, v. 2, p. 184–194, doi:10.1080/02723646.1981.10642213.

Winder, M., and Cloern, J.E., 2010, The annual cycles of phytoplankton biomass: Philosophical Transactions of the Royal Society B: Biological Sciences, v. 365, p. 3215–3226, doi:10.1098/rstb.2010.0125.

Winder, M., and Schindler, D.E., 2004, Climate change uncouples trophic interactions in an aquatic ecosystem: Ecology, v. 85, p. 2100–2106, doi:10.1890/04-0151.

Woerd, H.J. van der, and Wernand, M.R., 2015, True colour classification of natural waters with medium-spectral resolution satellites: SeaWiFS, MODIS, MERIS and OLCI: Sensors, v. 15, p. 25663–25680, doi:10.3390/s151025663.

Wong, W.H., Dudula, J.J., Beaudoin, T., Groff, K., Kimball, W., and Swigor, J., 2018, Declining ambient water phosphorus concentrations in Massachusetts' rivers from 1999 to 2013: Environmental protection works: Water Research, v. 139, p. 108–117, doi:10.1016/j.watres.2018.03.053.

Woolway, R.I., Kraemer, B.M., Lenters, J.D., Merchant, C.J., O'Reilly, C.M., and Sharma, S., 2020, Global lake responses to climate change: Nature Reviews Earth & Environment, p. 1–16, doi:10.1038/s43017-020-0067-5.

Woolway, R.I., and Merchant, C.J., 2019, Worldwide alteration of lake mixing regimes in response to climate change: Nature Geoscience, v. 12, p. 271–276, doi:10.1038/s41561-019-0322-x.

Wrigley, R.C., and Horne, A.J., 1974, Remote sensing and lake eutrophication: Nature, v. 250, p. 213–214, doi:10.1038/250213a0.

Wu, G., De Leeuw, J., Skidmore, A.K., Prins, H.H.T., and Liu, Y., 2008, Comparison of MODIS and Landsat TM5 images for mapping tempo–spatial dynamics of Secchi disk depths in Poyang Lake National Nature Reserve, China: International Journal of Remote Sensing, v. 29, p. 2183–2198, doi:10.1080/01431160701422254.

Wu, G., de Leeuw, J., Skidmore, A.K., Prins, H.H.T.T., and Liu, Y., 2007, Concurrent monitoring of vessels and water turbidity enhances the strength of evidence in remotely sensed dredging impact assessment: Water Research, v. 41, p. 3271–3280, doi:10.1016/j.watres.2007.05.018.

Wulder, M.A., Masek, J.G., Cohen, W.B., Loveland, T.R., and Woodcock, C.E., 2012, Opening the archive: How free data has enabled the science and monitoring promise of Landsat: Remote Sensing of Environment, v. 122, p. 2–10, doi:10.1016/j.rse.2012.01.010.

Xiang, B., Song, J.-W., Wang, X.-Y., and Zhen, J., 2015, Improving the accuracy of estimation of eutrophication state index using a remote sensing data-driven method: A case study of Chaohu Lake, China: Water SA, v. 41, p. 753, doi:10.4314/wsa.v41i5.18.

Xue, Z., Du, P., and Feng, L., 2014, Phenology-driven land cover classification and trend analysis based on long-term remote sensing image series: IEEE Journal of Selected Topics in Applied Earth Observations and Remote Sensing, v. 7, p. 1142–1156, doi:10.1109/JSTARS.2013.2294956.

Yacobi, Y.Z., Gitelson, A., and Mayo, M., 1995, Remote sensing of chlorophyll in Lake Kinneret using high spectral resolution radiometer and Landsat Thematic Mapper Spectral features of reflectance and algorithm development: Journal of Plankton Research, v. 17, p. 2155–2173.

Yang, X., 2020, Deepest point calculation for any given polygon using Google Earth Engine JavaScript API: Zenodo, doi:10.5281/zenodo.4136755.

Yang, X., Pavelsky, T.M., Allen, G.H., and Donchyts, G., 2020, RivWidthCloud: An automated Google Earth Engine algorithm for river width extraction from remotely sensed imagery: IEEE Geoscience & Remote Sensing Letters, v. 17, p. 217–221.

Zandaryaa, S., 2018, The UNESCO-IHP IIWQ World Water Quality Portal - Whitepaper -.:

Zhang, Y., and Hepner, G.F., 2017, The Dynamic-Time-Warping-based k-means++ clustering and its application in phenoregion delineation: International Journal of Remote Sensing, v. 38, p. 1720–1736, doi:10.1080/01431161.2017.1286055.

Zhang, H., Hu, W., Gu, K., Li, Q., Zheng, D., and Zhai, S., 2013, An improved ecological model and software for short-term algal bloom forecasting: Environmental Modelling and Software, v. 48, p. 152–162, doi:10.1016/j.envsoft.2013.07.001.

Zhou, X., Marani, M., Albertson, J., Silvestri, S., Zhou, X., Marani, M., Albertson, J.D., and Silvestri, S., 2017, Hyperspectral and Multispectral Retrieval of Suspended Sediment in Shallow Coastal Waters Using Semi-Analytical and Empirical Methods: Remote Sensing, v. 9, p. 393, doi:10.3390/rs9040393.

Zhou, B., Shang, M., Wang, G., Zhang, S., Feng, L., Liu, X., Wu, L., and Shan, K., 2018, Distinguishing two phenotypes of blooms using the normalised difference peak-valley index (NDPI) and Cyano-Chlorophyta index (CCI): Science of the Total Environment, v. 628–629, p. 848–857, doi:10.1016/j.scitotenv.2018.02.097.

Zhu, M., Paerl, H.W., Zhu, G., Wu, T., Li, W., Shi, K., Zhao, L., Zhang, Y., Qin, B., and Caruso, A.M., 2014, The role of tropical cyclones in stimulating cyanobacterial (Microcystis spp.) blooms in hypertrophic Lake Taihu, China: Harmful Algae, v. 39, p. 310–321, doi:10.1016/j.hal.2014.09.003.

Zhu, Z., Wang, S., and Woodcock, C.E., 2015, Improvement and expansion of the Fmask algorithm: Cloud, cloud shadow, and snow detection for Landsats 4-7, 8, and Sentinel 2 images: Remote Sensing of Environment, v. 159, p. 269–277, doi:10.1016/j.rse.2014.12.014.

Zou, H., and Hastie, T., 2005, Regularization and variable selection via the elastic net: Journal of the Royal Statistical Society: Series B (Statistical Methodology), v. 67, p. 301–320, doi:https://doi.org/10.1111/j.1467-9868.2005.00503.x.